UNIVERSITÉ DE SHERBROOKE
Faculté de génie
Département de génie civil

ASSESSMENT OF THE LONG-TERM PERFORMANCE OF GFRP BARS SUBJECTED TO DIFFERENT ENVIRONMENTAL EXPOSURES UNDER HIGH SUSTAINED LOADS

ÉVALUATION DE LA PERFORMANCE À LONG TERME DE BARRES D'ARMATURE EN PRFV SOUMISES À DIFFÉRENTES CONDITIONS ENVIRONNEMENTALES SOUS CHARGES DE TRACTION SOUTENUES ÉLEVÉES

Thèse de doctorat
Spécialité : génie civil

Yasin ESMAEILI HESAR

Sherbrooke (Québec) Canada
janvier 2021

MEMBRES DU JURY

Professeur Brahim Benmokrane
Directeur de thèse

Professeur John Newhook
Co-directeur

Professeur Mathieu Robert
Rapporteur et examinateur

Professeur P. Vijay
Examinateur

Dr. Patrice Cousin
Examinateur

ABSTRACT

The long-term performance of glass fiber reinforced polymer (GFRP) bars subjected to high sustained loads and aggressive environmental conditions is not entirely clear and very conservative limits are imposed by available FRP design guidelines and codes. A two-phase (Phase I and Phase II) experimental program was designed to address this issue.

Phase I included an experimental investigation and statistical approach to assess the long-term performance and to determine a safe creep-rupture strength value for glass fiber-reinforced polymer (GFRP) bars subjected to different types of environmental exposure. The study sample consisted of 160 bars of various sizes (10 mm, 12 mm, and two types of 15 mm) subjected to different levels of environmental conditioning (unconditioned and exposed to an alkaline solution at 23°C and 60°C) and a range of sustained load levels (40% to 90% of the ultimate tensile strength). The test results were analyzed with Weibull statistical analysis to determine the mean and characteristic creep-rupture strengths, and consequently, a safe design value was calculated. Limitations and variations of the strength degradation model for the life-span prediction was assessed. The impact of sustained load on strength reduction was more pronounced than the combined effect of the alkaline solution and high temperature. The GFRP bars with smaller diameters were more susceptible to creep rupture than the larger ones, while the conditioning had more effect on the bars with larger diameters than the smaller ones.

In Phase II, a set of experiments was conducted to assess the flexural behavior of concrete beams reinforced with GFRP bars subjected to a high sustained flexural load after 10 years of natural aging. The experimental program consisted of eight rectangular concrete beams measuring 250 × 250 × 2000 mm. All beams were reinforced with sand coated GFRP bars. Four beams were subjected to a high sustained load of up to 40% of the ultimate tensile capacity of their GFRP bars with simultaneous exposure to aggressive natural weathering (temperatures ranging from -25℃ to 35℃) for 10 years. The remaining four were stored in the laboratory and treated as control specimens without any loading. The conditioned beams were tested up to failure in a four-point bending setup. The results were compared in terms of load–displacement behavior, ultimate strength, displacement capacity, failure modes, and cracking pattern. In addition, the microstructure of the GFRP bars was studied to evaluate the physical changes of the bars, and their bond condition with surrounding concrete at different stress levels. The findings indicate a strength deterioration of only 16% for this early generation of GFRP bars under harsh natural conditioning and high sustained loads for 10 years. On the other hand, the bond between the concrete and GFRP bars as well as the glass transition temperature, infrared spectra and interlaminar shear strength of the GFRP bars remained unaffected. Finally, analytical approaches were implemented to predict the load–displacement behavior and crack widths of the tested beams.

Keywords: Creep rupture strength; GFRP bar; Durability; Environmental conditioning; Sustained load; Environmental reduction factor; Design codes; Natural weathering; High sustained stress; Failure mode; Bond behavior; Deflection; Non-destructive testing.

RÉSUMÉ

La performance à long terme des barres en polymère renforcé de fibres de verre (PRFV) soumises à des charges soutenues élevées et à des conditions environnementales agressives n'est pas tout à fait clairement définie et des limites sévères sont imposées par les guides de conception disponibles. Un programme expérimental en deux phases est conçu pour étudier cette question. Dans la phase I, la résistance à la rupture par fluage des barres de PRFV exposées à différentes conditions environnementales est évaluée pour la nouvelle génération de barres. La phase II examine le comportement en flexion de poutres en béton ayant subi un vieillissement naturel et qui ont été renforcées avec la génération précédente de barres de PRFV. La première phase est réalisée en laboratoire et la seconde phase est une étude sur le terrain.

La première série d'expériences est réalisée sur 170 barres et englobe une variété de diamètres de barres (10 mm, 12 mm et deux types de 15 mm), de conditionnement environnemental (non conditionné et exposé à une solution alcaline à 23 °C et 60 °C) et de charges soutenues imposées (40 à 90 % de la résistance ultime à la traction des barres). Les résultats des essais ont été analysés à l'aide d'une analyse statistique de Weibull afin de déterminer les résistances moyennes et les résistances caractéristiques de ruptures par fluage et par conséquent, une valeur sûre pour le dimensionnement a été calculée. Les limites et les variations du modèle de dégradation de la résistance pour la prédiction de la durée de vie ont été discutées. En outre, la microstructure des barres de PRFV non rompues a été

étudiée pour évaluer les changements physiques des barres. Les résultats de l'étude montrent que le taux de dégradation est prolongé pour des niveaux de charges soutenues plus faibles. L'impact d'une charge soutenue sur la réduction de la résistance est plus prononcé que l'effet couplé d'une solution alcaline et d'une température élevée. Les facteurs de réduction de la rupture par fluage (C_c) prescrits par les codes de conception actuels sont conservateurs pour les barres de PRFV dans cette étude. Un facteur de réduction environnemental égal à 1,0 peut être utilisé avec les limites de rupture par fluage spécifiées par les codes actuels pour les barres de PRFV noyées dans du béton, non en contact avec le sol et non exposées aux intempéries.

La deuxième série d'expériences a examiné le comportement en flexion de poutres en béton renforcées par des barres de PRFV et soumises à une charge soutenue élevée de flexion après 10 ans de vieillissement naturel. Le programme expérimental comprenait huit poutres rectangulaires en béton mesurant 250 x 250 x 2000 mm. Toutes les poutres ont été renforcées avec des barres de PRFV revêtues de sable. Quatre poutres ont été soumises à une charge élevée soutenue allant jusqu'à 40 % de la résistance ultime en traction des barres de PRFV, avec une exposition simultanée à un vieillissement naturel agressif (températures allant de -25°C à 35°C) pendant 10 ans. Les quatre autres poutres ont été entreposées au laboratoire comme spécimens témoins sans aucune charge. Les poutres conditionnées ont été testées en flexion quatre points jusqu'à la rupture. Les résultats ont été comparés en termes de comportement charge-déplacement, de résistance ultime, de capacité de déplacement, de modes de rupture et de patron de fissuration. De plus, la microstructure des barres de PRFV a été étudiée pour évaluer les changements physiques des barres et leur adhérence avec le

béton environnant à différents niveaux de contrainte. Les résultats indiquent une détérioration de la résistance de seulement 16 % pour cette première génération de barres de PRFV, dans des conditions naturelles difficiles et sous des charges élevées soutenues pendant 10 ans. En revanche, l'adhérence entre le béton et les barres de PRFV, ainsi que la température de transition vitreuse, les spectres infrarouges et la résistance au cisaillement interlaminaire des barres de PRFV n'ont pas été affectés. Enfin, des approches analytiques ont été mises en œuvre pour prédire le comportement charge-déplacement et l'ouverture des fissures des poutres testées.

Mots-clés : Résistance à la rupture par fluage, barre de PRFV, durabilité, conditionnement environnemental, charge soutenue, facteur de réduction environnemental, codes de conception, intempéries naturelles, contrainte soutenue élevée, mode de rupture, adhérence, flèche, essais non destructifs.

ACKNOWLEDGMENTS

I would like to sincerely thank my supervisor, Professor Brahim Benmokrane and my co-supervisor Professor John Newhook for initially believing in me and giving me the opportunity to perform this Ph.D. Their advice and guidance throughout the study period have been invaluable. Working with them has been inspirational for me and certainly, I have learnt a lot from them.

I am also very grateful to Dr. Khaled Ahmed MMohamed and Dr. Abolfazl Eslami for their constant support, continuous encouragement, consulting, and guidance throughout the Ph.D.

I am also I am also very grateful to the members of jury: Professor Mathieu Robert, Professor P. Vijay and Dr. Patrice Cousin for their time in reviewing my thesis.

My sincere gratitude goes to the Natural Science and Engineering Research Council of Canada (NSERC), the Network of Centre of Excellence (NCE) of Canada, the NSERC Research Chair in Innovative FRP Reinforcement for Sustainable Concrete Infrastructures, the Tier-1 Canada Research Chair in Composite Materials for Civil structures, and the University of Sherbrooke Research Centre on Composite Materials (CRUSMaC) from where the project received its financial support.

I would also like to thank all my colleagues and friends at the University of Sherbrooke for their support friendliness streamlined during the period of Ph.D. I wish to express my gratitude to the technical staff of the Center for Material Characterization (CCM) and the

materials and structural laboratory at the University of Sherbrooke and Dalhousie University.

Last but certainly not least, I would like to say a special thank you to all my family members, who were patient and helped me to complete this research work.

Yasin E. Hesar

TABLE OF CONTENTS

LIST OF TABLES

LIST OF FIGURES

CHAPTER 1 INTRODUCTION

1.1. Statement of the problem

When a new product is introduced to the market by a manufacturer, one of the main concerns is how to ensure the customers that what they buy is something durable and the performance of the product won't fade away. Can the life cycle of the product be predicted? Is it necessary we wait for several years to examine its service life performance or might there be other solutions? To answer these questions durability science suggests several techniques and methods of conducting experiments in order to anticipate behavior of the new product over its life cycle in a shorter period of time.

Because of the long time period required for natural conditioning of materials to occur, this kind of experiment is considered as an impractical approach to evaluate durability. For this reason, the idea of accelerated aging tests as a feasible, yet accurate method to investigate the life cycle of a material, predominates in the literature. This testing method is carried out based on vulnerable characteristic of composite polymers exposed to high temperatures (artificial aging). This can be considered as a treatment of FRP composite at elevated temperatures along with other artificially made environmental conditions (e.g. high humidity, freeze-thaw cycles, wet-dry cycles, seawater, de-icing salt effect, alkalinity, etc.) so as to accelerate the changes in the properties of that material.

Over the past years, a great number of studies (Vijay 1999; S. Debaiky 2006; Chen 2006; Robert et al. 2009; Huang 2010; Davalos et al. 2011; Zh. Dong 2016, Arczewska 2018) have justified the durability behavior of FRP bars subjected to different environmental conditions using the accelerated aging test method. However, a few studies investigated their long-term durability of these material in real-life conditions. Thus, fully exploiting this technology is still limited due to several remaining unknowns and issues related to its durability in actual conditions. To overcome this issue and broaden the knowledge of engineers on the long-term performance of GFRP material, different approaches have been adopted by engineers over the years. Besides aforementioned accelerated aging, Non-destructive Evaluation (NDE) of the existing structures is also reasonable option to acquire more information and anticipate life cycle of FRP bars. Non-Destructive tests, as a complementary data source for durability studies of FRP bars, have been extensively implemented by other researchers (Oakley, and Proctor 1981, Nkurunziza et al. 2005, Mufti et al. 2007, Robert et al. 2009, Wu et al. 2014, El-Hassan and El Maaddawy 2019). The method is comprised of a group of analysis techniques (microscopy and/or physicochemical analyses) to evaluate the properties of structural systems and components, without causing damage to them.

This research project aims at investigating the durability of GFRP bars in structural and micro structural scales. The experimental program included the two common experimental environments: 1- laboratory based (accelerated aging) conditions in which the creep strength of GFRP bars is studied under different environmental exposures; and, 2- Real-life environmental (natural aging) conditions. A field investigation in which retained flexural strength of the beams reinforced with GFRP bars is studied. The creep specimens were designed to satisfy requirements of ASTM D7337 (ASTM 2019) and the beam specimens

were designed based on the Canadian Highway Bridge Design Code CHBDC CSA S6 (CSA 2019). The outputs of this research will contribute to extend the use of GFRP-RC structural components, which is an innovative solution to overcome the corrosion problems and improve the product durability. The findings of this study are expected to support the idea of increasing in service capacity of GFRP bars, by design codes, in respect with creep strength, also reassuring for the design engineers of the durability performance of the internally used GFRP bars.

1.2. Motivation of the Research

Motivations behind this study can be summarized as:

- According to the clause 7.1.2.2, CSA S806 (CSA 2012), only 25% of the ultimate tensile capacity of GFRP reinforcing bars is used for serviceability limit state purposes. Similarly, the ACI 440.1R (ACI 2015) requires that the creep rupture strength be 20% of the design strength of GFRP bars. Nevertheless, advances made in manufacturing techniques have raised the hope to utilize more capacity of the GFRP bars for serviceability limit-state predictions.

- The creep rupture strength of GFRP is well known to affect by concrete alkalinity and environmental exposure; however, such an effect has not been quantified to ensure the safe service-life performance of structures and highlight the potential of relaxing the over-conservative assumptions of the current code provisions.

- Only a few studies have been carried out on existing in-service structures, and those that exist are based on non-destructive tests or solely considers environmental conditioning

effect without considering the deteriorating effect of sustained load. More experimental data for naturally aged GFRP RC structural components is required, so that the design code technical committees, engaged in developing standards and code provisions, can rely on more realistic data.

- It is important to understand what percentage of the total degradation of GFRP bar, after conditioning, is because of the effect of sustained load and what is the contribution of environmental conditioning. In addition, the environmental coefficients (CE) suggested by ACI440.1R (ACI 2015) is to be verified by experiments.

- The advancements of new generations of GFRP bars compared with old generations in terms of quality needs to be investigated. So that the design code provisions can be updated as per the-state-of-the-art.

1.3. Objectives and Scope

The objectives of the study are as follows:

The Phase I, a total of 160 GFRP bars have been tested for creep strength with varieties of bar sizes and types, different conditioning status, and a wide range of imposed sustained stress levels. The stress levels were defined by testing another 20 GFRP bars from the same types and sizes for longitudinal tensile properties. The objective of the study was to assess the long-term performance and creep-rupture strength for GFRP bars subjected to different environmental exposures. The Phase I of study also aims to assess the appropriateness of the

term $C_c \times C_E$ given by the ACI 440.1R (ACI 2015) and AASHTO LRFD (AASHTO 2018), and the long-term creep rupture limit specified by the Canadian Standards. A statistical analysis has been conducted to extrapolate a safe value of creep-rupture strength for conditioned and unconditioned GFRP bars. The extensive testing program devised for this project can provide detailed answers to many aspects of the creep-rupture problem of GFRP bars.

In Phase II, with the aim of increasing the serviceability limit state, the specimens in this study were loaded to 40% of the ultimate tensile strength of their GFRP bars and while exposed to harsh natural environmental conditioning for 10 years. This level of sustained stress is almost twice the threshold allowed in CSA S806 (CSA 2012), CSA S6 (CSA 2019), and ACI 440.1R (ACI 2015). It should be noted that the design codes tend to restrict GFRP bar capacity based on guaranteed tensile strength, but the sustained load applied in this study was a proportion (40%) of the ultimate tensile strength. A sustained load equal to 40% of the ultimate tensile strength is equivalent to 47% of the guaranteed tensile strength. Thus, the actual sustained stress level is 1.9 times higher than the allowable stress level for GFRP bars in CSA S806 (CSA 2012), CSA S6 (CSA 2019), and 2.4 times higher than threshold specified in ACI 440.1R (ACI 2015).

In order to achieve the objectives of this phase, two sets of tests were carried out: (1) destructive testing in which the structural flexural behavior of the beams up to failure point was evaluated using a four point bending setup, and (2) non-destructive testing in which physiochemical changes in the GFRP bar properties due to the likelihood of degradation were examined on the microstructural scale. The specimens were eventually loaded to

failure, offering an advantage over field studies which are normally carried out with non-destructive techniques.

The data obtained from the experiments were then used for analytical purposes and are discussed in terms of flexural responses of the GFRP RC beams before and after exposure to environmental conditions. Moreover, the accuracy of the existing provisions and models in the codes were verified based on the properties of the degraded GFRP bars. The outcomes can provide a detailed understanding on the durability performance of GFRP RC beams, and crucial information on increasing the serviceability limit state thresholds specified in design guidelines.

1.4. Outline of the Dissertation

This dissertation consists of five chapters; the following is a brief description of each chapter's content:

- Chapter 1 defines the problem, presents the main objectives, the motivations of the research, and provides an outline of the thesis with a brief description of each chapter.
- Chapter 2 presents a review of literature on relevant work related to durability of GFRP bars. The review includes the creep and flexural behaviour of GFRP bars and covers the available field studies and in-lab research projects.
- Chapter 3 presents the first paper in this dissertation entitled "Assessment of Creep Rupture Strength and Long-Term Performance of GFRP bars Subjected to Different Environmental Exposures under High-Sustained Loads". This chapter provides an investigation of design creep strength and environmental coefficient factor of GFRP

bars through performing creep testing on 160 bar specimens exposed to: a) normal laboratory conditions, b) immersed in alkaline solution with normal laboratory conditions at 23˚C, and c) immersed in alkaline solution with elevated temperature of 60˚C. A sustained load ranging from 40% to 90% UTS was applied on the specimens. The effect of conditioning and sustained load on creep strength investigated individually. A reliable design creep strength value was derived from test data and the results were compared with the current design codes limits.

- Chapter 4 presents the second paper in this dissertation entitled "Performance of GFRP-Reinforced Concrete Beams Subjected to High Sustained Load and Natural Aging for 10 Years". This chapter investigates the flexural behavior of eight RC beams (four unconditioned and four conditioned beams) constructed using early generation of GFRP bars. The beams were exposed to the combined effect of natural environmental conditioning and high sustained bending stress (40% of the ultimate tensile strength of the GFRP bars) for 10 years. Destructive and non-destructive testing were performed on the bar properties and the likelihood of degradation was investigated.

- Chapter 5 presents the summary, conclusions based on the test results, and recommendation for future research work.

CHAPTER 2 LITERATURE REVIEW

2.1. General

This chapter mainly reviews previous relevant studies into the durability of GFRP bars exposed to different environmental conditions and sustained load. The present durability study is mainly focused on the creep rupture behaviour of GFRP bars and the flexural behaviour of the beams reinforced with GFRP bars. The review attempts to address the degradation mechanisms, the effective parameters in the degradation process, most vulnerable areas of the bars against chemical attacks. The degradative effect of sustained load and conditioning is discussed individually and together. Furthermore, this chapter covers previous filed studies and laboratory-based studies also elaborates the difference between exposure to aggressive laboratory conditions and natural weathering. Design provisions of GFRP bars codes and guidelines are also presented in respect with creep rupture serviceability limit state and environmental coefficient factor in this chapter.

It is known that the long-term behavior of steel bars in corrosive environment is always accompanied by ruinous problems. This deteriorating effect of corrosion on steel would reduce the stiffness and strength of concrete structures (Wang et al. 2012). Undoubtedly, degradation of reinforcing bars entails massive repair and maintenance costs. For this reason, seeking possible alternatives for reinforcement of concrete structures appears to be a legitimate thought. Various solutions have been investigated so for, including galvanized

coating, electro-static-spray fusion bonded (powder resin) coating, polymer-impregnated concrete, epoxy coatings, alloyed steel bars, and glass FRP reinforcing bars [ACI440.1R (ACI 2015)].

Investigations on applicability of GFRP reinforcing bars in the field of civil engineering dates back to 1950s (ISIS Canada, 2007). However, they were not commercially available up until late 1970s. Corrosion-resistant feature of GFRP bars along with other advantages such as high-strength to weight ratio, electrically non-conductivity, transparency to the magnetic fields and radio frequencies, etc. have increased applicability of this material in construction industry [ACI440.1R (ACI 2015)]. Consequently, in the past decades, the studies investigating internally used FRP reinforcement have been noticeably boosted in the literature.

Today, the GFRP bars are broadly used in constructions subjected to aggressive media due to its low-cost manufacturing and can withstand better than steel bars when exposed to the combination of humidity, high temperature, and chloride. This condition is common in marine structures, bridges, and parking garages and wherever de-icing slat and chloride ions are in abundance. This environment reduces alkalinity of concrete, and leads to degradation of embedded steel bars, and this, in turn, results in concrete deterioration and overall stiffness reduction of the structure [ACI440.1R (ACI 2015)].

Past research attempts (Benmokrane et al. 2002a; Tobbi et al. 2012) to understand the applicability of GFRP bars in structures have revealed many important facts about their inherent features. Today, the short-term behavior of this structural material (features such as stiffness, bending strength, axial behavior, shear strength, bonding, and so forth) are almost

well known. Nonetheless, the long-term performance of GFRP bars still requires more research [ACI440.1R (ACI 2015)]. Particularly, their behavior under the combined effect of natural weathering and sustained stresses has received scant attention in the literature. The related durability problems of GFRP bars are commonly addressed by either laboratory accelerated aging studies (Ali et al. 2018; Park et al. 2014) or field investigations (Mufti et al. 2007; Gooranorimi and Nanni 2017; Benmokrane et al. 2018).

Despite three decades of extensive research on GFRP bars, still the subject requires supportive data and detailed studies. The everyday technological advances require the standards and the engineers to get updated with the-state-of-the-art. The variety of manufacturers, manufacturing techniques, different combination of constituent materials, sizing, shape and surface coating, fiber content, etc. are the parameters that play role in the quality of the final production. Therefore, more research is required to reach universal unity.

2.2. Creep

Creep is a time-dependent deformation that terminates in rupture when accumulated creep strains result in a deformation exceeding the design limits. Creep rupture takes place for all structural materials; however, with different intensity based on the material properties. GFRP bars experience considerable time-dependent deformation when subjected to a sustained load [ACI440.1R (ACI 2015)]. Researchers indicated that a sustained load corresponding to 40% of the Ultimate Tensile Strength (UTS) would cause a creep strain on GFRP bars of 10% from the initial tensile strain for 950 days of endurance time (Can et al.

2017). At relatively higher sustained load levels, the creep elongation is accompanied by cumulative creep failure.

The early generations of GFRP bars showed 45% UTS creep strength at an extrapolated 50-year endurance time (Renaud and Greenwood 2000; Seki et al. 1997; Yamaguchi et al. 1997). However, due to insufficient material information and lack of standard test methods, the creep-rupture stress level of internal GFRP reinforcement at serviceability is strictly limited by design codes and guides [ACI440.1R (ACI 2015); CSA S806 (CSA 2012)]. Today, standard testing methods are available to the form of material specifications issued by ASTM. The requirements of ASTM D7337 (ASTM 2019) provide detailed instructions in respect with creep testing procedures.

In a more recent study, Benmokrane et al. (2019) evaluated the creep rupture strength of a collected database of 204 creep-rupture tests conducted following the requirements of ASTM D7337 (ASTM 2019). The authors extrapolated a creep-rupture strength at 10^6 h (114 years) of 50.7% of the average UTS. Similar results were also shown by Weber (2005) for GFRP bars with three different bars sizes of 8, 16, and 25 mm. Rossini et al. (2019) performed a refined analysis to creep-rupture data handling of two types of GFRP bars (with 13 mm diameter) and predicted a safe value for design purposes of more than 39% UTS. However, all these studies were conducted on unconditioned GFRP bars, while the presence of sufficiently adverse environmental conditions such as high temperature and high alkalinity could adversely decrease creep rupture endurance time of GFRP bars [ACI440.1R (ACI 2015)].

Very limited studies addressed the effect of environmental conditions on the creep rupture behavior of GFRP bars. Renaud and Greenwood (2000) examined the creep rupture performance of small-sized GFRP bars (6.35 mm diameter) exposed to several environments at ambient temperature and elevated temperature of 60°C. The early generation of GFRP bars resulted in a 50-years average creep rupture strength of 45.9% UTS for the reference sample, reduced to 24% and 18.8% when conditioned in cement extract (pH = 12.6) at ambient temperature and 60°C, respectively. In a more recent study, Keller et al. (2017) investigated the creep rupture strength of GFRP bars with size #5 exposed to moist concrete (pH > 13.0) at 60°C and extrapolated an average 10^6-h creep rupture strength of 29.7% UTS.

2.3. Aggressive environmental conditions

Despite exhibiting good corrosion resistance, long-term exposure of GFRP bars to aggressive environments could reduce their creep strength (Dejke and Tepfers 2001; Shi et al. 2017). Davalos et al. (2012) studied the behavior of GFRP bars with E-glass and vinyl ester resin embedded in a saturated concrete at 10°C and subjected to low levels of sustained loading (corresponding to 1100-1300 με - tensile strain). The findings showed that the GFRP bars could maintain 38% of their tensile strength after 50 years. Robert and Benmokrane (2013) investigated the behaviour of GFRP bars embedded in concrete designed to simulate the alkaline environment of saturated concrete. Different exposure temperatures were implemented, moderate temperature of 23°C, 40°C, and 50°C, and warm, humid application environment of 70°C. The authors predicted a long-term tensile strength retention of GFRP bars of 77% for mean annual temperature of 10°C. Similar results were also reported by Ali et al, (2018) when aging GFRP bare bars in an alkaline solution for 1000, 3000, and 5000

hours at different elevated temperature of 22°C, 40°C, and 60°C. Benmokrane et al. (2020) predicted tensile-strength retention equal to 85% UTS after 100 years for GFRP bars with vinyl ester resin subjected to an alkaline solution at 10°C. These discrepancies make design codes take conservative measures in defining safety factors for GFRP RC structures exposed to different environmental conditions.

It should be noted that the most significant deterioration of GFRP rebars as reported by many researchers was caused by the alkaline environment (Chen el al. 2006, Al-Salloum et al. 2013, D'Antino et al. 2018, Manalo et al. 2020). The alkaline solution could damage glass fibres. The ingression of alkaline solution can also degrade the fibre/matrix interface, reducing the stress transfer between fibres and consequently reducing the tensile strength. Nevertheless, the laboratory conditioning could be too severe and exposing GFRP bars to a high alkaline solution at high temperatures would not accurately represent real-life scenarios. Studies on the durability of GFRP bars exposed to natural environment (Mufti et al. 2007, Gooranorimi and Nanni 2017, Benmokrane et al. 2018) reported no degradation of GFRP bars after up to 15 years in service.

2.3.1. Degradation Mechanism in GFRP Bars

The internal concrete environment has high alkalinity and moisture. Depending on the type of cement and the design mixture used for concrete, pH level within concrete varies between 10.5 and 13.5 (neglecting the effect of carbonation). This alkalinity is a result of moisture uptake and hydration process in concrete, which causes growth of hydration products (mainly Ca $(OH)_2$) in the pore fluids. This moist alkaline environment of concrete together

with the sustained stresses applied during in-service conditions, are the major threats of durability performance of GFRP bars.

The degradation can begin at any of three major components of GFRP bars: a) fibers; b) matrix and; c) the fiber/matrix interface. Depend on different combination of constituent materials (fiber, resin, sizing chemistry, additives and fillers) different mechanisms of degradation might occur. The items discussed below elaborate more on the possible degradation scenarios of FRP bars (Dong et al. 2017).

2.3.1.1. **Resin**

Vinyl ester resin matrix is prone to degradation by hydrolysis when hydroxyl ions (OH^-)/water, present in concrete pore solution, diffuse inside. Water molecules act as a plasticizer, resulting a swelling stress, which in turn can cause matrix cracking and fiber/matrix de-bonding. That is why it is important to use fully cured resins in GFRP reinforcing bars, as they contain less voids, holes, cracks and imperfections compared to under-cured resins. Therefore, fully cured resins more efficiently can protect the fibers from penetration of hydroxyl ions. Vinyl-ester and epoxy resins have shown low permeability and high resistance to alkaline attack and are quite tough in resisting micro-crack development. On the contrary, polyester resins are not recommended at all for this purpose.

2.3.1.2. **Fiber**

The fibers damage occurs due to chemical attack on the glass fibers by the alkaline environment (Yilmaz 1992). The diffusion of alkali ions in fiber structure cause leaching of Si and Na from fiber and dissolution of these atoms. This chemical reaction occurs due to

the breaking of Si-O-Si structure by hydroxyl ions (Eq. 1). In other words, the ingress of water hydrolyzes Si-0-Si bonds and is accompanied by inward diffusion of Ca ions arising from the cement, while sodium and silicon from the fiber migrate outward into the adjacent concrete paste. This phenomenon can be also observed by scanning electron microscopy (SEM) photomicrograph in two general forms: a) the formation of a thin layer (shell) around the fibers, known as “etching” (see Fig. 2-1); b) the formation of pits or notches on the surface of fibers (see Fig. 2-2). The consequence of degradation on fibers would be reduced flexibility, and deteriorated mechanical properties (Yilmaz et al. 1991).

$$\equiv \mathrm{Si} - \mathrm{O} - \mathrm{Si} \equiv + \mathrm{OH}^- \rightarrow \mathrm{Si} - \mathrm{OH} \quad + \quad \mathrm{O}^- - \mathrm{Si} \equiv \qquad (1)$$

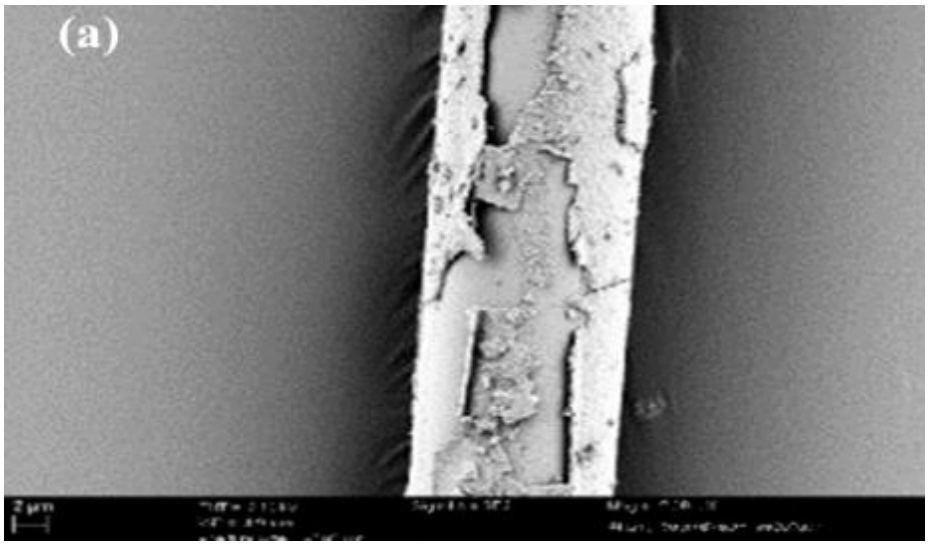

Fig. 2-1 A thin layer formed around the fiber - "etching phenomenon"(Yilmaz 1992)

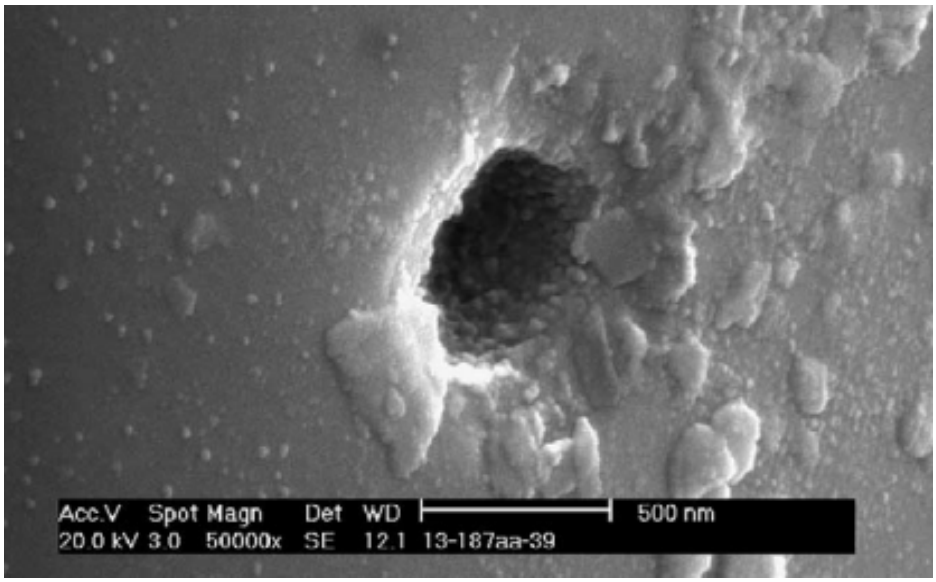

Fig. 2-2 Small pits appear on the surface of fiber as a result of corrosive reaction and out-migration of silicon atoms from fiber structure (Helbling et al. 2006)

2.3.1.3. Fiber/Matrix Interface

Fiber/matrix interface is the weakest link in the system can be degraded easily. Numerous studies on degradation mechanism of FRP bars, all agree that the bond between fiber and resin is the most critical and vulnerable region to corrosion. Any damage in this area reduces the tensile strength of the FRP bar (Davalos et al. 2012), because the load transfer from matrix to fibers would not function properly.

It is also worth mentioning that for the bars embedded in concrete, the interface of concrete and the FRP bar also matters and should be considered as a potential degradation region.

Based on three degradation mechanisms discussed above, it can be concluded that improving the permeability features of the resin as well as improving the hydrolytic stability of the fiber/ matrix interface, can improve the durability of FRP bar (Davalos et al. 2012).

2.3.2. The Synergic Effect of Sustained Load and Aggressive Environment

Benmokrane et al. (2002) investigated corrosion of GFRP bars embedded in moist concrete under different stress levels. Based on this research three types of corrosion mechanisms had been identified: 1-diffusion dominated corrosion, 2-crack-propogation-dominated corrosion, 3-stress dominated corrosion. This study tends to divide sustained stress into three separate levels: a) low stress levels (perhaps below 20% of ultimate tensile load), b) moderate stress level (e.g. 20% to 40%) c) high stress levels (above 40%). According to this classification the corrosion condition of fiber/matrix interface of GFRP bars embedded in moist concrete under different stress levels falls under each of these categories. For the stress levels below 20% resin, the stress is not sufficient to expand the voids and the micro-cracks of the matrix, so no direct attack on the interface takes place. In other words, the hydroxyl ions are only able to penetrate to the fiber/matrix interface by diffusion. For the moderate stress levels (20-40%), the stress is able to extend and expand the micro-cracks and voids of the resin. The more stress is applied the more micro-cracks appear in the resin. This allows alkaline environment of concrete attack the fiber/matrix interface directly. The degree of crack propagation is a critical factor for the residual tensile strength. Therefore, this phase is named crack-propagation-dominated stage. At last, for the stress levels above 40%, creep characteristics of the GFRP bars brings the bars to rupture after a period of time even without contact with corrosive medium. However, the alkaline environment shortens the time needed for the bar failure. It should be noted that the findings of Benmokrane et al. (2002) attributed to earlier generations of GFRP bars and should not be taken valid for the newer generations.

The synergetic effect of sustained load and moisture is shown in Fig. 2-3. The figure points out accelerating effect of sustained stress on corrosion. Sustained load widens the micro-cracks and the voids of resin matrix, and this allows easier penetration of the hydroxyls to the resin matrix. Consequently, accelerates erosion of the fibers/ matrix bond. Fig. 2-4 refers to the schematic correlation between applied stress/conditions and time-to-failure for GFRP bars in general.

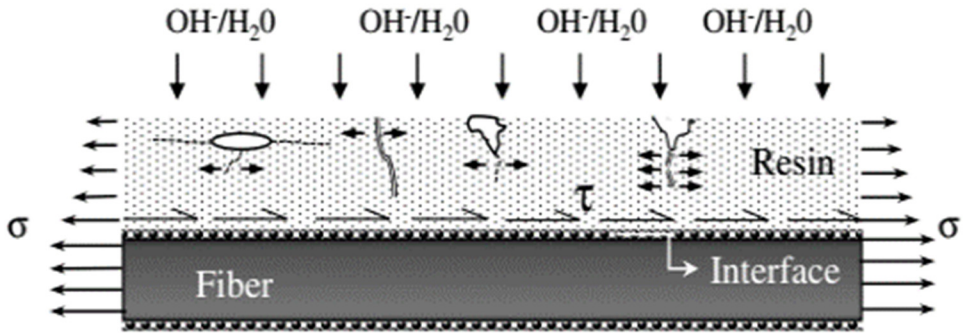

Fig. 2-3 Coupled effect of sustained load and moisture absorption (Wu et al. 2014)

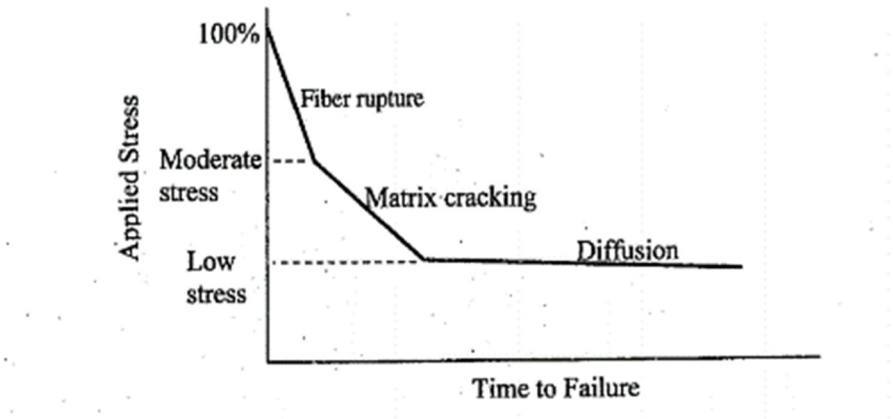

Fig. 2-4 Effect of applied stress and failure mechanism on time-to-failure (schematically) (Nkurunziza et al. 2005)

2.3.3. Accelerated Aging Tests of GFRP Bars

Accelerated aging tests have been widely used in durability studies due to their simplicity in establishing the life span of the GFRP bars. In this method, the alkaline solutions represent concrete pore water and the elevated temperature yields accelerated aging. He et al. (2017) conducted accelerated durability tests on GFRP reinforcement embedded in concrete beams. The bars were extracted from the beams immersed in alkaline solution at 60°C and subjected to sustained loads (20% and 40% of ultimate bending strength). After 18 months exposure to alkaline solution, the bars retained tensile strength of about 80% and 75% for the bars subjected to sustained loads of less than 20% and 40% of ultimate bending strength, respectively. Debonding of glass fibers and matrix has also been reported for GFRP bars under a sustained load equal to 40% of their ultimate bending strength. At the same time, no significant evidence of degradation was observed for sustained flexural loads of less than 20% of bar ultimate bending moment. Moreover, the authors stated that the degree of degradation could be more pronounced at the interface of the glass fibers and resin matrix. Ali et al. (2018) predicted tensile-strength retention of 85% and 75% after 200 years for GFRP bars with vinyl ester resin subjected to an alkaline solution at 10°C and 30°C, respectively. Park et al. (2014) studied the flexural behavior of 36 beams reinforced with either GFRP or steel bars subjected to the combined effect of sustained load and accelerated-aging conditions (i.e., 47°C and 80% relative humidity) for 300 days. Their experimental outcomes indicated different rates of degradation for different types of GFRP bars under artificial aggressive environments. The studies confirmed, however, that one advantage of

using GFRP bars in concrete is that they are not subjected to corrosion unlike the conventional steel reinforcement.

In contrast, some contradictory outcomes have also been reported based on the findings of accelerated tests conducted on GFRP RC structures. For instance, Davalos et al. (2012) studied the behavior of GFRP bars with E-glass and vinyl ester resin embedded in a saturated concrete at 10°C and subjected to relatively low levels of sustained loading (1100-1300 με - tensile strain). They indicated that the GFRP bars could maintain 38% of their tensile strength after 50 years. This would lead to the conclusion that GFRP bars should not be used in concrete. This paradox might be due to the variety of constituent materials in GFRP bars and the available processing techniques. These uncertainties; however, have a massive influence on the safety margin of the design process forcing engineers to adopt high safety factors for GFRP RC structures exposed to different environmental conditions.

2.3.4. Performance of GFRP Bars Under Natural Aging

Unlike accelerated-aging tests, natural aging is a very slow process as the properties of GFRP reinforcement are less affected by natural weathering than accelerated-aging conditions (Bakis et al. 2005; Micelli and Nanni 2004; Mufti et al. 2007; Gooranorimi and Nanni 2017; Benmokrane et al. 2018). Since the results obtained from the natural weathering conditions are more realistic and reliable than that from accelerated aging tests, conducting field studies is crucial to validate design code provisions. In an attempt, Trejo et al. (2011) studied 160 actual field-conditioned GFRP bars embedded in unsaturated cracked concrete for seven years to evaluate the effects of environmental degradation. Their results indicated lower rates

of strength deterioration compared to data available for the accelerated exposure. No sustained load was imposed on the bars, however, over seven years of exposure. In another study, Gooranorimi and Nanni (2017) performed a field study to evaluate the long-term durability conditions of GFRP bars in a 15-year old bridge (Sierra de la Cruz Bridge in Texas, USA). The durability of the GFRP bars embedded in the concrete deck and exposed to the natural environmental conditions was evaluated through a series of microstructural tests. The test results showed that the GFRP bars were in good condition even after 15 years. Nonetheless, due to limitation in obtaining data for the control specimens, the results of interlaminar shear tests were inconclusive.

Mukherjee and Arwikar (2005, 2006) conducted a comprehensive study comparing the performance of GFRP bars under accelerated aging and natural weathering in a tropical environment. The specimens for the accelerated aging test were immersed in tanks containing water at 60°C for 3, 6, and 12 months.The conditioning time of the naturally aged specimens was 18 or 30 months. In addition, 50% of the ultimate load was imposed on the beams as a sustained load. The outcomes were discussed on the structural (Mukherjee and Arwikar 2006), and microstructural (Mukherjee and Arwikar 2005) scales. Failure of the control beams was associated with the design-intended flexural-compression mode. On the other hand, the conditioned beams failed with reinforcement rupture and withstood higher loads. The tests on constituent materials showed that the concrete gained substantial strength due to conditioning in the tank at 60°C. The testing of reinforcing bars taken from the conditioned beams also revealed that the bars experienced strength drops of about 42%, 56%, and 65% with 3, 6, and 12 months of accelerated aging, respectively. Even given natural weathering, strength reductions of about 35% and 39% were observed after 18 and

30 months, respectively. The increase in concrete strength and decrease in reinforcing-bar strength shifted the failure mode from concrete crushing to reinforcement rupture. Moreover, although the resin matrix was made of vinyl ester, the extrapolated life span showed that the GFRP bars would lose 65% of their strength over a service life of 32 years. The microstructural observations also verified the degradation. The authors stated, however, that the SEM analysis points to bubbles and microcracks in the matrix that could have formed during the manufacturing process. Bubbles and microcracks facilitate the diffusion of moisture and alkaline solution.

He et al. (2013) conducted a durability investigation on E-glass reinforced vinyl-ester bars. The bars were conditioned in concrete beams for three years. During conditioning, the specimens were subjected to a sustained load equal to 11% of the ultimate tensile strength of the GFRP bars combined with different environments, including ambient indoor laboratory, natural outdoor weathering in central Pennsylvania, a high alkaline aqueous solution at 60°C, and alternating 17°C dry freeze and room-temperature water immersion. Based on the results, the tensile strength decreased by 28% for the artificially aggressive environments, while it remained unchanged for the indoor and outdoor conditioning. An extrapolation to 50 years predicted a residual strength of 50% of the ultimate strength for the former condition.

2.3.5. Micro-Structural and Physicochemical Analyses

Microstructural and physicochemical analyses, or so called “non-destructive tests”, are widely used in durability studies nowadays. They can provide invaluable information for

engineers and manufacturers. Microstructural tests such as Scanning Electron Microscopy (SEM), fiber volume content, water absorption, penetration, Fourier Transform Infrared Spectroscopy (FTIR), Xray test (XRF), Differential Scanning Calorimetry (DSC) and so on are useful in evaluating the long-term performance. These testing techniques are essential part of quality control/assurance process of FRP rod production lines, and are of high importance for the industrial manufacturers (Benmokrane et al. 2002).

2.3.6. Design Code Provisions

ACI440.1R (ACI 2015) and AASHTO LRFD (AASHTO 2018) require that material properties provided by FRP manufactures be considered as raw properties that do not include the deteriorating effect of long-term environmental exposure. The specification requires using environmental reduction factors (C_E) to reduce the material properties used in design equations, based on the type and level of environmental exposure. The C_E factor for GFRP reinforced concrete components not exposed to earth and weather suggested by ACI440.1R (ACI 2015) is 0.8 and for the members exposed to earth and weather is 0.7. According to the concept of environmental reduction factor, the design creep strength, F_c^*, defined by ACI440.1R (ACI 2015) and AASHTO LRFD (AASHTO 2018) should be determined as

$$F_c^* = C_c . C_E . F_u^*$$

where F_u^* is guaranteed ultimate tensile strength of GFRP bars and C_c is the creep knock-down factor (Rossini et al. 2019). The current edition of ACI440.1R (ACI 2015) specifies a creep rupture reduction factor equals to 0.2, leading to a creep-rupture tensile strength

corresponding to 0.16 or 0.14 of F_u^* for elements not exposed or exposed to earth and weather, respectively. The second edition of AASHTO LRFD (AASHTO 2018), however, relaxed creep rupture reduction factor to 0.3 benefiting from the adoption of the standardized creep rupture test method, and the recent advancements in GFRP manufacturing process and material constituents. However, by using the environmental reduction factor accompanied with C_c, the creep-rutpure tensile strength is reduced to 0.24 or 0.21 for elements not exposed or exposed to earth and weather, respectively.

Canadian Standards are pursuing a different strategy in this respect [CSA S806 (CSA 2012); CSA S6 (CSA 2019)]. Canadian design code uses resistance factor ϕ_f to account for uncertainties of material (including but not limited to environment-induced effects). In other words, CSA S806 (CSA 2012) and CSA S6 (CSA 2019) recommend resistance factors, ϕ_f, equal to 0.75 and 0.65, respectively, for internally reinforced FRP structures where the effect of environment is taken in this coefficient. However, the resistance factors do not apply to serviceability limit states such as creep.

CHAPTER 3 ASSESSMENT OF CREEP RUPTURE AND LONG-TERM PERFORMANCE OF GFRP BARS SUBJECTED TO DIFFERENT ENVIRONMENTAL EXPOSURE CONDITIONS UNDER HIGH SUSTAINED LOADS

Authors and affiliations:

Yasin Esmaeili,[1] Khaled Mohamed,[2] John Newhook,[3] Brahim Benmokrane[4*]

[1]PhD candidate, Department of Civil Engineering, University of Sherbrooke, Sherbrooke, QC, Canada, J1K 2R1, E-mail: Yasin.Esmaeili.Hesar@usherbrooke.ca

[2]Postdoctoral Fellow, Department of Civil Engineering, University of Sherbrooke, Sherbrooke, QC, Canada, J1K 2R1, E-mail: Khaled.Mohamed@usherbrooke.ca

[3]Professor, Faculty of Engineering, Dalhousie University, Sexton Campus, Halifax, NS, Canada, B3H 4R2, E-mail: John.Newhook@dal.ca

[4]Professor of Civil Engineering, Tier-1 Canada Research Chair of Advanced Composite Materials for Civil Structures and Senior NSERC Research Chair in Innovative FRP Reinforcement for Sustainable Concrete Infrastructure, Department of Civil Engineering, University of Sherbrooke, Sherbrooke, QC, Canada, J1K 2R1, Phone: (819) 571-6923; E-mail: Brahim.Benmokrane@usherbrooke.ca **([*]Corresponding Author)**

Journal Title and Paper Status:

Submitted to Journal of Construction and Building Materials in January 02, 2021.

Contribution to the Thesis:

The long-term creep rupture strength of GFRP bars is well known to be affected by environmental exposure, such as concrete alkalinity and earth or weather. However, no investigation has reported such an effect. Consequently, code provisions conservatively assumed a long-term reduction of the GFRP bars creep rupture strength based on the committee consensus, and recommended future research to assess the stipulated reductions. The current study assesses and quantifies the effect of creep rupture strength of GFRP bars exposed to the alkaline solution at ambient and elevated temperature.

Abstract

This paper presents an experimental investigation and statistical approach to assess the long-term performance and to determine a safe creep-rupture strength value for glass fiber-reinforced polymer (GFRP) bars subjected to different types of environmental exposure. The study sample consisted of 160 bars of various sizes (10 mm, 12 mm, and two types of 15 mm) subjected to different levels of environmental conditioning (unconditioned and exposed to an alkaline solution at 23°C and 60°C) and a range of sustained load levels (40% to 90% of the ultimate tensile strength). The test results were analyzed with Weibull statistical analysis to determine the mean and characteristic creep-rupture strengths, and consequently, a safe design value was calculated. Limitations and variations of the strength degradation model for the life-span prediction are discussed. The impact of sustained load on strength reduction was more pronounced than the combined effect of the alkaline solution and high

temperature. The GFRP bars with smaller diameters were more susceptible to creep rupture than the larger ones, while the conditioning had more effect on the bars with larger diameters than the smaller ones. The creep-rupture reduction factors prescribed in current design codes are conservative for the GFRP bars in this study.

Author keywords: Creep-rupture strength; GFRP bar; durability; environmental conditioning; sustained load; environmental reduction factor; design codes.

3.1. Introduction

Creep is a time-dependent deformation that terminates in rupture when the accumulated creep strains result in deformation exceeding the design limits. Creep rupture occurs in all structural materials, although the intensity varies according to material properties. Glass fiber-reinforced polymer (GFRP) bars experience considerable time-dependent deformation when subjected to sustained load (ACI 440.1R [ACI 2015]). Researchers have indicated that a sustained load corresponding to 40% of the ultimate tensile strength (UTS) would cause 10% creep strain in GFRP bars from the initial tensile strain for 950 days of endurance time (Can et al. 2017). At relatively higher sustained load levels, creep elongation is accompanied by cumulative creep failure.

The early generations of GFRP bars showed 45% UTS creep strength at an extrapolated 50-year endurance time (Greenwood 2002, Seki et al. 1997, Yamaguchi et al. 1997). Due to insufficient material information and lack of standard test methods, however, the creep-rupture stress level of internal GFRP reinforcement at serviceability is strictly limited by design codes and guides (ACI 440.1R [ACI 2015], CSA S806 [CSA 2012]). Today, standard

testing methods are available in the form of material specifications issued by ASTM. The requirements of ASTM D7337 (ASTM 2019) provide detailed instructions with respect to creep testing procedures.

In a more recent study, Benmokrane et al. (2019) evaluated the creep-rupture strength of a collected database of 204 creep-rupture tests conducted according to the requirements of ASTM D7337 (ASTM 2019). The authors extrapolated a creep-rupture strength of 50.7% of the average UTS at 106 h (114 years). Weber (2005) presented similar results for GFRP bars of three different sizes (8, 16, and 25 mm). Rossini et al. (2019) performed a refined analysis of creep-rupture data for two types of GFRP bars (13 mm in diameter) and predicted a safe value for design purposes of more than 39% UTS. All these studies, however, were conducted on unconditioned GFRP bars, while the presence of sufficiently adverse environmental conditions—such as high temperature and high alkalinity—could irreversibly decrease the creep-rupture endurance time of GFRP bars (ACI 440.1R [ACI 2015]).

Very limited studies have addressed the effect of environmental conditions on the creep-rupture behavior of GFRP bars. Renaud and Greenwood (2005) examined the creep-rupture performance of small GFRP bars (6.35 mm in diameter) exposed to several environments at ambient temperature and a high temperature of 60°C. This early generation of GFRP bars had a 50-year average creep-rupture strength of 45.9% UTS for the reference sample, which decreased to 24% and 18.8% when conditioned in cement extract (pH = 12.6) at ambient temperature and 60°C, respectively. In a more recent study, Keller et al. (2017) investigated the creep-rupture strength of #5 GFRP bars exposed to moist concrete (pH > 13.0) at 60°C and extrapolated an average 10^6-h creep-rupture strength of 29.7% UTS.

To account for the effect of environmental exposure on the creep-rupture strength of GFRP, ACI 440.1R (ACI 2015) and AASHTO LRFD (AASHTO 2018) require that the design-creep strength be multiplied by an environmental reduction factor (C_E) to reduce the material properties used in design equations, based on the type and level of environmental exposure. The C_E factor for GFRP-reinforced concrete components not exposed to earth and weather suggested by ACI 440.1R (ACI 2015) and AASHTO LRFD (AASHTO 2018) is 0.8; the value for members exposed to earth and weather is 0.7. Canadian standards are pursuing a different strategy in this respect (CSA S806 [CSA 2012], CSA S6 [CSA 2019]). The Canadian design code uses a resistance factor φ_f to account for material uncertainties (including but not limited to environmentally induced effects). These resistance factors do not, however, apply to serviceability limit states such as creep.

In this study, a total of 160 GFRP bars were tested for creep strength of various bar sizes and types under different conditioning types and a wide range of imposed sustained stress levels. The stress levels were defined by testing another 20 GFRP bars of the same types and sizes for longitudinal tensile properties. Few studies have been investigated the effect of creep rupture under harsh environmental exposure conditions on the long-term behavior of GFRP bars. The objective of this study was to assess the creep-rupture strength of GFRP bars subjected to severe environmental exposure throughout a comprehensive experimental investigation. A statistical analysis was conducted to extrapolate a safe value of creep-rupture strength for the conditioned and unconditioned GFRP bars. The extensive testing program devised for this project can provide detailed answers to many aspects of the creep-rupture problem of GFRP bars.

3.2. Experimental Investigation

3.2.1. Material Properties

The creep rupture test specimens included three different bar sizes #3, #4 and #5 (diameters of 10 mm, 13 mm, and 16 mm, respectively). Two types of #5 GFRP bars were used in this study with different constituent materials and fiber contents. Type A was sand coated with a helically wrapped surface, while Type B was helically grooved, as shown in Fig. 3-1. On the other hand, the #3 and #4 GFRP bars had a smooth surface. The bars were manufactured according to a pultrusion process and were comprised of vinyl-ester resin and E-CR glass fibers meeting the requirements of ASTM D578 (ASTM 2018). The physical and mechanical properties of the specimens and the pertained testing method are presented in Table 3-1. The properties in Table 3-1 were measured for five different replicates cut from the bars based on the test requirement. Generally, the physical and mechanical properties of the GFRP bars were following the requirements of ASTM D7957 (ASTM 2017) and CSA S807 (CSA 2019b) specifications. Table 3-1 shows that the GFRP had various tensile strength and modulus, ranging between 1123-1670 MPa and 51-69.2 GPa, respectively.

Fig. 3-1. GFRP bars used for creep rupture tests.

Table 3-1. Physical and mechanical properties of the specimens.

Property	Bar #3	Bar #4	Bar #5A	Bar #5B	Standard
Nominal bar size (mm)	10	13	16	16	ASTM D7925 (ASTM 2017)
Nominal cross-sectional area (mm^2)	71	129	199	199	ASTM D7925 (ASTM 2017)
Actual cross-sectional area by immersion (mm^2)	78	141	214	207	ASTM D7205 (ASTM 2016)
Ultimate tensile strength (MPa)	1180±53	1679±51	1270±54	1123±58	ASTM D7205 (ASTM 2016)
Characteristic tensile strength (MPa)*	1118	1601	1212	1050	ASTM D7205 (ASTM 2016)
Guaranteed tensile strength (MPa)*	1067	1588	1164	991	ACI 440.1R (ACI 2015)
Modulus of elasticity (GPa)	54.5±0.6	69.2±4.7	59.6±3.7	51.0±1.6	ASTM D7205 (ASTM 2016)
Ultimate strain (%)	2.2±0.1	2.7±0.3	2.3±0.2	2.3±0.1	ASTM D7205 (ASTM 2016)
Fiber content by weight (%)	81	84	84	76	ASTM D3171 (ASTM 2015a) Method II Procedure G
Glass transition temperature (℃)	118	130	122	117	ASTM D3418 (ASTM 2015b)
Cure ratio (%)	95	98	100	99	CSA S807 (CSA 2019)
Moisture absorption at full saturation (%)	0.29	0.14	0.13	0.32	ASTM D570 (ASTM 2018b)

Note: Tensile properties were calculated based on the nominal cross-sectional area.

* The characteristic and guaranteed tensile strengths were calculated using normal distribution based on probability of 0.05% and 0.001%, respectively.

3.2.2. Testing scheme

The initial stage of the experimental program involved the tensile testing of the GFRP bars to determine their tensile properties. Five samples of each bar type were tested to estimate the average ultimate tensile strength (UTS) $F_{u,m}$, characteristic tensile strength $F_{u,k}$, guaranteed tensile strength F_u^*, and modulus of elasticity. Table 1 gives the tensile properties of the tested bars. Note that the nominal cross-sectional area of the bars was used in the pertinent calculation.

The ensuing step was to conduct creep-rupture tests using the test results obtained in the initial stage. The testing scheme was divided into three parts in terms of exposure conditions: (a) the first group (Group A) of experiments involved 70 bars bearing sustained load without environmental conditioning, (b) the second group (Group B) consisted of 60 bars subjected to sustained load and exposed to the alkaline solution at ambient temperature (23°C), and (c) the third group (Group C) was comprised of ٣٠ bars maintaining sustained load and exposed to the alkaline solution and a high temperature of 60°C. The imposed sustained load varied between 40% and 90% of the average UTS of the bars. Table 3-2 presents the details of the sustained load levels for each size and exposure medium. Five specimens were tested at each load level for each size and per each exposure conditioning.

The creep rupture testing scheme was prepared following the principles of ASTM D7337 (ASTM 2019). The purpose of the current study was to generate creep rupture data under different exposure conditions and using different sizes of GFRP bars. Therefore, stress levels in Table 3-2 were chosen to induce creep rupture failure, while only bars #3 were exposed

to lower sustained stress levels (40% UTS) to have run-out results as recommended by the ASTM D7337 (ASTM 2019). The chosen stress levels for GFRP exposed to the alkaline solution (Group B and C) were lower than that for Group A samples; consequently, the endurance time would be longer for Group B and C effect of alkaline environment exposure to take place.

Table 3-2. Load level and environmental conditioning of the tested GFRP for creep rupture

Group	Bar size	Loading level (% of UTS)	Exposure media	Temperature
A	#3	40, 60, 70, 80, and 90	-	Ambient temperature (23°C)
	#4	60, 70, and 90		
	#5-A	60, 80, and 90		
	#5-B	60, 80, and 90		
B	#3	50, 60, and 70	Alkaline solution (pH ≥ 12.5)	Ambient temperature (23°C)
	#4	40, 50 and 70		
	#5-A	40, 50, and 70		
	#5-B	40, 50, and 70		
C	#4	50, 60, and 70	Alkaline solution (pH ≥ 12.5)	High temperature (60°C)
	#5-A	40, ٥٠, and ٦٥		

3.2.3. Loading protocol and test setup

All the GFRP bars were cut into 1800 mm lengths for tensile testing and creep-rupture testing. Steel anchors were installed as specified in ASTM D7205 (ASTM 2016) with expansion grout, while the surfaces of the smooth bars were roughened The ends of the steel

anchors were threaded in order to anchor the specimen to the test frame with a nut, as shown in Fig. 3-2a. Fig. 3-2a also shows the dimensions of the tested specimens.

A customized loading system was developed for this study to ensure sustained loads on the GFRP bars, as shown in Fig. 3-2b. The loading frames were designed to withstand a sustained load of up to 500 kN. The loads were applied to the GFRP bars using a hollow hydraulic jack and were simultaneously monitored with a load cell connected to a data-acquisition system. Fig. 3-2c illustrates the sustained load application system. The jack was supported by a U-shaped steel assembly that, in turn, rested on the loading frames. After the desired load level was reached, nut 2 (see Fig. 3-2c) was tightened on the threaded bar rubbing against the reaction frame. The load on the hydraulic jack was then released. The loading system was calibrated by monitoring the evolution of stresses with an extensometer connected to a data-acquisition system (see Fig. 3-2d). The highest relaxation occurred during the first 15 to 20 min. Therefore, the loading was maintained with the hydraulic jack for 20 min to ensure a constant load on the GFRP bars. Additionally, loads were kept constant by periodically monitoring the load on the bar and adjusting the load level as necessary. The time to rupture was recorded for each loaded specimen.

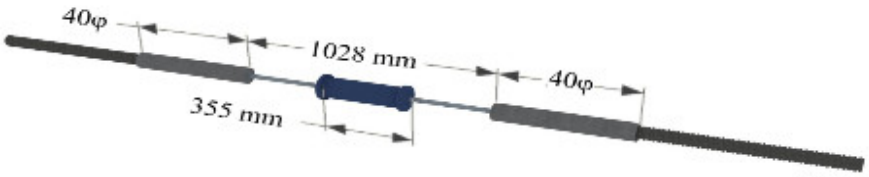

(a)

(b)

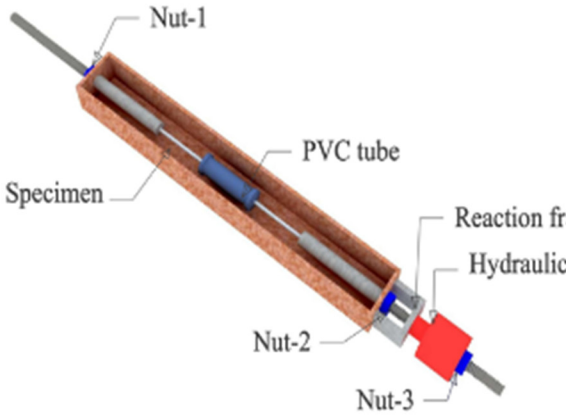

(c)

(d)

Fig. 3-2 .Loading and conditioning system used for Specimens: a) dimensions and overview of the GFRP specimens b) testing frame, c) device for sustained load application, d) readjustment of sustained load level, in an inspection session, using extensimeter and data acquisition system.

3.2.4. Conditioning

The middle part of the bars for Group B and C series was exposed to alkaline solution to simulate the high alkalinity of concrete pore solution. The alkaline solution was prepared using calcium hydroxide, potassium hydroxide, and sodium hydroxide (118.5 g of Ca(OH)2 + 0.9 g of NaOH + 4.2 g of KOH in 1 L of deionized water) according to ASTM D7705 (ASTM D7705 2019). The pH level of the solution was held constant at 12.8 and was controlled during the conditioning period to ensure the same pH level. The alkaline solution was injected into plastic tubes installed in the middle of the bars and measuring 75 mm in diameter and 355 mm in length (see Fig. 3-2a). For samples from Group C, the entire frame was placed in the temperature-controlled chamber at 60˚C throughout the aging duration.

The high temperature of 60°C has been used by many researchers for accelerated aging in order to perform durability studies in a reasonable amount time (Chen et al. 2006; Micelli and Nanni 2004). Robert et al. (2010) explained that high temperature would increase the reaction rate of alkalis, pH, and moisture diffusion across the resin/matrix interface. Robert et al. (2010) suggested a conditioning temperature of 60°C and it is used as accelerated aging for GFRP bars in ASTM D7705 (ASTM 2019) and CSA S807 (CSA 2019). The effect of a high temperature of 60°C for accelerated aging on the creep-rupture results was investigated in this study. Furthermore, this temperature was used in this study to assess the creep-rupture behavior of GFRP bars exposed to severe environmental conditions.

3.3. Test Results

The test results are presented individually for each GFRP bar. Table 3-3 shows the elapsed time under sustained loads for the creep tests for bars tested under standard laboratory conditions (Group A conditioning). Table 3-4 presents the data for the bars under sustained load and exposed to the alkaline solution at ambient temperature (23°C) (Group B conditioning). Table 3-5 gives the data of the bars under sustained load and exposed to the alkaline solution and high temperature (60°C) (Group C conditioning). Note that specimen labelling begins with the bar number (and, if applicable, the type, e.g. #5A), followed by the conditioning group (e.g., A for Group A), and ends with the number of the tested specimen. When the bar did not rupture at the time of data collection, the result was marked with a dagger to indicate the status of the specimen. In addition, of each bar type tested for creep, 5 bars were tested from the same lot number to determine the average, characteristic, and guaranteed tensile strength of the GFRP bars. The static tensile test performed on the bars according to ASTM D7205 (ASTM 2016), and the results of tensile tests are presented in Table 3-1.

Table 3-3. Creep rupture test results for bar exposed to conditioning Group A.

Specimen ID	Sustained load/UTS %	Time to failure (h)	Specimen ID	Sustained load/UTS %	Time to failure (h)
#3-A-1	90	0.025	#4-A-9	70	200.6
#3-A-2	90	0.03	#4-A-10	70	282.86
#3-A-3	90	0.032	#5A-A-1	90	0.01
#3-A-4	90	0.033	#5A-A-2	90	0.02
#3-A-5	90	0.082	#5A-A-3	90	0.03
#3-A-6	80	0.5	#5A-A-4	90	0.03
#3-A-7	80	0.517	#5A-A-5	90	0.04
#3-A-8	80	0.6	#5A-A-6	80	0.38
#3-A-9	80	0.683	#5A-A-7	80	0.39
#3-A-10	80	0.75	#5A-A-8	80	0.4
#3-A-11	70	46	#5A-A-9	80	0.4
#3-A-12	70	50.42	#5A-A-10	80	0.42
#3-A-13	70	69.33	#5A-A-11	60	2800.00
#3-A-14	70	92.13	#5A-A-12	60	3500.00
#3-A-15	70	115.53	#5A-A-13	60	4032.00
#3-A-16	60	3456	#5A-A-14	60	4500.00
#3-A-17	60	3816	#5A-A-15	60	4872.00
#3-A-18	60	6816	#5B-A-1	90	0.010
#3-A-19	60	7272	#5B-A-2	90	0.018
#3-A-20	60	10766	#5B-A-3	90	0.022
#3-A-21	40	24048 †	#5B-A-4	90	0.025
#3-A-22	40	24048†	#5B-A-5	90	0.030
#3-A-23	40	24048†	#5B-A-6	80	0.17
#3-A-24	40	24048†	#5B-A-7	80	0.2
#3-A-25	40	24048†	#5B-A-8	80	0.24
#4-A-1	90	0.03	#5B-A-9	80	0.37
#4-A-2	90	0.05	#5B-A-10	80	0.59
#4-A-3	90	0.05	#5B-A-11	60	2208.00
#4-A-4	90	0.06	#5B-A-12	60	3302.00
#4-A-5	90	0.07	#5B-A-13	60	4572.00
#4-A-6	70	86.23	#5B-A-14	60	5806.00
#4-A-7	70	90.29	#5B-A-15	60	7104.00
#4-A-8	70	135.98			

† runout test result.

Table 3-4. Creep rupture test results of bars exposed to conditioning Group B.

Specimen ID	Sustained load/UTS %	Time to failure (h)	Specimen ID	Sustained load/UTS %	Time to failure (h)
#3B-B-1	70	65.33	#5A-B-4	70	27
#3B-B-2	70	66.08	#5A-B-5	70	51.33
#3B-B-3	70	73.08	#5A-B-6	50	3504
#3B-B-4	70	78	#5A-B-7	50	3768
#3B-B-5	70	90	#5A-B-8	50	3960
#3B-B-6	60	3387	#5A-B-9	50	4920
#3B-B-7	60	4800	#5A-B-10	50	4920
#3B-B-8	60	4800	#5A-B-11	40	10728†
#3B-B-9	60	9648	#5A-B-12	40	10728†
#3B-B-10	60	9648	#5A-B-13	40	10728†
#3B-B-11	50	8356	#5A-B-14	40	10728†
#3B-B-12	50	9025	#5A-B-15	40	10728†
#3B-B-13	50	9816	#5B-B-1	70	52.50
#3B-B-14	50	10124	#5B-B-2	70	52.83
#3B-B-15	50	10546	#5B-B-3	70	55.33
#4B-B-1	70	60.5	#5B-B-4	70	55.83
#4B-B-2	70	73	#5B-B-5	70	59.50
#4B-B-3	70	77.33	#5B-B-6	50	7476
#4B-B-4	70	264	#5B-B-7	50	8024
#4B-B-5	70	456	#5B-B-8	50	10728†
#4B-B-6	50	3456	#5B-B-9	50	10728†
#4B-B-7	50	4008	#5B-B-10	50	10728†
#4B-B-8	50	4752	#5B-B-11	40	10728†
#4B-B-9	50	4920	#5B-B-12	40	10728†
#4B-B-10	50	6216	#5B-B-13	40	10728†
#5A-B-1	70	6.17	#5B-B-14	40	10728†
#5A-B-2	70	13.75	#5B-B-15	40	10728†
#5A-B-3	70	26.67			

† runout test result.

Table 3-5. Creep rupture test results of bars exposed to conditioning Group C

Specimen ID	Sustained load/UTS %	Time to failure (h)	Specimen ID	Sustained load/UTS %	Time to failure (h)
#4-C-1	70	36.4	#5A-C-1	60	47.5
#4-C-2	70	38.33	#5A-C-2	60	49.3
#4-C-3	70	48	#5A-C-3	60	50
#4-C-4	70	74	#5A-C-4	60	74
#4-C-5	70	76	#5A-C-5	60	76
#4-C-6	60	30	#5A-C-6	50	576
#4-C-7	60	48	#5A-C-7	50	744
#4-C-8	60	80	#5A-C-8	50	984
#4-C-9	60	92	#5A-C-9	50	1392
#4-C-10	60	92.5	#5A-C-10	50	1392
#4-C-11	50	144	#5A-C-11	40	6696†
#4-C-12	50	168	#5A-C-12	40	6696†
#4-C-13	50	1000	#5A-C-13	40	6696†
#4-C-14	50	2000	#5A-C-14	40	6696†
#4-C-15	50	3000	#5A-C-15	40	6696†

† runout test result.

3.4. Data analysis methodology

The experimental data were used to extrapolate the creep-rupture strength of the tested GFRP bars at 114 years (10^6 h) for each type of conditioning. Such extrapolations cannot, however, be implemented for design purposes without a safety factor. Therefore, a margin of safety for the GFRP bars was also determined based on statistical and probabilistic analyses to avoid unacceptable creep performance and, subsequently, to introduce a design creep strength.

3.4.1. Statistical Distributions

The five data points obtained from the tensile-strength test are barely one standard deviation away from the average value. For this reason, employing a normal distribution model for the data set obtained for the tensile test could reasonably approximate the data. It is not clear, however, if normal distribution is suitable with respect to the creep behavior of GFRP bars. The data points from the creep-rupture tests are usually dispersed around the average value. Compared to the tensile-test results, they are scattered over a wide range about a large coefficient of variation. For instance, a coefficient of variation of up to 100% was obtained in this study for the data points of a #4 bar at 50% UTS sustained load level subjected to type C conditioning. A similar variation in range has been reported in the literature for the creep-rupture tests (Devalapura et al. 1998; Greenwood 2002).

Weibull distribution was adopted for this study to account for the higher degree of variability in creep-rupture test results. Because of it being a right-skewed distribution, Weibull distribution matches suitably with the creep-test data points. The use of Weibull distribution for failure and survival time analysis has been repeatedly reported in the literature (Franke and Meyer 1992; Noël 2019; Rossini et al. 2019). The implementation of this statistical method in predicting the creep behavior of the GFRP bars was outlined by Rossini et al. (2019) and briefly discussed below.

By assuming a simple form of the Weibull distribution equation for the long-term creep behavior of the GFRP bars, the distribution model can be described by Eq. (1):

$$P(t) = 1 - exp\left[-\left(\frac{t}{t_0}\right)\right]^m \quad (1)$$

where t_0 and m are Weibull parameters. The scale factor t_0 can be considered as the mean value, and the shape factor m provides a measure of spread of the variable t.

Determining the Weibull parameters on the basis of creep rupture requires transforming Eq. (1) into a graph with the x- and y-axes representing $ln(t)$ and $ln\ ln[1\text{-}1/(1\text{-}P)]$, respectively, where the distribution equation appears as a straight line with a regression line. Therefore, the slope of the bar determines the shape factor (m) and the intersection of the regression line with $ln(t)$ equates t_0. Fig. 3-3 explains this transformation and determination of the Weibull parameters, for instance, for a #3 bar at 60% stress level under Group A conditioning.

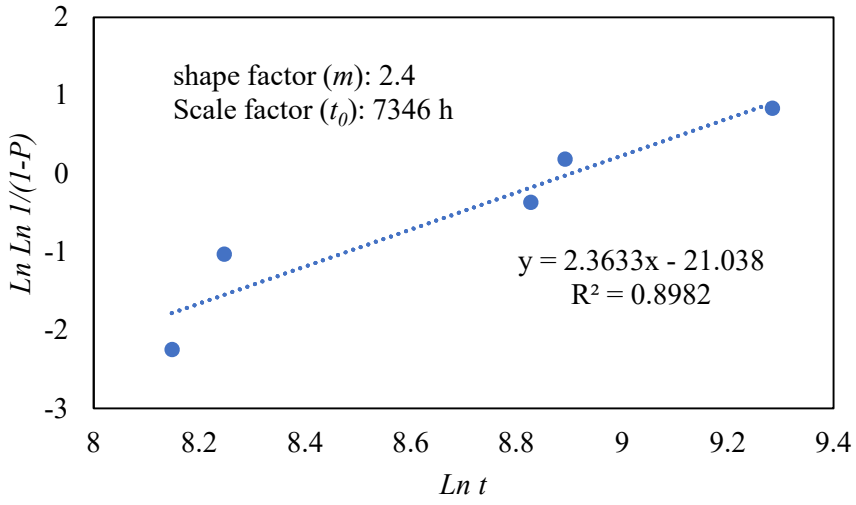

Fig. 3-3. Weibull distribution parameters for a #3 bar subjected to Group A conditioning at 60% sustained load.

3.4.2. Creep rupture curves

The creep-rupture results of each bar size tested were plotted on a logarithmic diagram in which the x-axis shows the logarithmic time-to-failure, and the y-axis shows the level of sustained load. Weibull statistical analysis was performed on each data set to obtain the mean and characteristic creep-rupture strengths for each sustained load level. The mean creep-rupture strength has a breakdown point of 50%, meaning that 50% of the specimens would fail beyond this point. The characteristic creep-rupture strength has a breakdown point of 5%, meaning that 95% of the specimens would fail beyond this point. The creep-rupture curves were then obtained by fitting regression lines through the statistically predicted points. Fig. 3-4 shows the typical mean and characteristic creep-rupture curves for the tested GFRP bars (dotted green and dashed red lines, respectively).

In order to establish consistency between the creep- and tensile-test results, the regression line passing through the creep-rupture data points was intercepted by the corresponding tensile-test value on the vertical axis. This means, for example, that the mean creep-rupture curve must intersect the bar's average UTS. Indeed, the tensile test can be seen as a creep-rupture test result with an endurance time equal to a fraction of a moment. The tensile-test duration should be approximately 10 min based on ASTM D7205 (ASTM 2016) requirements. Rossini et al. (2019) explained, however, that the maximum load is maintained on the specimen for only an instant, corresponding to the final step in the load ramp. For this reason, the endurance time of the bars during tensile testing was assumed to be 0.0001 h. Equation (2) presents the general format of the mean creep-rupture curve of the bars,

$$\frac{F_{c,m}}{F_{u,m}} = 1 - \beta_m log_{10}\left(\frac{t}{t_0}\right) \quad (2)$$

where $F_{c,m}$ is the mean creep-rupture strength at the endurance time t, $F_{u,m}$ is the ultimate tensile strength at time zero (t_0), and β_m is the regression parameter. It can be deduced from Eq. (2) that, when t equals t_0, the mean creep-rupture strength equals the average tensile strength.

Likewise, the characteristic creep-rupture curve of the bars can be defined by Eq. (3):

$$\frac{F_{c,k}}{F_{u,k}} = 1 - \beta_k log_{10}\left(\frac{t}{t_0}\right) \quad (3)$$

where $F_{c,k}$ is the characteristic creep-rupture strength at the endurance time t, $F_{u,k}$ is the characteristic tensile strength at time zero t_0, and β_k is the regression parameter. Similarly, substituting t for t_0 in Eq. (3) gives a characteristic creep-rupture strength equal to the characteristic tensile strength.

The results of both the tensile test and creep-rupture test are statistically variable. The endurance time is of no importance in tensile tests: the variable is strength, so the results are scattered along the load axis. The variability attributed to tensile-test results is represented by a normal distribution (bell-shaped curve) along the *y*-axis in Fig. 3-4. In contrast, in creep-rupture tests, the sustained load is constant: the endurance time varies, so the results are scattered along the time axis. The right-tailed bell curve along the *x*-axis in Fig. 3-4 represents the creep-rupture test results at a certain sustained load level. The slope of the

characteristic creep-rupture curve depends on variation in the datasets. A small coefficient of variation in a dataset reflects closeness of the characteristic creep-rupture curve to mean creep rupture.

3.4.3. Safety factor

The characteristic creep-rupture curve is still not safe enough to be used for design purpose, so an additional safety margin is required. Rossini et al. (2019) provided further conservatism by applying the design-assisted-by-testing outlines in BS EN (1992). BS EN (1992) assumes a normal distribution for the mechanical property of the tested material. Therefore, the 99.9th strength percentile can be used as a safe value for design purposes with only a 0.001 probability of failure. According to BS EN (1992)**,** the design strength can be assessed by applying the safety factor to characteristic strength, as follows in Eqns. (4) and (5):

$$F_u{}^* = \frac{F_{u,k}}{\gamma} \tag{4}$$

$$\gamma = \frac{(1 - 1.80 \times COV)}{(1 - 3.0 \times COV)} \tag{5}$$

where *COV* is the coefficient of variation, γ is the safety factor, $F_{u,k}$ is the characteristic tensile strength, and $F_u{}^*$ is the guaranteed tensile strength. Subsequently, by dividing the characteristic creep-rupture strength (F_{ck}) in Eq. (3) to the safety factor (γ) stated in Eq. (5), the guaranteed creep-rupture strength ($F_c{}^*$) is derived as:

$$\frac{F_c^*}{F_u^*} = 1 - \beta_k log_{10}\left(\frac{t}{t_0}\right) \quad (6)$$

It can be deduced from Eq. (6) that, when t is equal to t_0, the guaranteed creep-rupture curve intersects the guaranteed tensile-strength value in Fig. 3-4. Moreover, it is evident that the guaranteed creep rupture curve is shifted downward in respect to characteristic curve. Consequently, this downward displacement of the curve provides the required safety margin for design purpose.

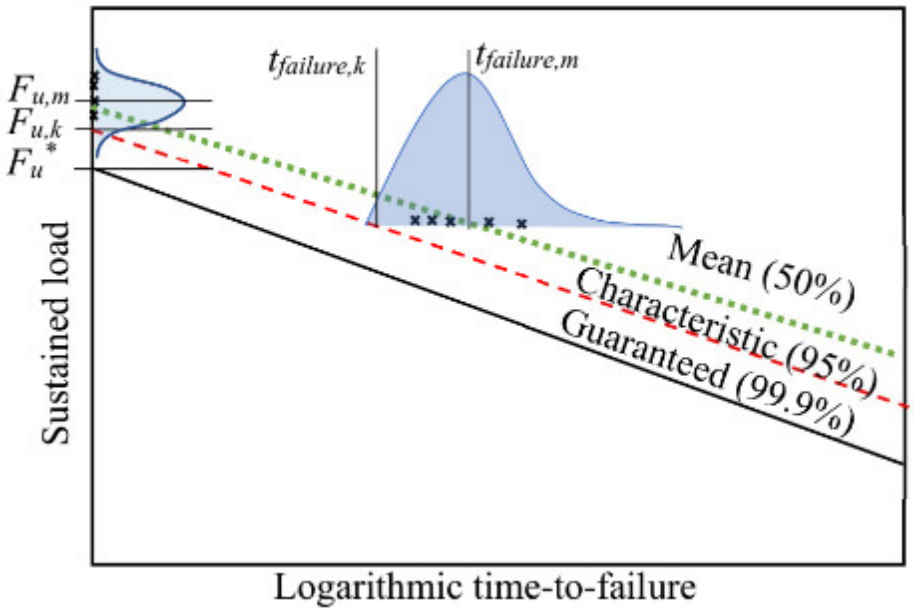

Fig. 3-4. Typical of creep rupture curves

3.5. Analyses and Discussions

Following the statistical procedure above and implementing the data analyses, the creep-rupture curves were plotted as specified in ASTM D7337 (ASTM 2019). The ratio of applied sustained load to UTS was plotted against a logarithmic time-to-failure scale to present the

endurance time of the GFRP bars over a million hours. The creep-rupture strength limit in AASHTO LRFD (AASHTO 2018) is presented as a knockdown factor multiplied by a guaranteed tensile strength. For this reason, the axis on the right side of the figures—which is a function of the ratio of UTS to the guaranteed tensile strength (GTS)—is added in order to compare the test results with the value permitted in the codes and design guides. Note that the run-out points were not considered in the analyses. Furthermore, Table 3-6 the test results by reporting the predicted values of creep-rupture strength and the safety factors used in statistical analysis.

3.5.1. Conditioning Group A

The curves in Fig. 3-5a through d are the results of the creep-rupture test for bars #3, #4, #5A, and #5B, subjected to sustained load alone. By projecting the linear regression line, passing through data points, over a prediction interval of 10^6 h (approximately 114 years of service life), the average creep rupture $F_{c,m}$, characteristic creep $F_{c,k}$, and guaranteed creep-rupture strengths F_c^*, were estimated (Table 3-6). In addition, the safe sustained stress levels 30% of GTS, recommended in AASHTO LRFD (AASHTO 2018)], is shown in the figures for comparison purposes. Furthermore, the goodness-of-fitness curve for each bar is presented in Fig. 3-6a through d for Group A, confirming fitness of the Weibull model predicting the data points.

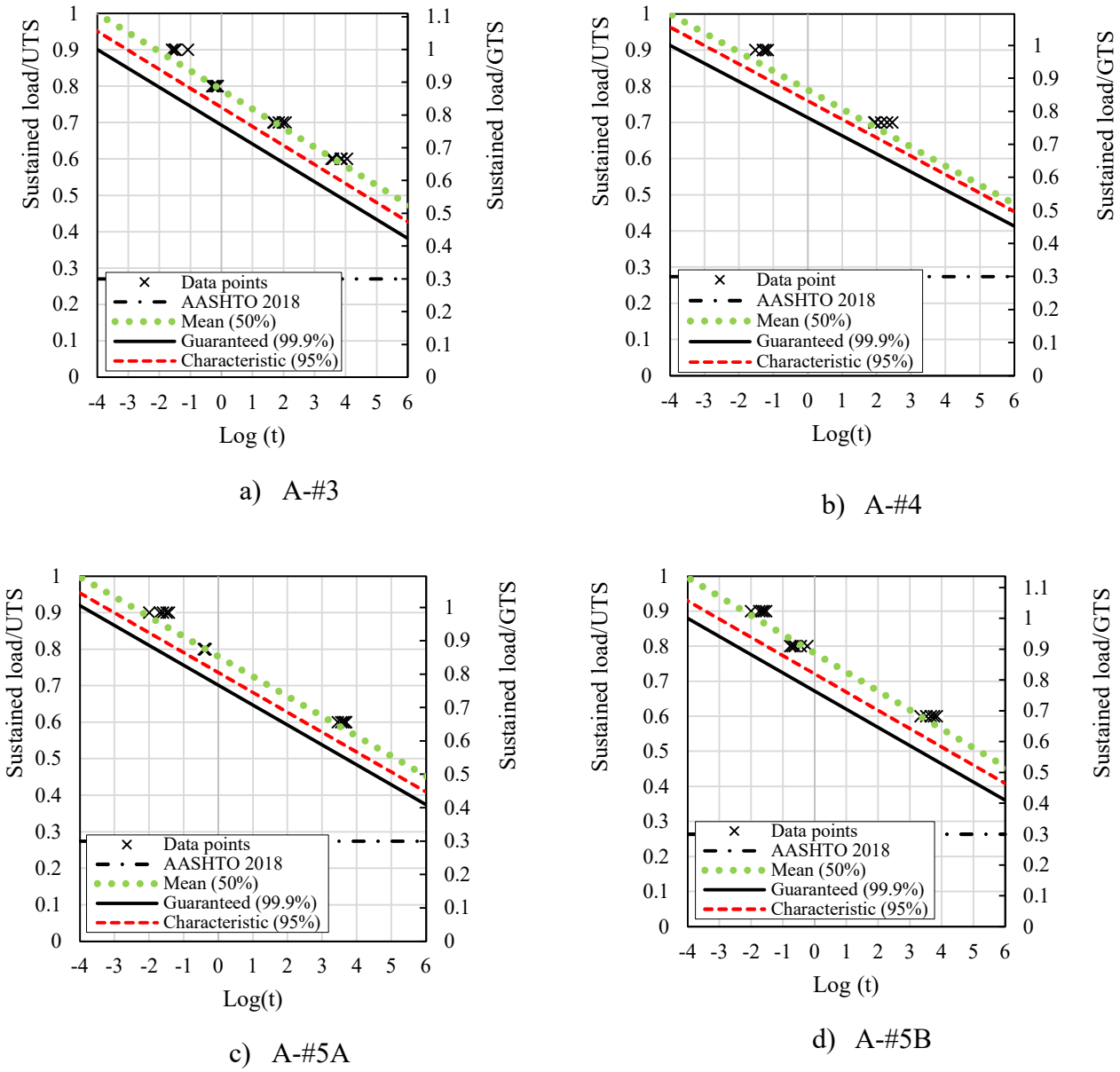

Fig. 3-5. Sustained load versus logarithmic time-to-failure, for a) bar #3, b) bar #4, c) bar #5A and d) bar #5B, subjected to conditioning type A.

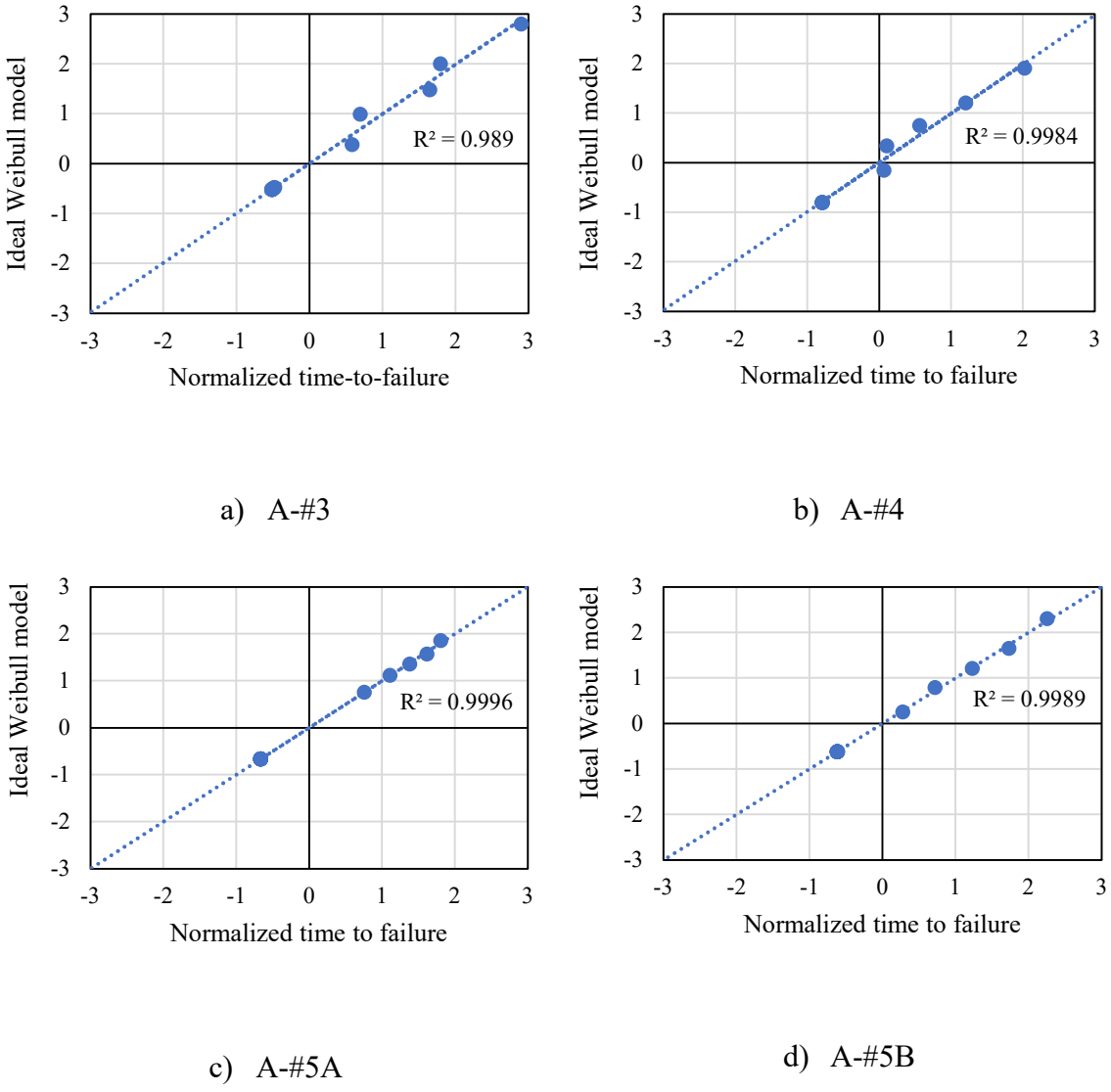

Fig. 3-6. Actual time to failure fitting to Weibull model for a) bar #3, b) bar #4, c) bar #5A, d) bar #5B, subjected to conditioning type A

The average creep rupture of the bars varies from 47% to 51% UTS, while the guaranteed creep rupture ranges from 41% to 45% GTS. Table 3-6 shows that smaller bar size yielded lower creep-rupture strength with Group A conditioning. The smallest average creep-rupture strength (47% UTS) was experienced by bar #3, whereas the smallest guaranteed creep-rupture strength (41% GTS) obtained for bar #5A. This discrepancy is due to the variability

of guaranteed creep rupture associated with the dispersion of data points. The safety margins between the sustained load level recommended in the available code provisions and the smallest guaranteed creep rupture obtained from the tests (41% GTS) were 21%, 26%, and 11% GTS compared to ACI 440.1R (ACI 2015), CSA S806 (CSA 2012), AASHTO LRFD (AASHTO 2018), respectively. Clearly, the recommended safety levels in the codes are very conservative.

Benmokrane et al. (2019) reported average and guaranteed creep-rupture values of 50.7% and 39.1% UTS, respectively. These values were determined considering a regression line passing through aggregate data points corresponding to the average points and the lower bound for 99% prediction intervals. The findings of Rossini et al. (2019) on the other hand, approximated the guaranteed creep rupture equal to 39% UTS (46% GTS) for the tests performed on two varieties of #4 GFRP bars. These values are comparable to the outcomes of the current study.

3.5.2. Conditioning Group B

Fig. 3-7a through d show the results obtained for the combined effect of the alkaline solution and sustained load on the creep strength of the tested GFRP bars. Fig. 3-8a through d give the curves of goodness-of-fitness for each bar. The obtained average and guaranteed creep rupture of the bars varied from 37% to 44% UTS and from 30% to 40% GTS, respectively. It is evident that larger size bars were more susceptible to alkaline exposure. The #3 bars retained 44% UTS after 106 h, with less than a 3% reduction in creep strength compared to the bars exposed to sustained load alone (Group A). Likewise, this loss in the expected creep-

rupture strength was estimated as 8%, 13%, and 11% for bars #4, #5A, and #5B, respectively, compared to the creep-rupture strength of the counterpart bars in Group A. These results confirm the finding of Benmokrane et al. (2017) that the effect of conditioning on tensile properties is expected to be greater for bars with larger diameters.

By assuming that a bar exposed to the alkaline solution and sustained load resembles an embedded bar in a concrete component not exposed to earth and weather, according to ACI 440.1R (ACI 2015) and AASHTO LRFD (AASHTO 2018), the suggested environmental factor (C_E) can be taken as 0.8. The product of the C_E factor multiplied by the suggested creep-rupture knock-down factor as per ACI 440.1R (ACI 2015) and AASHTO LRFD (AASHTO 2018) : 0.2 and 0.3, equal to 16% and 24% GTS, respectively. CSA S806 (CSA 2012) , on the other hand, uses the same creep-rupture strength (25% GTS) for all GFRP bars without endorsing an environmental reduction factor. Table 3-6 shows that all the guaranteed creep-rupture strengths of the bars were above code limits with at least a 5% GTS margin of safety, reflecting that the current code provisions are overly conservative.

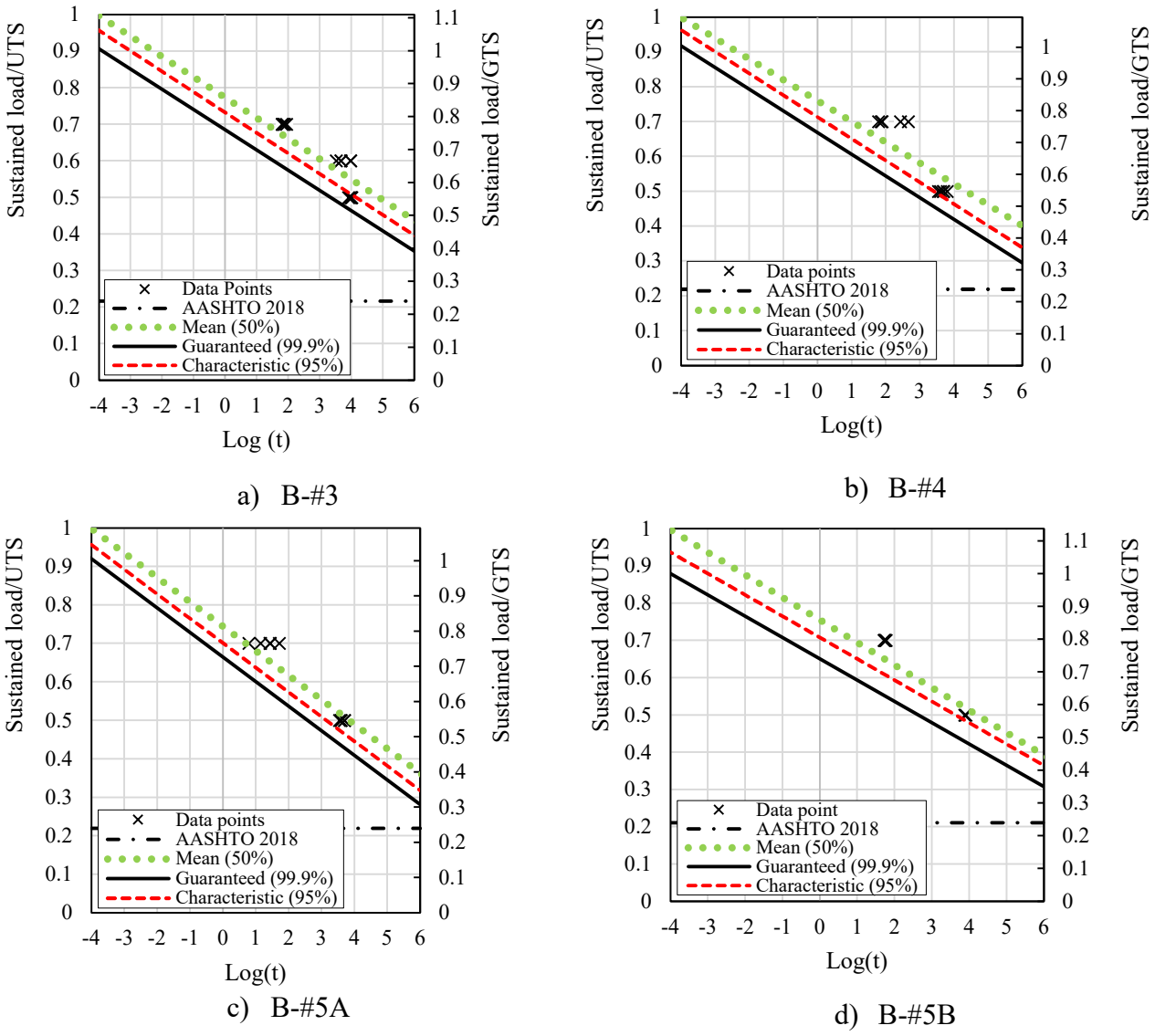

Fig. 3-7. Sustained load versus logarithmic time-to-failure, for a) bar #3, b) bar #4, c) bar #5A and d) bar #5B, subjected to conditioning type B.

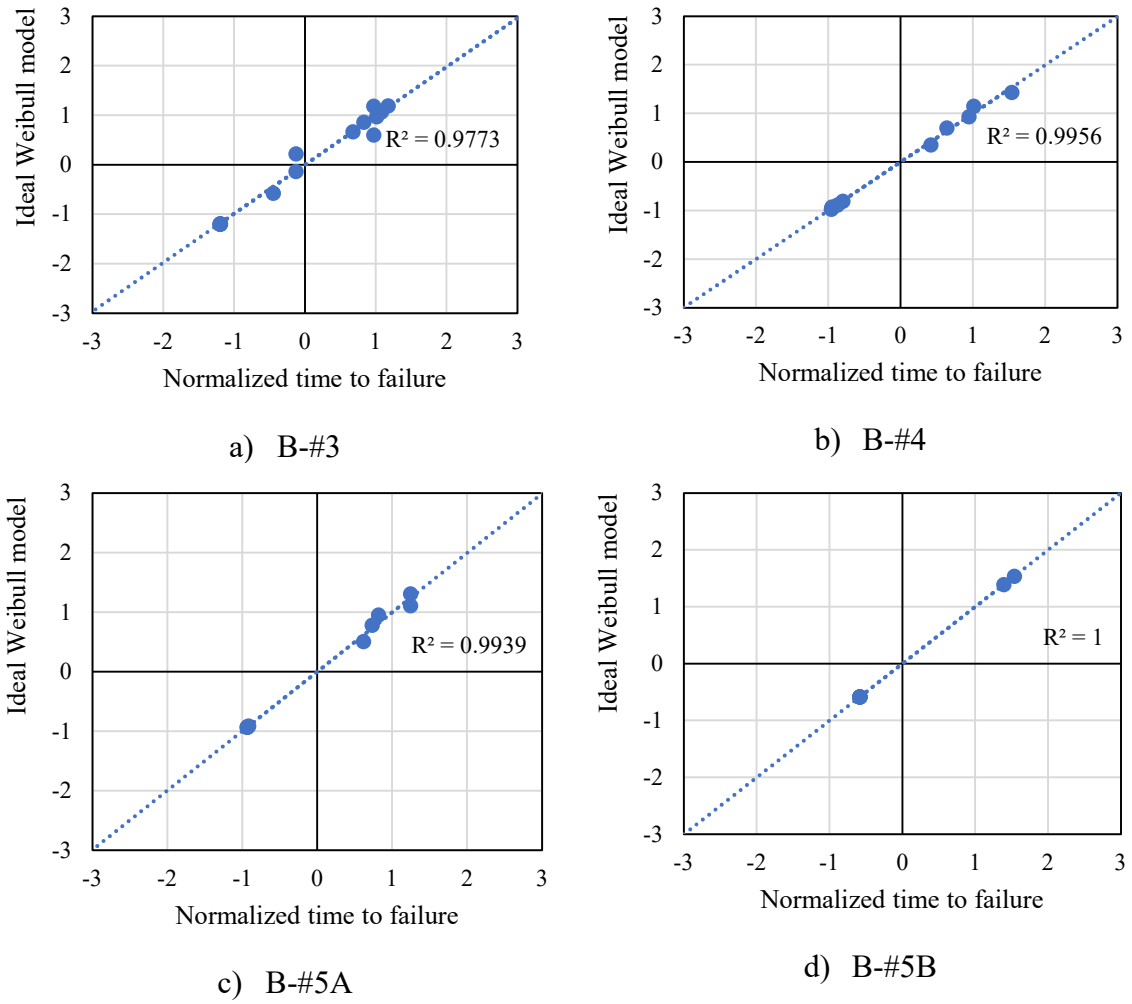

Fig. 3-8. Actual time to failure fitting to Weibull model for a) bar #3, b) bar #4, c) bar #5A, d) bar #5B, subjected to conditioning type B.

The recommended C_E values in ACI 440.1R (ACI 2015) were based on a consensus of ACI 440 committee members and is believed to be conservative. Benmokrane et al. (2020) reassessed the environmental reduction factor using data compiled from the literature and suggested a value of 0.85 for an assumed service life of 75 to 100 years for #3 bars or larger, which would result in creep-rupture strengths of 17% and 25.5% GTS using the creep-rupture limits in ACI 440.1R (ACI 2015) and AASHTO LRFD (AASHTO 2018),

respectively. These values are still well below the obtained guaranteed creep-rupture strength in this study (ranging from 30% to 40% GTS).

3.5.3. Conditioning Group C

For the case of the conditioning Group C, only bar #4 and bar #5A were involved in the experiment due to the limited space of the heating chambers. Fig. 3-9a-b show the results obtained for the bars subjected to the effect of the trio of alkaline solution, elevated temperature (60˚C) and sustained load on creep strength of the bars. The goodness-of-fitness curves shown in Fig. 3-10a-b show how well the observed values fit the data obtained from the prediction model. The severity of the exposure condition used as an accelerated ageing shifted down the creep rupture strength of the bars. The deleterious effect of the trio of conditioning on bar #4 and #5A was 8% UTS accelerated the creep rupture endurance time and caused a drop in creep rupture strength of both bars compared to conditioning Group B (coupled effect of alkaline solution and sustained load). Moreover, in comparison to conditioning Group A (only the effect of sustained load), the trio caused 16% UTS and 21% UTS drop for bar #4 and #5A, respectively. This again confirms the speculation that the greater degradation takes place in the larger bar size (Benmokrane et al. 2017).

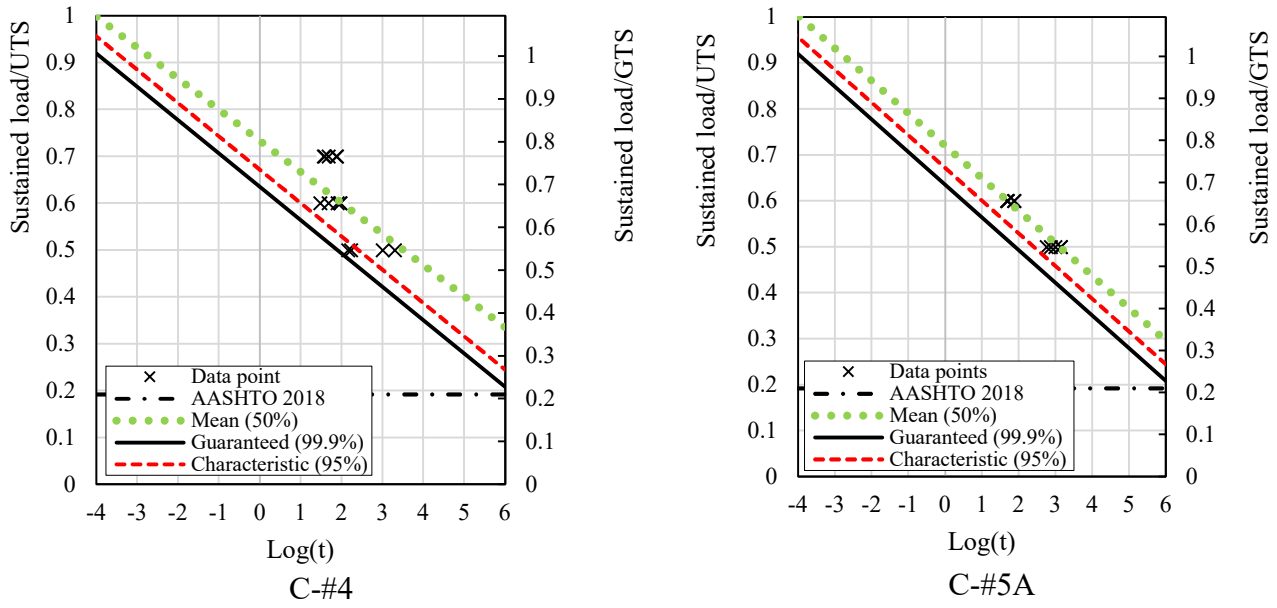

Fig. 3-9. Sustained load versus logarithmic time-to-failure, for a) bar #4, b) bar #5A, subjected to conditioning type C.

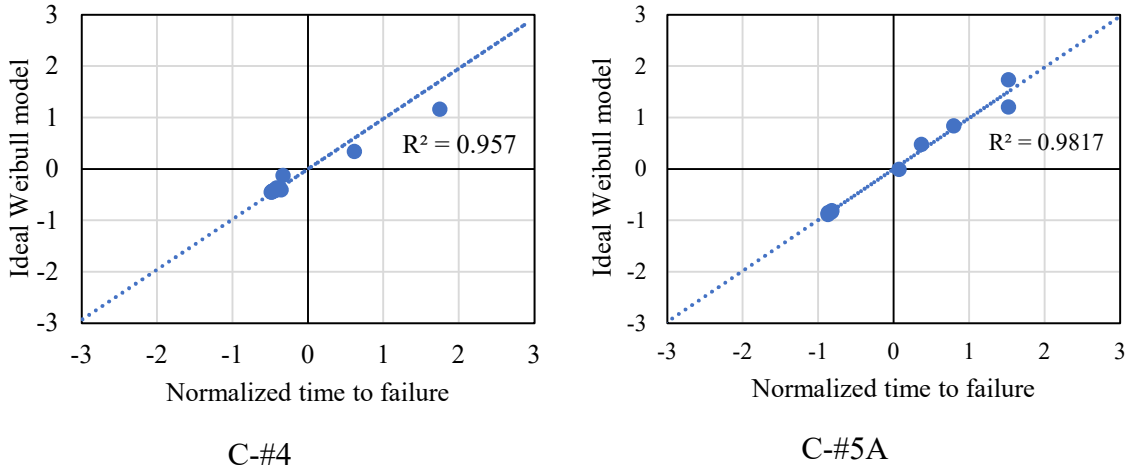

Fig. 3-10. Actual time to failure fitting to Weibull model for a) bar #4, b) bar #5A, subjected to conditioning type C.

The CSA S806 (CSA 2012), on the other hand, requires the designer to consider the effect of elevated temperature on the performance of FRP reinforcement, however, without clear guidance on such effect. The results in Table 3-6 shows that a service temperature of 60°C

has an adverse effect on the creep rupture strength of tested GFRP bars. Therefore, a creep rupture strength of 0.25 GTS recommended by the CSA S806 (CSA 2012) cannot be used solely without considering the effect of temperature for a service life performance of 10^6 h (114 years). The results of the current study suggest that a creep rupture strength of 0.23 GTS can be used with a service temperature of 60°C.

The environmental reduction factor recommended by the ACI 440.1R (ACI 2015) accounts for the effect of high temperatures up to the glass transition temperature of the resin (117°C in Table 3-1), while AASHTO LRFD (AASHTO 2018) provides no guidance on the service life temperature for GFRP bars. For the trio of conditioning of Group C, the C_E value was presumed to be 0.7, reflecting GFRP bars embedded in concrete and exposed to earth or weather. The product of the C_E factor multiplied by the suggested creep rupture knock-down factor equals 0.14 and 0.21 GTS, according to ACI 440.1R (ACI 2015) and AASHTO LRFD (AASHTO 2018), respectively. From Table 3-6 it is evident that despite a harsh laboratory environment, all the guaranteed creep-rupture strengths of the bars were above 23% GTS, with at least 2% GTS margin of safety. However, it is recommended to implement lower C_E factors for GFRP bars in special application that might be exposed to service temperatures higher than 60°C. More investigations are needed to address this point.

Table 3-6. Estimated average and guaranteed creep rupture strengths for the tested GFRP bars.

Group	GFRP Bar	EN 1990 Safety factor (γ)	Mean Creep Rupture strength (% of UTS)	Guaranteed Creep Rupture strength (% of GTS)	CSA S806 (CSA 2012) and CSA S6 (CSA 2019) (% of GTS)	AASHTO LRFD (2018) (% of GTS)	ACI 440.1R (ACI 2015) (% of GTS)
A	#3	1.044	47	42	25	30	20
	#4	1.038	48	45	25	30	20
	#5A	1.038	50	41	25	30	20
	#5B	1.055	51	41	25	30	20
B	#3	1.044	٤٤	٤٠	25	24	16
	#4	1.038	٤٠	٣٣	25	24	16
	#5A	1.038	٣٧	٣٠	25	24	16
	#5B	1.055	٤٠	٣٦	25	24	16
C	#4	1.038	32	23	25	21	14
	#5A	1.038	29	23	25	21	14

3.6. CONCLUSION

The current study evaluated design creep strength and an environmental coefficient factor of GFRP bars by performing creep testing on 160 bar specimens made of E-CR fibers and vinyl-ester resin. The bars were exposed to three different environmental conditions and concurrently applied sustained loads ranging from 40% to 90% UTS. The conditioned bars were exposed to (a) normal laboratory conditions (Group A), (b) immersed in alkaline solution under normal laboratory conditions at 23°C (Group B), and c) immersed in alkaline

solution at a high temperature of 60°C (Group C). The findings of the study can be outlined as follows.

1- The consistency of the Weibull distribution in accounting for variabilities in creep testing of GFRP composite materials was confirmed with a correlation of coefficient of more than 95% for the predicted and experimental data points.

2- The extrapolation of the creep-rupture results of Group A GFRP bars (#3, #4, #5A, and #5B at an endurance time of 10^6) resulted in mean creep-rupture strengths equal to 47%, 48%, 50%, and 51% UTS, respectively. These values decreased due to additional exposure to the alkaline solution at ambient temperature (23°C) by 3%, 8%, 13%, and 11% UTS for bars #3, #4, #5A, and #5B, respectively (i.e., the extrapolated creep-rupture strengths were 44%, 40%, 37%, and 40%, respectively). Moreover, when the conditioning in alkaline solution combined with high temperature (60°C), the extrapolated mean creep strengths of bars #4 and #5A were 32% and 29% UTS, for a reduction of 16% and 21%, respectively, compared to the sole creep-rupture test results of the same bars (Group A).

3- Larger bar sizes exhibited higher degradation rates than smaller bar in all conditioning groups. Therefore, it can be concluded that there was an inverse correlation between bar diameter and reduced creep strength.

4- A guaranteed creep-rupture threshold associated with the 99.9^{th} strength percentile at an endurance time of 10^6 h equal to 0.41 can be used for the tested bars (#3, #4, #5A, and #5B). This value is approximately 105% and 37% higher

than the 0.30 and 0.2 coefficients currently recommended in ACI 440.1R (ACI 2015) and AASHTO LRFD (AASHTO 2018), respectively.

5- The guaranteed creep-rupture strengths with an endurance time of 10^6 h obtained for the bars exposed to Group B conditioning was at least 30% GTS. This value is higher than the creep-rupture limits in the codes when presuming that the exposure conditions can represent a C_E factor of 0.8, corresponding to bars not exposed to weather, leading to creep-rupture limits of 0.16 and 0.24 according to ACI 440.1R (ACI 2015) and AASHTO LRFD (AASHTO 2018), respectively. Furthermore, the obtained design creep-rupture limit (30% GTS) is higher than that required by CSA S806 (CSA 2012), CSA S6 (CSA 2019a) of 25% GTS.

6- The harsh exposure conditioning in Group C substantially reduced the 10^6 h guaranteed creep-rupture strength to 23% GTS. The resultant creep-rupture strengths were 9% and 2% higher than that according to ACI 440.1R (ACI 2015) and AASHTO LRFD (AASHTO 2018), respectively, when assuming that such conditioning can be simulated by bars exposed to weather with a C_E factor of 0.7. Nevertheless, the 60°C exposure temperature is very severe and was presented herein to assess the creep-rupture behavior of the bars under extreme conditioning. These results confirm that the creep-rupture limits in the codes are overly conservative.

It shall be noted that the laboratory conditioning by exposing GFRP bars to a high alkaline solution at high temperatures would not accurately represent real-life scenarios, therefore, additional research is needed to mimic the creep rupture behavior of GFRP bars in natural environments. Additional tests are also needed to investigate the creep rupture behavior and

long-term performance of larger sizes GFRP bars. Furthermore, the guaranteed creep rupture strength was estimated in the current study based on the design-assisted-by-testing outlined by the BS EN (1992), while future studies can calibrate and implemented other safety models.

CHAPTER 4 PERFORMANCE OF GFRP-REINFORCED CONCRETE BEAMS SUBJECTED TO HIGH SUSTAINED LOAD AND NATURAL AGING FOR 10 YEARS

Authors and affiliations:

Yasin Esmaeili,[1] Abolfazl Eslami,[2] John Newhook,[3] Brahim Benmokrane[4*]

[1]PhD candidate, Department of Civil Engineering, University of Sherbrooke, Sherbrooke, QC, Canada, J1K 2R1, E-mail: yasin.esmaeili.hesar@usherbrooke.ca

[2]Postdoctoral Fellow, Department of Civil Engineering, University of Sherbrooke, Sherbrooke, QC, Canada, J1K 2R1, E-mail: abolfazl.eslami@usherbrooke.ca

[3]Professor, Faculty of Engineering, Dalhousie University, Sexton Campus, Halifax, NS, Canada, B3H 4R2, E-mail: John.newhook@dal.ca

[4]Professor of Civil Engineering, Tier-1 Canada Research Chair of Advanced Composite Materials for Civil Structures and Senior NSERC Research Chair in Innovative FRP Reinforcement for Sustainable Concrete Infrastructure, Department of Civil Engineering, University of Sherbrooke, Sherbrooke, QC, Canada, J1K 2R1, Phone: (819) 571-6923; E-mail: brahim.benmokrane@usherbrooke.ca.
([*]Corresponding Author)

Journal Title and Paper Status:

Published in Journal of Composites for Construction, ASCE, Volume 24 Issue 5 - October 2020. https://doi.org/10.1061/(ASCE)CC.1943-5614.0001065

Contribution to the Thesis:

Laboratory conditioning could be too severe and exposing GFRP bars to a high alkaline solution at high temperatures – as presented in Chapter 3 - would not accurately represent real-life scenarios. This Chapter addresses the long-term performance of GFRP bars under high levels of sustained load combined with real field conditioning. GFRP bars were embedded in concrete beams exposed to aggressive natural weathering (temperatures ranging from -25°C to 35°C) for 10 years and sustained loads of up to 40% of the ultimate tensile capacity of their GFRP bars. The beams were tested to failure in a four-point bending setup, and the obtained results were compared to that of unconditioned beams. The results confirmed that natural exposures are less aggressive than the concentrated alkaline solution and high temperature.

Abstract

The long-term performance of glass fiber-reinforced polymer (GFRP) bars under high levels of sustained load combined with real field conditioning has not yet been thoroughly investigated. Our experimental investigation examined the flexural behavior of concrete beams reinforced with GFRP bars subjected to high sustained bending load after 10 years of natural aging. The experimental program consisted of eight rectangular concrete beams measuring 250 x 250 x 2000 mm. All beams were reinforced with sand coated GFRP bars. Four beams were subjected to a high sustained load of up to 40% of the ultimate tensile capacity of their GFRP bars with simultaneous exposure to aggressive natural weathering (temperatures ranging from -25℃ to 35℃) for 10 years. The remaining four were stored in

the laboratory and treated as control specimens without any loading. The conditioned beams were tested up to failure in a four-point bending setup. The results were compared in terms of load–displacement behavior, ultimate strength, displacement capacity, failure modes, and cracking pattern. In addition, the microstructure of the GFRP bars was studied to evaluate the physical changes of the bars, and their bond condition with surrounding concrete at different stress levels. The findings indicate a strength deterioration of only 16% for this early generation of GFRP bars under harsh natural conditioning and high sustained loads for 10 years. On the other hand, the bond between the concrete and GFRP bars as well as the glass transition temperature, infrared spectra and interlaminar shear strength of the GFRP bars remained unaffected. Finally, analytical approaches were implemented to predict the load–displacement behavior and crack widths of the tested beams.

KEYWORDS: GFRP bar; durability; natural weathering; high sustained stress; failure mode; bond behavior; deflection; strength; non-destructive testing.

4.1. Introduction

The corrosion resistance of fiber-reinforced polymer (FRP) reinforcing bars has introduced them as an alternative to conventional steel reinforcement in reinforced concrete (RC) structures subjected to harsh environments. Glass FRP (GFRP) bars are the more common type of fiber-reinforced polymer bars used in the construction industry due to their low cost [ACI 440. 1R (ACI 2015)].

Past research attempts (Benmokrane et al. 2002a; Tobbi et al. 2012) to understand the applicability of GFRP bars in structures have revealed many important facts about their

inherent features. Today, the short-term behavior of this structural material (features such as stiffness, bending strength, axial behavior, shear strength, bonding, and so forth) are almost well known. Nonetheless, the long-term performance of GFRP bars still requires more research [ACI 440. 1R (ACI 2015)]. Particularly, their behavior under the combined effect of natural weathering and sustained stresses has received scant attention in the literature. The related durability problems of GFRP bars are commonly addressed by either laboratory accelerated aging studies (Park et al. 2014; Ali et al. 2018) or field investigations (Mufti et al. 2007; Gooranorimi and Nanni 2017; Benmokrane et al. 2018).

4.1.1. Accelerated Aging Tests of GFRP Bars

Accelerated aging tests have been widely used in durability studies due to their simplicity in establishing the life span of the GFRP bars. In this method, the alkaline solutions represent concrete pore water and the elevated temperature yields accelerated aging. He et al. (2017) conducted accelerated durability tests on GFRP reinforcement embedded in concrete beams. The bars were extracted from the beams immersed in alkaline solution at 60°C and subjected to sustained loads (20% and 40% of ultimate bending strength). After 18 months exposure to alkaline solution, the bars retained tensile strength of about 80% and 75% for the bars subjected to sustained loads of less than 20% and 40% of ultimate bending strength, respectively. Debonding of glass fibers and matrix has also been reported for GFRP bars under a sustained load equal to 40% of their ultimate bending strength. At the same time, no significant evidence of degradation was observed for sustained flexural loads of less than 20% of bar ultimate bending moment. Moreover, the authors stated that the degree of degradation could be more pronounced at the interface of the glass fibers and resin matrix.

Ali et al. (2018) predicted tensile-strength retention of 85% and 75% after 200 years for GFRP bars with vinyl ester resin subjected to an alkaline solution at 10°C and 30°C, respectively. Park et al. (2014) studied the flexural behavior of 36 beams reinforced with either GFRP or steel bars subjected to the combined effect of sustained load and accelerated-aging conditions (i.e., 47°C and 80% relative humidity) for 300 days. Their experimental outcomes indicated different rates of degradation for different types of GFRP bars under artificial aggressive environments. The studies confirmed, however, that one advantage of using GFRP bars in concrete is that they are not subjected to corrosion unlike the conventional steel reinforcement.

In contrast, some contradictory outcomes have also been reported based on the findings of accelerated tests conducted on GFRP RC structures. For instance, Davalos et al. (2012) studied the behavior of GFRP bars with E-glass and vinyl ester resin embedded in a saturated concrete at 10°C and subjected to relatively low levels of sustained loading (1100-1300 με - tensile strain). They indicated that the GFRP bars could maintain 38% of their tensile strength after 50 years. This would lead to the conclusion that GFRP bars should not be used in concrete. This paradox might be due to the variety of constituent materials in GFRP bars and the available processing techniques. These uncertainties; however, have a massive influence on the safety margin of the design process forcing engineers to adopt high safety factors for GFRP RC structures exposed to different environmental conditions.

4.1.2. Performance of GFRP Bars Under Natural Aging

Unlike accelerated-aging tests, natural aging is a very slow process as the properties of GFRP reinforcement are less affected by natural weathering than accelerated-aging conditions (Micelli and Nanni 2004; Bakis et al. 2005; Mufti et al. 2007). Since the results obtained from the natural weathering conditions are more realistic and reliable than that from accelerated aging tests, conducting field studies is crucial to validate design code provisions. In an attempt, Trejo et al. (2011) studied 160 actual field-conditioned GFRP bars embedded in unsaturated cracked concrete for seven years to evaluate the effects of environmental degradation. Their results indicated lower rates of strength deterioration compared to data available for the accelerated exposure. No sustained load was imposed on the bars, however, over seven years of exposure. In another study, Gooranorimi and Nanni (2017) performed a field study to evaluate the long-term durability conditions of GFRP bars in a 15-year old bridge (Sierra de la Cruz Bridge in Texas, USA). The durability of the GFRP bars embedded in the concrete deck and exposed to the natural environmental conditions was evaluated through a series of microstructural tests. The test results showed that the GFRP bars were in good condition even after 15 years. Nonetheless, due to limitation in obtaining data for the control specimens, the results of interlaminar shear tests were inconclusive.

Mukherjee and Arwikar (2005, 2006) conducted a comprehensive study comparing the performance of GFRP bars under accelerated aging and natural weathering in a tropical environment. The specimens for the accelerated aging test were immersed in tanks containing water at 60°C for 3, 6, and 12 months.The conditioning time of the naturally aged specimens was 18 or 30 months. In addition, 50% of the ultimate load was imposed on the

beams as a sustained load. The outcomes were discussed on the structural (Mukherjee and Arwikar 2006), and microstructural (Mukherjee and Arwikar 2005) scales. Failure of the control beams was associated with the design-intended flexural-compression mode. On the other hand, the conditioned beams failed with reinforcement rupture and withstood higher loads. The tests on constituent materials showed that the concrete gained substantial strength due to conditioning in the tank at 60° C. The testing of reinforcing bars taken from the conditioned beams also revealed that the bars experienced strength drops of about 42%, 56%, and 65% with 3, 6, and 12 months of accelerated aging, respectively. Even given natural weathering, strength reductions of about 35% and 39% were observed after 18 and 30 months, respectively. The increase in concrete strength and decrease in reinforcing-bar strength shifted the failure mode from concrete crushing to reinforcement rupture. Moreover, although the resin matrix was made of vinyl ester, the extrapolated life span showed that the GFRP bars would lose 65% of their strength over a service life of 32 years. The microstructural observations also verified the degradation. The authors stated, however, that the SEM analysis points to bubbles and microcracks in the matrix that could have formed during the manufacturing process. Bubbles and microcracks facilitate the diffusion of moisture and alkaline solution.

He et al. (2013) conducted a durability investigation on E-glass reinforced vinyl-ester bars. The bars were conditioned in concrete beams for three years. During conditioning, the specimens were subjected to a sustained load equal to 11% of the ultimate tensile strength of the GFRP bars combined with different environments, including ambient indoor laboratory, natural outdoor weathering in central Pennsylvania, a high alkaline aqueous

solution at 60°C, and alternating 17°C dry freeze and room-temperature water immersion. Based on the results, the tensile strength decreased by 28% for the artificially aggressive environments, while it remained unchanged for the indoor and outdoor conditioning. An extrapolation to 50 years predicted a residual strength of 50% of the ultimate strength for the former condition.

To augment the available data related to the durability of GFRP RC members, our study focuses on the flexural performance of concrete beams reinforced with sand coated GFRP bars under the combined effect of natural environmental conditioning and high sustained bending load.

4.1.3. Research Significance

Design guides and codes such as CSA S6 (CSA 2019a) and ACI 440. 1R (ACI 2015) restrict the maximum stress in GFRP bars at the serviceability limit state to 20% and 25% of their guaranteed tensile strength, respectively. With the aim of increasing the serviceability limit state, the specimens in this study were loaded to 40% of the ultimate tensile strength of their GFRP bars and while exposed to harsh natural environmental conditioning for 10 years. This level of sustained stress is almost twice the threshold allowed in CSA S806 (CSA 2012), CSA S6 (CSA 2019a) and ACI 440. 1R (ACI 2015).

In order to achieve the objectives of this study, two sets of tests were carried out: (1) destructive testing in which the structural flexural behavior of the beams up to failure point was evaluated using a four point bending setup, and (2) non-destructive testing in which physiochemical changes in the GFRP bar properties due to the likelihood of degradation

were examined on the microstructural scale. The specimens were eventually loaded to failure, offering a prime merit over field studies which are normally carried out with non-destructive techniques.

The data obtained from the experiments were then used for analytical purposes and are discussed in terms of flexural responses of the GFRP RC beams before and after exposure to environmental conditions. Moreover, the accuracy of the existing provisions and models in the codes were verified based on the properties of the degraded GFRP bars. The outcomes can provide a detailed understanding on the durability performance of GFRP RC beams, and crucial information on increasing the serviceability limit state thresholds specified in design guidelines.

4.1.4. Review of Code Provisions

According to ACI 440. 1R (ACI 2015), the material properties provided by FRP manufacturers should be considered as raw properties that would not take into account deterioration due to long-term environmental exposure. The specification requires using environmental reduction factors (C_E) to reduce the material properties used in the design expressions, based on the type and level of environmental exposure. According to ACI 440. 1R (ACI 2015), the suggested C_E factor for GFRP reinforced-concrete components not exposed to earth and weather is 0.8, compared to 0.7 for members exposed to earth and weather. In addition, ACI 440. 1R (ACI 2015) recommends that, in order to avoid creep rupture failure, service-load sustained stress not exceed 0.20 times the design tensile strength of GFRP) reinforcement.

Pursuing a different strategy, CSA S806 (CSA 2012) uses a resistance factor ($\emptyset_f$) to account for uncertainties about the materials that include but are not limited to environmentally induced effects. In other words, CSA S806 (CSA 2012), recommends a resistance factor of $\emptyset_f = 0.75$ for FRP RC structures when the long-term degradation effect is implicitly considered. Furthermore, due to the low stiffness and high ultimate strength of FRP bars, design of FRP reinforced members is usually controlled by the serviceability limit states. Thus, CSA S806 (CSA 2012) suggests two more provisions to reduce the tensile capacity of GFRP bars at the service level: 1) the maximum stress in GFRP bars at the serviceability limit state shall not exceed 25% of the characteristic tensile strength; 2) the maximum strain in GFRP reinforcement under sustained service loads shall not exceed 0.002. Similarly, CSA S6 (CSA 2019a) recommends using a resistance reduction factor of 0.55 for the ultimate state design and 0.25 for the service limit state design.

The design codes tend to restrict GFRP bar capacity based on guaranteed tensile strength, but the sustained load applied in this study was a proportion (40%) of the ultimate tensile strength. A sustained load equal to 40% of the ultimate tensile strength is equivalent to 47% of the guaranteed tensile strength. Thus, the actual sustained stress level is 1.9 times higher than the allowable stress level for GFRP bars in CSA S806 (CSA 2012), CSA S6 (CSA 2019a) and 2.4 times higher than threshold specified in ACI 440. 1R (ACI 2015).

4.2. Experimental Program

The experimental test consisted of eight beams; six of them for destructive purpose and the remainder for non-destructive evaluation. In destructive phase, three beams out of six were

stored in the lab until tested under a four-point bending setup a year after casting to serve as the control specimens. The reason for testing the unconditioned beams one year after casting was to allow the concrete compression strength to stabilize. The remainder were subjected to high sustained bending stress applied by a steel frame and left in aggressive natural weathering conditions in Halifax (Nova Scotia, Canada) for 10 years starting from December 2008. This conditioning included freeze–thaw and wet–dry cycles with temperatures fluctuating from -25°C to 35°C. Fig. 4-1 gives the variation in maximum and minimum daily temperature records for the Halifax international airport from 2008 to 2018 (The official website of the Government of Canada 2019). The objective of this phase was to compare the flexural behavior of the conditioned beams under the combined effect of natural weathering and sustained load with those of the unconditioned beams.

To obtain control specimens for non-destructive phase, one beam was kept in the lab. The second beam was conditioned following similar approach implemented in the beams used for destructive phase. The objective was to scrutinize the likelihood of degradation signs on the microstructural scale.

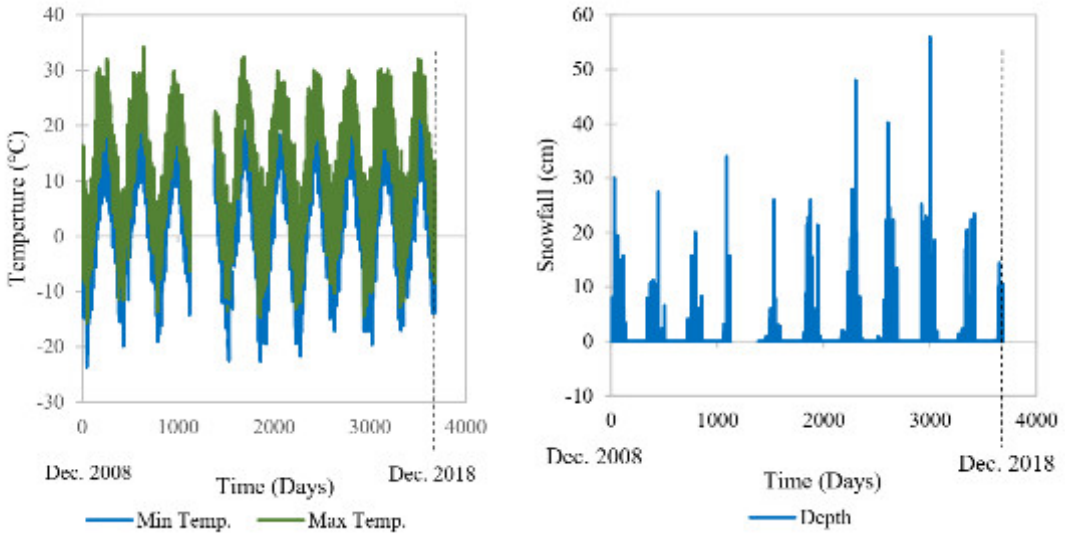

Fig. 4-1. The variation in temperature extremities and snowfall at the Halifax international airport's climatological monitoring station (2008–2018) (The official website of the Government of Canada 2019)

4.2.1. Description of Test Specimens

Specimen identification consists of a letter indicating the conditioning status (C for the conditioned and U for the unconditioned beams) followed by a digit representing the number of repeated specimens. The conditioned beams are labeled C1, C2, C3, and C4 and the unconditioned beams U1, U2, U3, and U4. Beams (U4 and C4) were used for non-destructive tests while the remainder were tested in the destructive phase. Note that the unconditioned beams were stored in a standard laboratory condition (i.e. at 23-24℃ and 50% relative humidity) without exposure to weather conditioning or sustained load.

FRP RC beams are often over-reinforced to take advantage of the inelastic behavior of concrete and thus experiencing significant deflection before failure (Nanni 1993; ACI 2015). However, the beam specimens of the current study were designed with under

reinforced sections to assess the effect of conditioning on the tensile strength of GFRP bars. In such cases, the flexural strength of beam would be lower upon deterioration of the GFRP bars.

Fig. 4-2 provides the geometric and reinforcement details of the test specimens. Each specimen measured 250 × 250 × 2000 mm with a clear span of 1900 mm. The tensile reinforcement consisted of two No. 4 bars in the longitudinal direction with stirrups and compression reinforcement made of No. 3 bars of the same type. The flexural reinforcement ratio of the beams was 0.0049 with a balanced reinforcement ratio of 0.0053. Due to the lack of closed stirrups at the time, the transverse reinforcement consisted of combining two U-shaped ties as illustrated in Fig. 4-2.

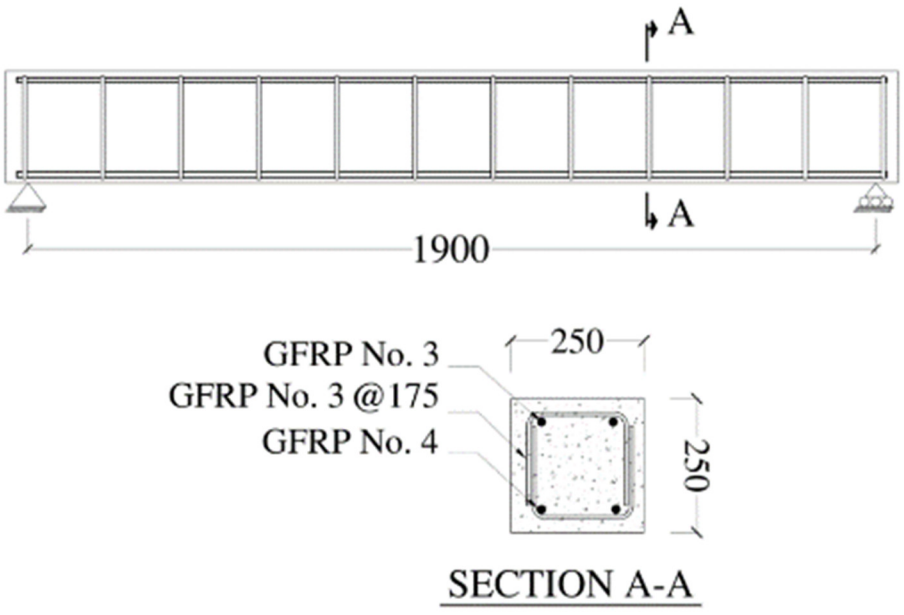

Fig. 4-2. Geometric and reinforcement details of the test specimens (all dimensions are in mm)

4.2.2. Material Properties

No. 4 (12.7 mm in diameter) and No. 3 (9.5 mm in diameter) sand coated GFRP bars were used as longitudinal and transverse reinforcement, respectively. Table 4-1 presents the mechanical properties of the longitudinal and transverse GFRP bars. The GFRP bars were made of vinyl-ester resin and E-glass fibers. The tensile properties of the GFRP bars were determined in accordance with CSA S806 (CSA 2012), Annex C, while the actual cross-sectional area of the bars was measured according to CSA S806 (CSA 2012), Annex A.

All the beams were cast with a normal weight ready mix concrete containing 20% fly ash. The target concrete compressive strength was 40 MPa. The 28-day compressive strength of concrete was determined by averaging the results of six cylinders (measuring 100×250 mm), was 28.2 MPa. In addition, the average compressive strength of six cores taken from the unconditioned beams on the testing day (one year after casting) was about 36.7 MPa, while core samples of the conditioned beams, indicated an average compressive strength of 37.3 MPa.

Table 4-1. Mechanical properties of the longitudinal GFRP reinforcement and the stirrups

Property	Longitudinal Bar	Stirrup[#]	Standard
Nominal bar size (mm)	12.7	9.5	
Actual cross-sectional area (mm^2)	146.8	84.2	CSA S806 annex A
Ultimate tensile strength (MPa)	756±13	816±19	CSA S806 annex C
Guaranteed tensile strength (MPa)	718	689	
Modulus of elasticity (GPa)	45.8	47.8	
Ultimate strain (%)	1.9±0.11	1.6 ±0.09	
Fiber content by weight (%)	80.9	77.5	ASTM D5028
Glass transition temperature (℃)	136	125.8	ASTM E1356
Cure ratio (%)	99.5	99.1	CSA S807
Moisture absorption at full saturation (%)	0.52	0.65	ASTM D570
Bar surface	Sand coated	Sand coated	

[#] Data corresponding to straight portions of bent bars
Note: Properties calculated based on nominal cross-sectional area.

4.2.3. Application of Sustained Load

The stressing level applied to the beams over 10 years was about 40% of the ultimate tensile strength of the GFRP bars. As shown in Fig. 4-3, this load was applied by clamping one pair of beams together with steel frames placed 50 mm from the beam ends and fastened together with 12.7 mm threaded bars. Two hollow steel sections (HSS) were placed between the beams 750 mm apart and 625 mm from the beam ends. These hollow steel sections could provide supports to the beams while separating them from each other. The length between

the two steel supports was under a constant bending moment. The magnitude of torque applied to the nuts at the end of each frame was verified with a load cell. The verification was aimed at relating the amount of torque to the applied load to achieve the correct amount of stress in each beam. The correlation between the torque and applied force can be seen in Fig. 4-4. In order to reach 40% of the ultimate tensile strength of the GFRP bars, each threaded steel rod should impose 13.1kN of load on the beam. Therefore, 13.6 N.m of torque was applied to the nuts. This produced 348 MPa of stress on the GFRP bar, while the stress on the concrete beam at 40% of the ultimate strength was 27.2 MPa. The clamping-mechanism force was readjusted twice a year for the first five years and annually for the rest of conditioning period to compensate for the creep and temperature deformations.

The conditioned beams cracked as a result of stressing, which was expected at 40% stress in the constant-moment zone. Note that cracking moment was determined to be about 9.54 kN.m, whereas the moment corresponding to 40% of ultimate load was around 15.01 kN.m. Fig. 4-5a-d indicate the status of the beams and the initial cracks—formed due to sustained loading—at the initial stages of conditioning. The initial cracks formed in the constant-moment zone in all the conditioned beams. As reported in Table 4-2, the crack widths—determined with a crack-measuring microscope—varied between 0.31 mm and 0.64 mm.

Table 4-2. The size of initial cracks

Beam	Crack Size (mm)		
	Crack 1	Crack 2	Crack 3
C1	0.45	0.64	n/a
C2	0.31	0.46	0.38
C3	0.52	0.39	n/a
C4	0.55	0.42	n/a

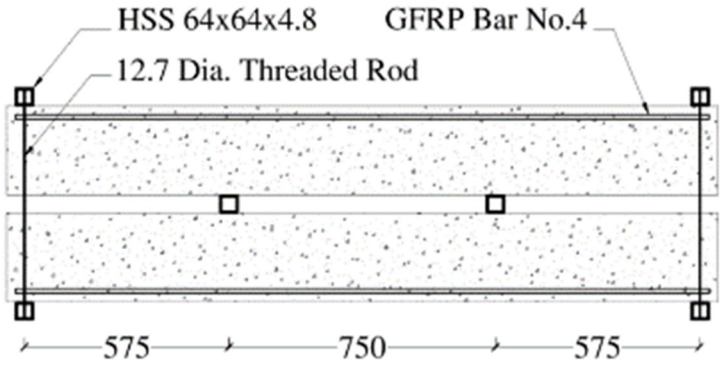

Fig. 4-3. Apparatus used to apply the sustained load (all dimensions are in mm)

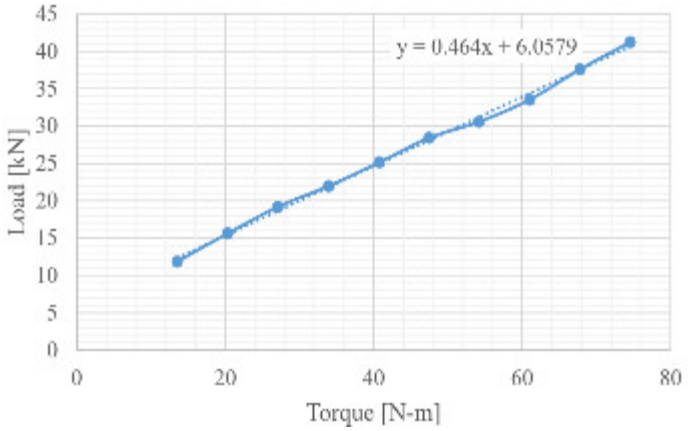

Fig. 4-4. Relationship between torque and applied load for the long-term stressing frames

Fig. 4-5. a) the beams under sustained load and natural weather conditioning (December 2008); b) the beams under sustained load and natural weather conditioning (October 2009); c) number of cracks formed along the length of a conditioned beam; d) a close-up photo of a crack

4.2.4. Test Setup and Instrumentation

The destructive phase of the experimental program was conducted using a four-point bending setup with a shear span identical to that used for the application of the sustained load as shown in Fig. 3-6. The testing was conducted with a 500 kN actuator with a displacement-controlled rate of 1.2 mm/min., while the variation of mid-span deflection was measured with two potentiometers. Moreover, the variation of crack width in the conditioned beams was recorded with a set of linear variable differential transformers (LVDTs) installed after the formation of early cracks. During testing, the variations of the load, potentiometers and LVDTs, were recorded using a programmed data acquisition system. In addition, crack formation along the side of the beams was marked and recorded.

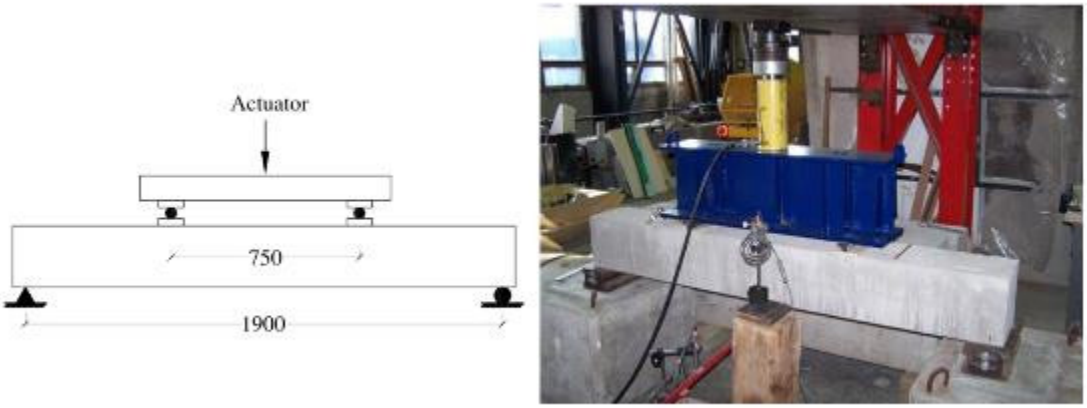

Fig. 4-6. A specimen under loading (dimensions are in mm)

4.3. Experimental Results and Discussion

After testing, the results of the conditioned beams were compared to their unconditioned counterparts in terms of flexural behavior, cracking pattern, and failure mode. The conditioned and unconditioned beams have failed with a similar behavior. As anticipated from their initial design, both have indicated a flexural–tension mode. Nonetheless, the crack spacing was found to be negligibly greater (average of 120±30 mm) in the conditioned beams. However, the total number of cracks in both the conditioned and unconditioned beams were identical, as illustrated in Figs. 4-7 and 4-8. This may refer to the adequate bond strength between the GFRP bar and concrete.

Fig. 4-7. Typical failure of the unconditioned beams

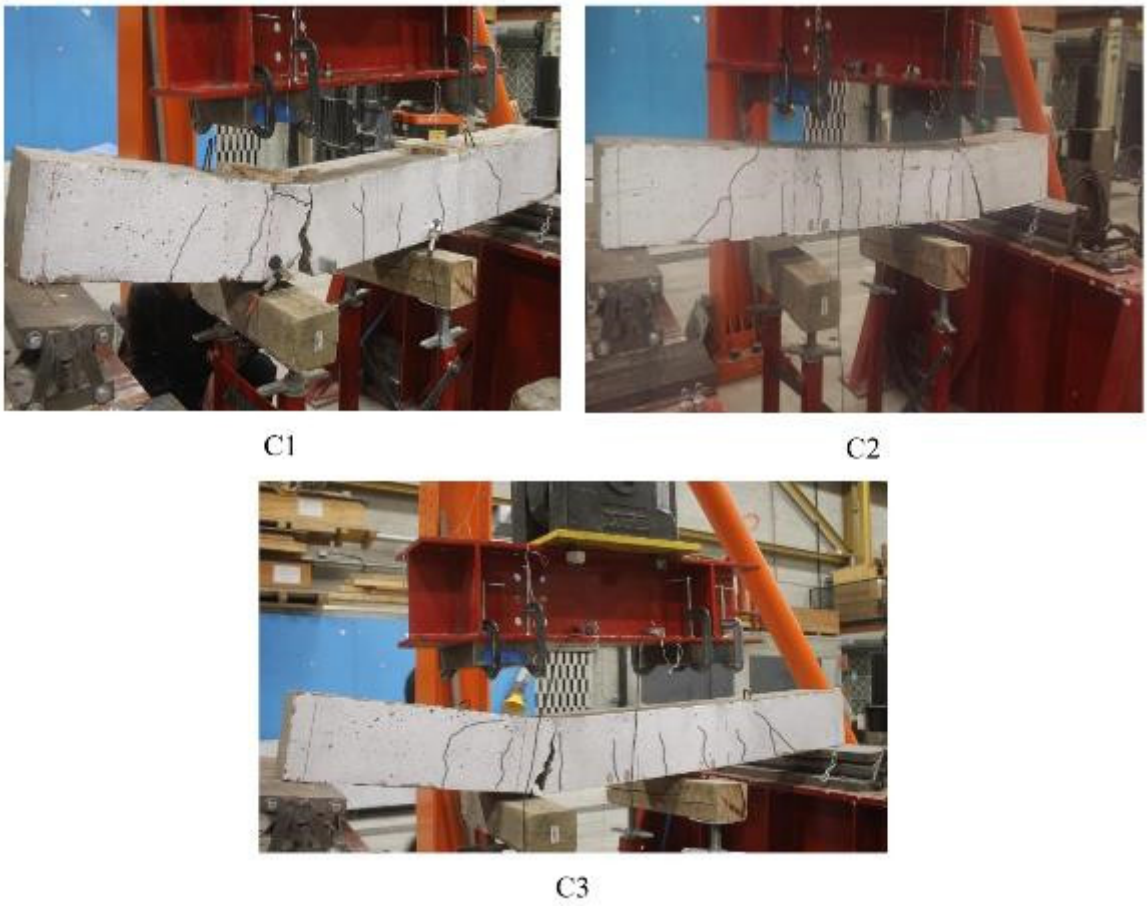

Fig. 4-8. Cracking patterns of the conditioned beams (C1, C2, and C3)

When GFRP bars are subjected to tensile tests, they usually exhibit a broom-like rupture (Benmokrane et al. 2002b; El-Hassan et al. 2017) due to individual fiber fracture over a large length of reinforcing bar. This is why, with flexural-tension failure of the beams, all the GFRP bars used in the aged beams experienced a different mode of failure with an almost flat fracture surface. The bars marked A and B in Fig. 4-9 are examples of the flat failure mode. A similar failure mode was also reported by Mukherjee and Arwikar (2006) for conditioned GFRP bars. A justification for this phenomenon can be failure over a short

length. When the bars are placed in concrete, a bunch of fibers are ruptured along a certain length by the surrounding concrete, whereas they rupture individually over a longer length during tensile testing.

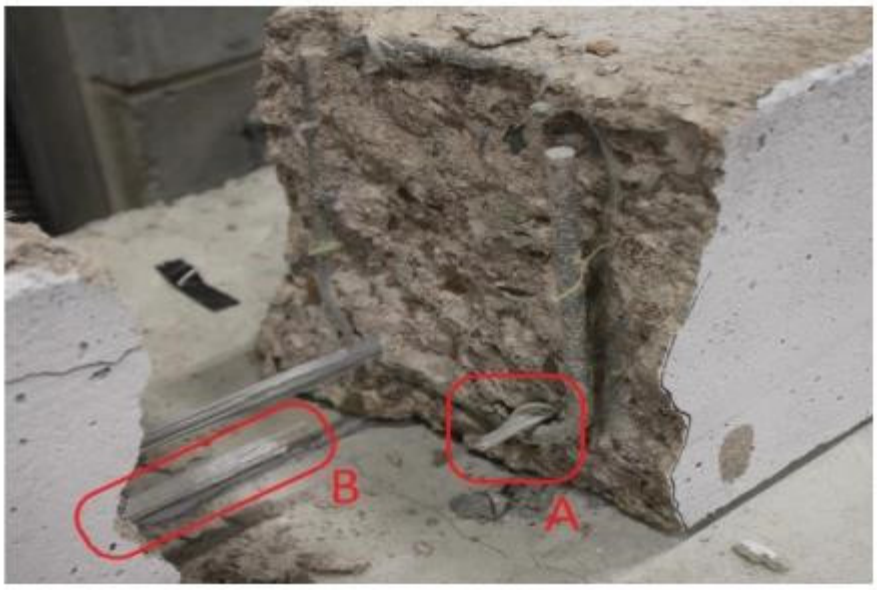

Fig. 4-9. Failure mode of GFRP bars in an aged beam

4.3.1. Moment-Deflection Response

The load–displacement responses of both the conditioned and unconditioned beams were similar before cracking, as indicated in Fig. 4-10. The general trend of the load–displacement curves was bilinear with a decrease in stiffness at the cracking point (M_{cr}). Since the sustained load imposed on the conditioned beams was higher than M_{cr}, the sections were already cracked. The remaining portions of the curves followed two slightly different paths for the unconditioned and conditioned beams. Table 4-3 summarizes the variations in the responses of beam. It should be noted that the results of the beams with the maximum capacities (U2 and C2) are compared. The stiffness, ultimate flexural strength, and deflection

at ultimate load of the conditioned beam (C2) were respectively, 4%, 16%, and 17% lower than those of the unconditioned beam (U2). This inferior flexural behavior can be attributed to the degradation of the GFRP reinforcement bars over time due to the creep and environmental effects.

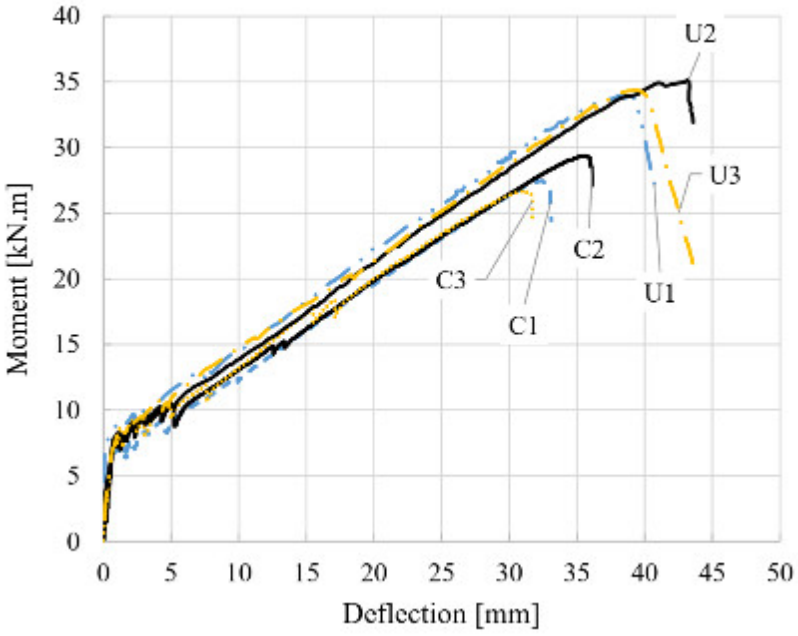

Fig. 4-10. Load–deflection curves for the unconditioned and conditioned beams reinforced with GFRP bars

Table 4-3. Values and variations in the flexural response of the beams reinforced with GFRP bars before and after conditioning

Beam No.	Ultimate Deflection (mm)			Ultimate strength (kN.m)			Stiffness (kN.m/m)		
	Uncond.	Cond.	Var.* (%)	Uncond.	Cond.	Var.* (%)	Uncond.	Cond.	Var.* (%)
1	37.8	32.	-17%	33.8	27.2	-16%	771	661	-4%
2	43.2	35.6		35.1	29.4		648.6	655.7	
3	39.4	31.2		34.3	26.5		885.2	666	
Average	40.2	33.3		34.4	27.7		780.2	660.9	
SD	2.1	2.1		0.65	1.5		100.6	5.15	
CV	5.2%	6.3%		1.9%	5.4%		112.8%	0.77%	

*Determined based on the flexural response of the beams with maximum capacities (U2 and C2)

4.3.2. Bond Interface

The similar cracking patterns (in terms of both number of cracks and spacing) and the slight change in stiffness of the conditioned and unconditioned beams can refer to negligible effect more than 10 years of conditioning had on the bond strength. However, the bond condition between the GFRP bar and concrete was assessed based on illustrations of the optical microscopy and scanning electron microscopy (SEM). For this purpose, a thin layer of concrete was cut obliquely from a concrete-core sample. To consider the influence of sustained stress intensity (i.e., stress levels of 0% to 40%), the core samples were extracted from both the conditioned and unconditioned beams at different stress levels, as well as from the beam tested to failure, as shown in Fig. 4-11. Then a circular core containing a portion of GFRP (an oval section) and concrete was drilled out. Fig. 4-12 shows the samples extracted for the SEM and optical microscopy analyses.

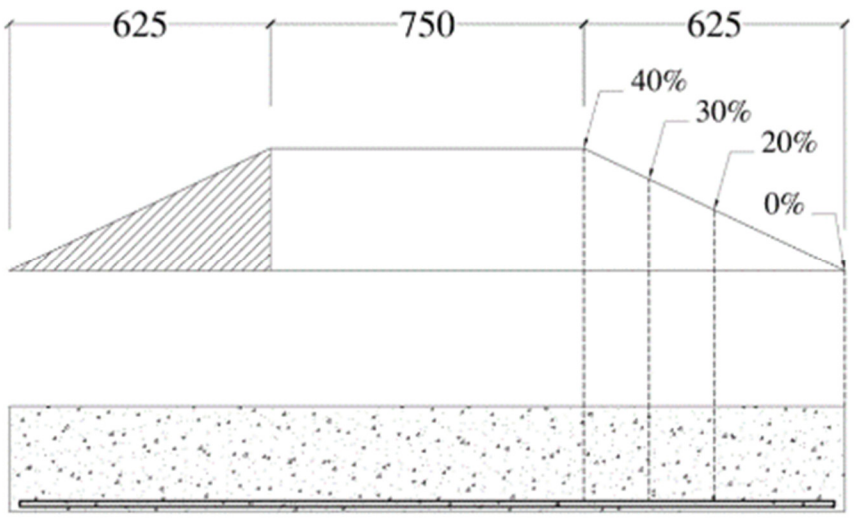

Fig. 4-11. The moment diagram of the beams and positions of the different stress levels (all dimensions are in mm)

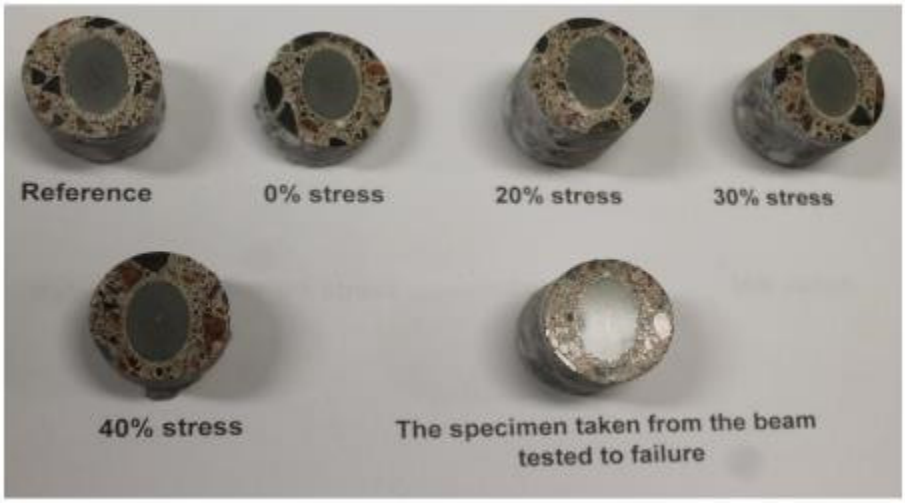

Fig. 4-12. Illustration of drilled samples

Optical microscopy of the bond condition at different stress levels has not indicated any damage to the GFRP bar–concrete interface. As observed in the magnified shots of Figs. 4-13a-f, the interface between the bar and concrete has not changed over time, and an intact connection still existed between the bar and concrete interface after 10 years of exposure to adverse natural environmental conditions at different levels of sustained stresses.

Nevertheless, this conclusion was also rigorously examined with SEM analysis at higher rates of magnification. Thus, Figs. 4-14a-f compare shots of the specimens at different stress levels with that obtained from the control specimen using SEM. The results confirm the findings of the optical microscopy, since an intact bond was observed at the bar–concrete interface with the control bar and, in general, for all the specimens taken from the conditioned beams at different stress levels. Some minor scattered detachments were observed in the specimen taken at a stress level of 30% (Fig. 4-14d). Since these detachments were not continuous along the interface, they might be attributed to the sample preparation process.

Fig. 4-14f shows the bonding conditions for the bars taken from conditioned beam C2 after failure under the flexural testing. This sample was taken as close as possible to the section in which the beam failed (100 mm). The bonding condition of the sample extracted from the beams that failed in flexure was still promising. This indicates that the bond remained intact even in the vicinity of the rupture and failure point of the bar.

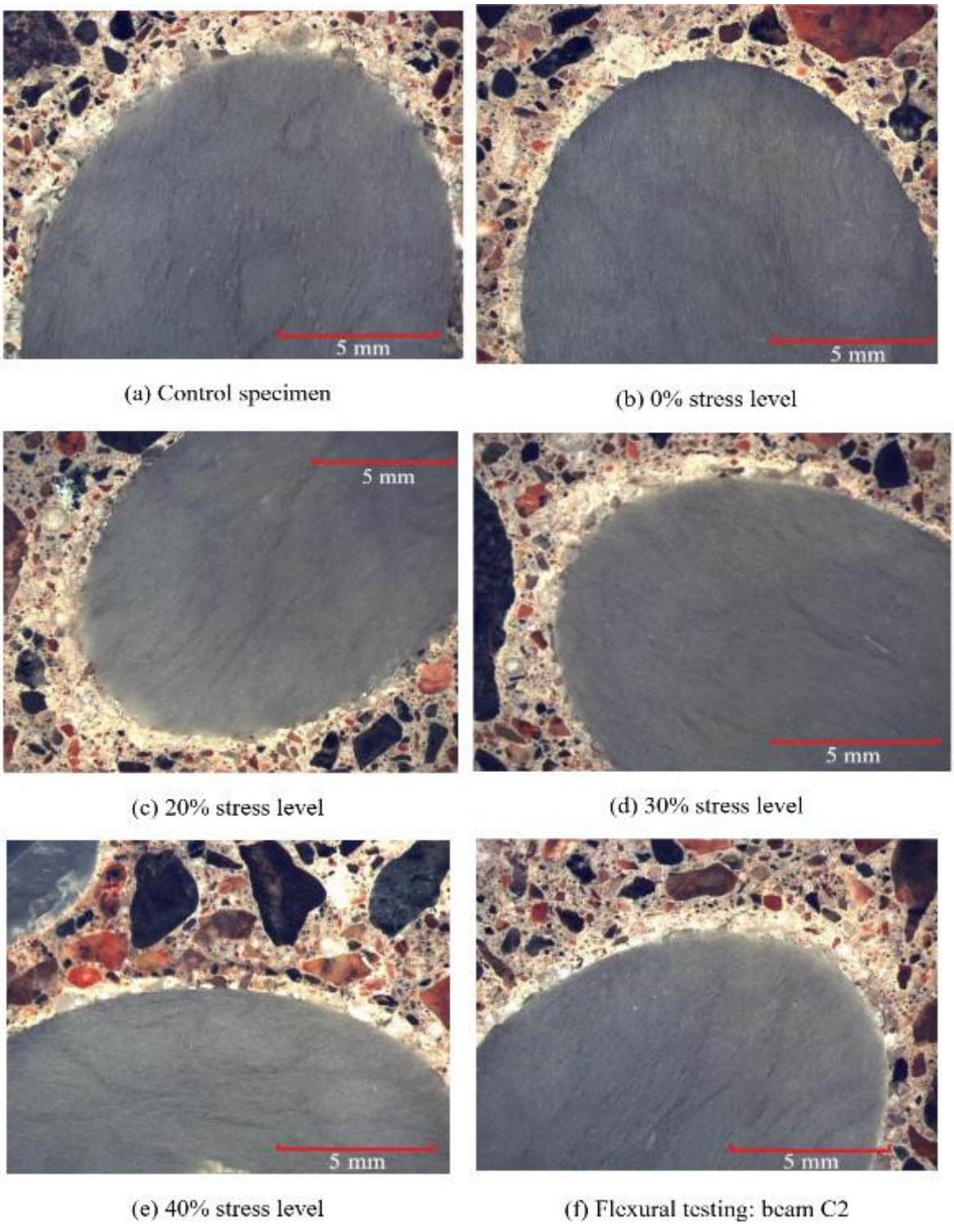

Fig. 4-13. Images taken by optical microscopy of the specimens at different stress levels

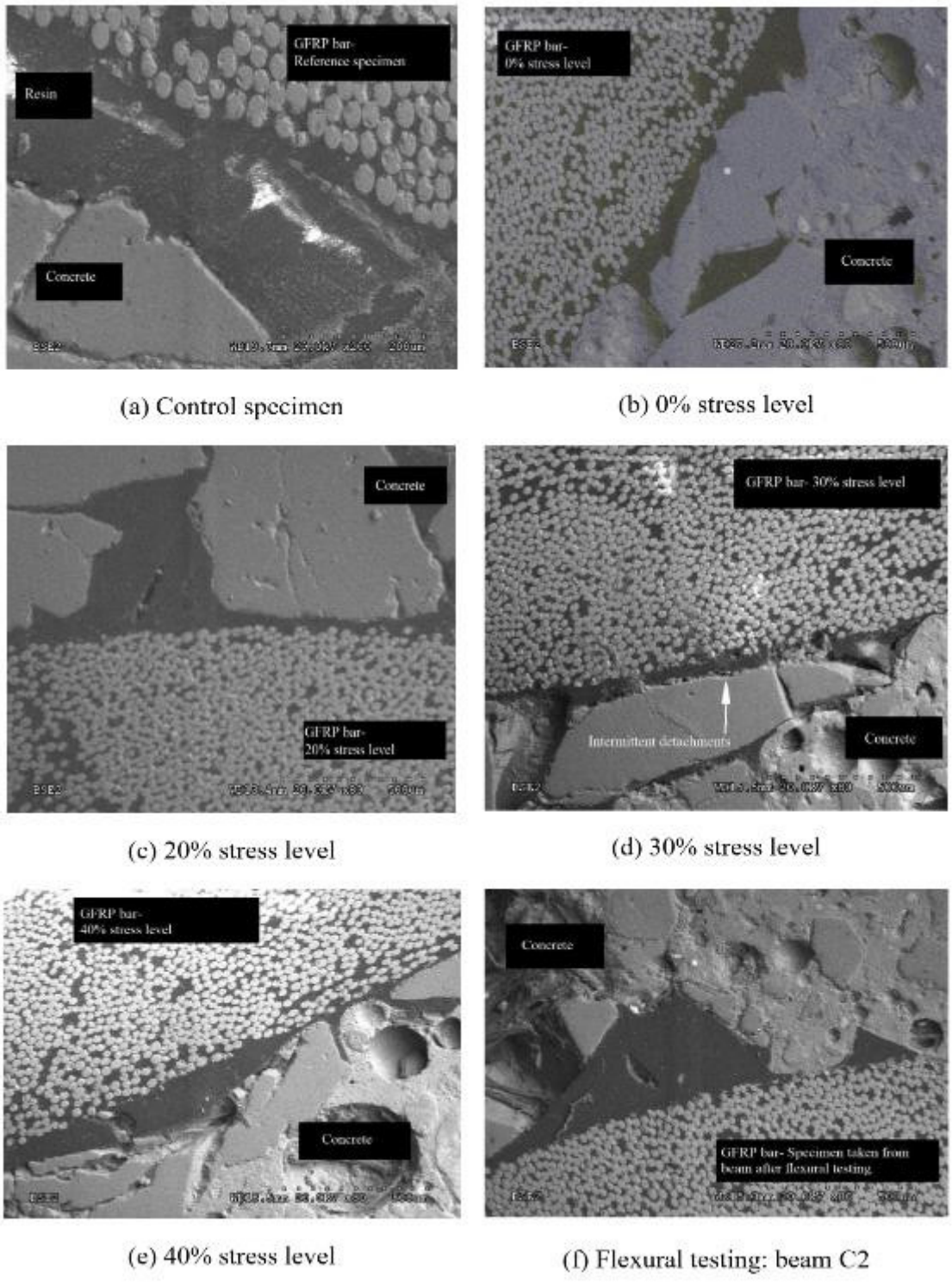

Fig. 4-14. Images taken with SEM of the specimens at different stress levels at 80 times magnification

4.3.3. Differential Scanning Calorimetry

The objectives of differential scanning calorimetry (DSC) analysis were to obtain the glass transition temperature (T_g) and cure ratio in accordance with ASTM E1356 (ASTM 2014) and CSA S807 (CSA 2019b), respectively. Resin matrix degradation can decrease T_g, since the polymeric chains might rupture due to hydrolysis reactions taking place in the presence of alkalis. In addition, water can reduce T_g since it has plasticizing effect on the resin. On the other hand, cure ratio can also be measured with DSC analysis. If the composite material has not been properly cured during the manufacturing process, subsequent crosslinking might occur in the polymeric chains during the concrete curing process. This is mainly attributed to the elevated temperature caused by the cement hydration. The T_g of an optimally cured composite material is expected to be higher than that with a lower cure ratio. This is due to the formation of a sound crosslinking network in the polymeric chains of an ideally cured composite material (Kumar et al. 2015).

Herein, the glass transition temperature (T_g) of the GFRP bars was determined according to the procedure described in ASTM E1356 (ASTM 2014). The measurements were conducted under air on a TA DSC apparatus between 40°C and 200°C at a heating rate of 20°C/min. The samples used for T_g were extracted from the control bars (taken from the unconditioned beam), and the conditioned bars located at sustained stress levels of 0% and 40% (taken from the conditioned beam). If noticeable decreases in T_g were observed due to a likelihood of degradation, more samples at other stress levels (20%, 30%, 35%, etc.) were to be incorporated in the analysis. For each type, five GFRP samples were taken to obtain more precise results. Moreover, all the GFRP test samples for DSC analysis were saturated before

testing in accordance with CSA S807 (CSA 2019b). For this purpose, the GFRP samples were immersed in distilled water at 50°C for saturation in accordance with ASTM D570 (ASTM 2018). After full saturation, the increase in bar weight due to water absorption was less than 1%.

Table 4-4 summarizes the values of T_g and cure ratios obtained. Fig. 4-15 shows a typical calorimetry result from DSC analysis. In this figure, '*Delta Cp'* refers to the difference between the heat capacity of the sample and the reference. The term '*Half Cp Extrapolated'* is the method used by the software to calculate T_g. This method is measured by midpoint temperature (T_m), which is the point on the thermal curve corresponding to 1⁄2 the heat flow difference between the extrapolated onset and extrapolated end. Moreover, the term Endo in the label of the vertical axis, Heat Flow Endo Up, refers to endothermic. Endothermic means heat flows into the sample (*Cp* increasing) as a result of heating or an endothermic process, e.g. glass transition.

According to CSA S807 (CSA 2019b), the minimum values of T_g and cure ratio are equal to 110°C and 95% for bars with high durability resistance (*D1*). Considering the obtained results, all of the conditioned and control specimens had shown values higher than the limit requirement of CSA S807 (CSA 2019b). In addition, no sign of post-curing issue was observed, because the resin had been fully cured during the manufacturing process. The T_g value dropped from 136°C for the control specimens to 126.5°C for the conditioned specimens with 40% sustained stress. This decrease (6.9%) in the T_g values of the conditioned GFRP specimens was still very low and cannot be attributed to resin degradation, as proven below with FTIR analysis.

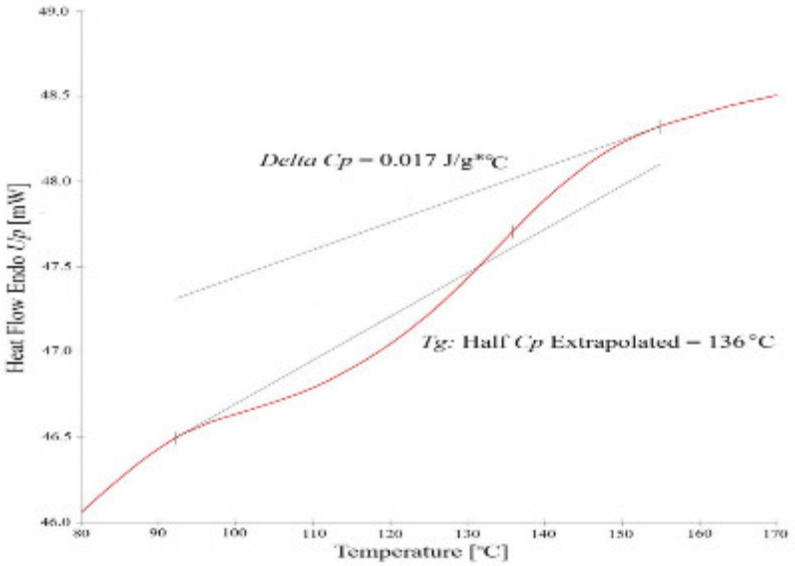

Fig. 4-15. A typical calorimetry curve indicating 100% cure ratio of the GFRP bar

Table 4-4. Average values of T_g and cure ratios obtained from DSC tests

Specimens	T_g (°C)	Cure Ratio (%)
Control	136	100
0% stress level	128.1	100
40% stress level	126.5	100
Average	130.3	
Standard deviation	5.3	

4.3.4. FTIR Analysis

The presence of alkaline ions within concrete may cause degradation of the GFRP bars. The degradation reaction occurs as a result of hydroxylation of the polymer. Hydroxyl ions (OH^-) attacking the polymer chains of the resin matrix can result in the formation of alcohols or carboxylic acids (hydroxyl groups). A common approach to determine the occurrence of hydrolysis reactions is conducting FTIR testing.

Vinyl-ester resins are known to be highly resistant to chemical attacks (Nkurunziza et al. 2005). Since this resin inherently contains hydroxyl groups, a stretch of hydroxyl appears in the graphs. Any variations between the results obtained from the conditioned and unconditioned specimens within the range of the hydroxyl band can be an indication of hydroxylation. Fig. 4-16 shows the results of FTIR tests on the unconditioned and conditioned GFRP bars at different stress levels. Comparison of the spectra clearly shows no difference between the graphs. Therefore, no signs of degradation were observed in the resin matrix. This finding, once again, proves that vinyl-ester resin has reliable durability to moisture diffusion and alkali attacks.

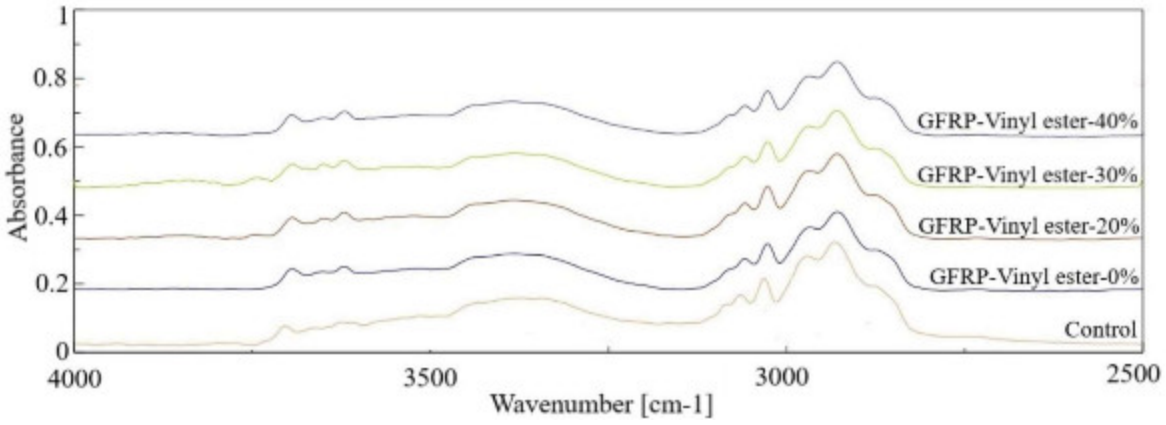

Fig. 4-16. FTIR spectra of the unconditioned and conditioned GFRP bars at different stress levels

4.3.5. Interlaminar Shear Strength

The interlaminar shear strength is a mechanical property representing the resistance of the resin and fiber interface. Micelli and Nanni (2004) indicated that the decrease in apparent horizontal shear strength of the conditioned GFRP bars resulted from potential damage to the resin can be caused by penetrating fluids. There is a positive relationship between the

quantity of degraded and broken fibers on the surface and lower failure load in the interlaminar shear test.

The interlaminar shear test was performed according to ASTM D4475 (ASTM 2016) on short GFRP bar segments taken from different stress levels along the length of the beams (U4, C4). The test was carried out with MTS 810 testing machine equipped with a 500 kN load cell with a controlled displacement rate of 1.3 mm/min. Three replicates from each stress level were prepared and tested. As the nominal diameter of the bars was 12.7 mm, the span length was set to 63.5 mm (five times the nominal diameter of the GFRP bar). Fig. 4-17a provides an illustration of the test setup. The applied load and displacement magnitudes were recorded using a data acquisition system. The interlaminar shear strength (S_u) of the bars was determined according to ASTM D4475 (ASTM 2016).

Table 4-5 provides a summary of the results for the specimens at different stress levels. All the specimens showed horizontal planes of failure perpendicular to the loading plane and cross section, as depicted in Figs. 4-17b-h. The test results show that none of the specimens subjected to natural weathering and sustained stress experienced a degradation in the interlaminar shear strength as a result of conditioning. In addition, the failure modes of all the bars were similar. Accordingly, the residual properties of the conditioned specimens remained the same as or even higher than those measured for the control ones. The conditioned specimens having slightly higher strength values than the control specimens might be due to the inherent discrepancy in the experimental results. It is also worth noting that the interlaminar shear strength values obtained for the GFRP bars in this study—which represent the early generation of GFRP bars—are comparable with that of the new

generation. For instance, the interlaminar shear results obtained by Benmokrane et al. (2017) for No. 4 GFRP bars (52.9 MPa) are approximately the same as the results of the current study.

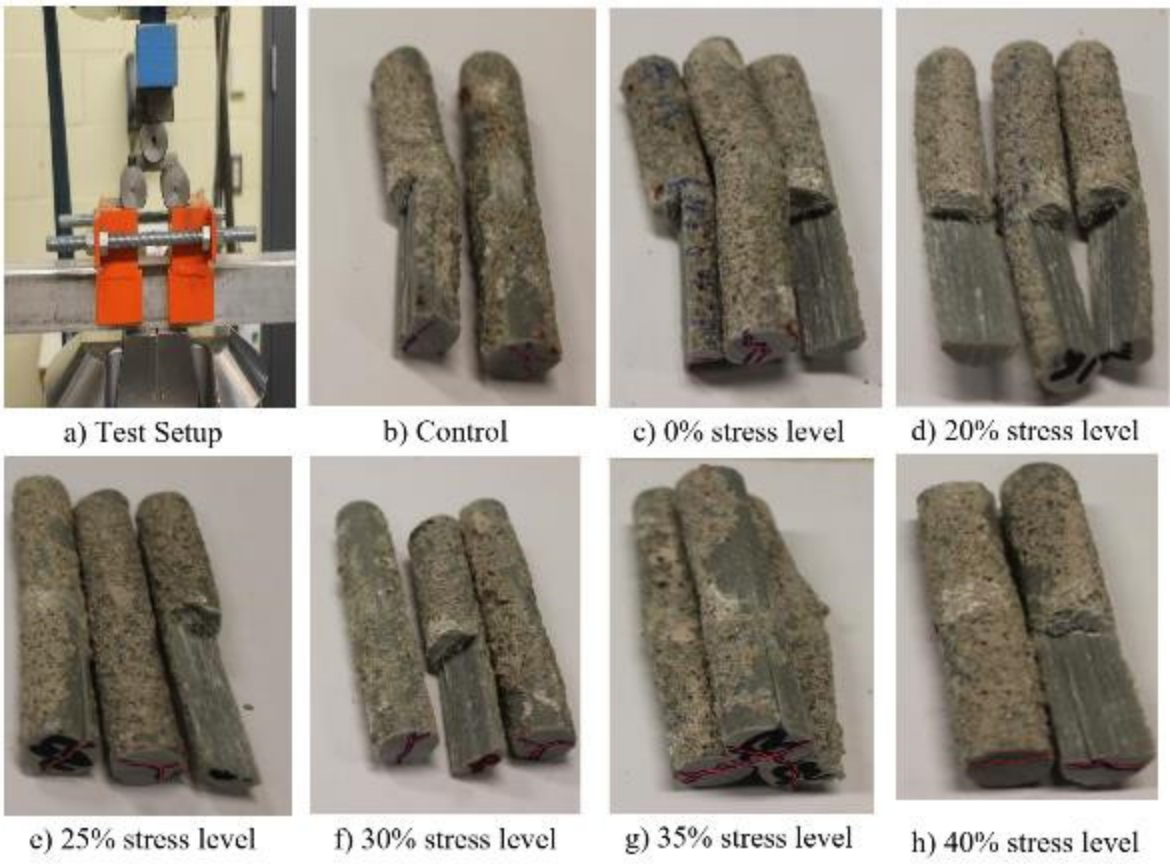

Fig. 4-17. Interlaminar shear test setup and mode of failure of the specimens extracted from different stress levels along the length of the beams (U4, C4)

Table 4-5. Results of the horizontal shear test performed on the GFRP bars extracted from different stress levels

Samples	Control	0%	20%	25%	30%	35%	40%
Apparent shear strength (MPa)	50.0	53.7	50.4	51.5	51.7	56.4	59.4
	52.5	56.1	57.1	56.4	51.7	57.2	55.2
	58.4	55.0	51.5	58.0	58.6	55.5	49.0
Mean value of Strength (MPa)	53.6	54.9	53.0	55.3	54.0	56.3	54.5
Standard deviation	4.3	1.2	3.6	3.4	4.0	0.8	5.3
Coefficient of variation (%)	8.1	2.2	6.8	6.1	7.4	1.5	9.7

4.4. Analytical Evaluation

This section describes the flexural behavior of the tested beams in terms of predicted moment–deflection response and crack width.

4.4.1. Deflection

Despite the superior corrosion resistance and high strength of FRP bars than steel, they possess lower modulus of elasticity. This feature results in a substantial loss of stiffness in an FRP RC beam that has reached the cracking moment (M_{cr}). As the modulus of elasticity is inversely proportional to deflection, unacceptable deflections might be observed in an FRP RC beam under service conditions. Thus, the design of such members is usually governed by serviceability limit states, including the maximum allowable deflection and crack width (Mota et al. 2006). For this reason, calculations related to the deflection of FRP reinforced beams are a common part of the design procedure.

ACI440.1R (ACI 2015) suggests an expression for the effective moment of inertia of FRP RC members that originated from Bischoff and Gross (2011) and defined by

$$I_e = \frac{I_{cr}}{1 - \gamma\left(\frac{M_{cr}}{M_a}\right)^2\left[1 - \frac{I_{cr}}{I_g}\right]} \leq I_g \tag{1}$$

where γ is a parameter reflecting the variation of curvature (accounting for variation of stiffness) along the length of member. For a beam subjected to four-point loading, the expression is given as

$$\gamma = \frac{3\left(\frac{a}{L}\right) - 16\left(\frac{M_{cr}}{M_a}\right)\left(\frac{a}{L}\right)^2 + 12\left(\frac{a}{L}\right)^3}{3\left(\frac{a}{L}\right) - 4\left(\frac{a}{L}\right)^3} \tag{2}$$

Fig. 4-18 compares the distribution of the experimental deflections for all three conditioned beams with those calculated according to ACI440.1R (ACI 2015). Despite some minor discrepancies, the predictions of ACI440.1R (ACI 2015) model fits the curves of the conditioned beams with a reliable accuracy, provided that the environmental coefficient factor is employed in the prediction model.

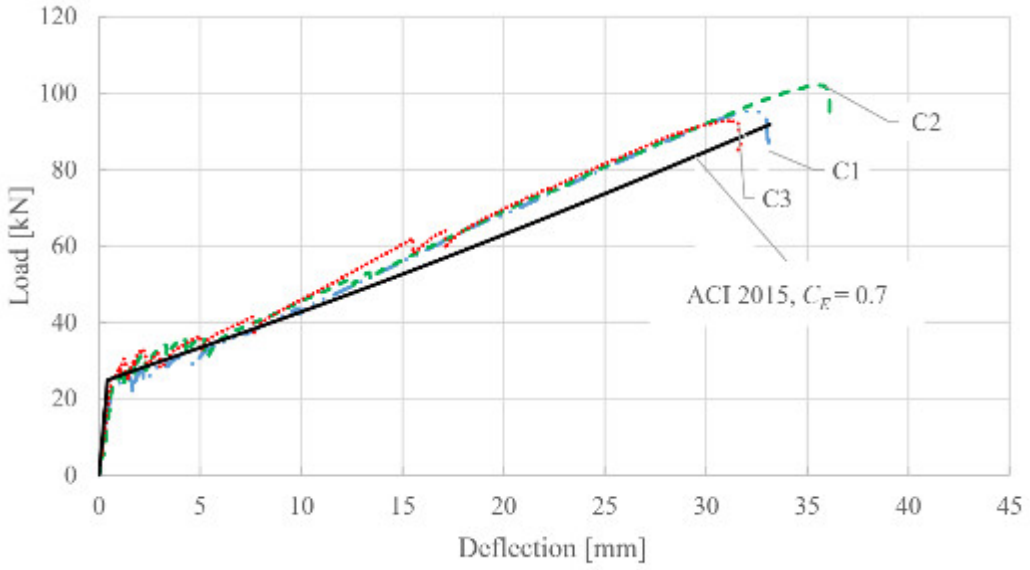

Fig. 4-18. Comparison of the deflection values obtained from experimental tests with those predicted by ACI440.1R (ACI 2015) model for the conditioned beams

4.4.2. Crack Width

As the crack width values were not available for the unconditioned beams of the present study, a clear comparison could not be made between the conditioned and unconditioned beams. However, for comparison purpose, our study used the expression stipulated in CSA S6 (CSA 2019a) to evaluate the crack width in the unconditioned beams which is defined by

$$w = 2\frac{f_f}{E_f}\frac{h_2}{h_1}k_b\sqrt{{d_c}^2 + (0.5s)^2} \qquad (3)$$

In the above equation, the value of k_b—which is known as the bond-dependent coefficient—was obtained from technical literature (Thériault and Benmokrane 1998; Tobbi et al. 2012). Two studies conducted by Shield et al. (2019) on GFRP bars from the same manufacturer with the same bar size as those used in the present study as well as a study by McCallum

(2013) on No. 5 GFRP bars from the same manufacturer were considered. The former investigation proposed a k_b of 0.84, the latter a k_b of 1.07. For the beams tested in the current study, the concrete cover and spacing of longitudinal reinforcement were 25 and 167 mm, respectively. Moreover, the crack widths were measured on the side of the beams at the same level as the longitudinal reinforcement.

Fig. 4-19 compares the predicted crack width of the unconditioned beams with those measured during testing of the conditioned beams. Despite some discrepancies that might be attributed to the inherent feature of the concrete and analytical prediction, the crack-width curves of the conditioned beams (C1, C2, and C3) were analogous with the predictions provided by both k_b values adopted.

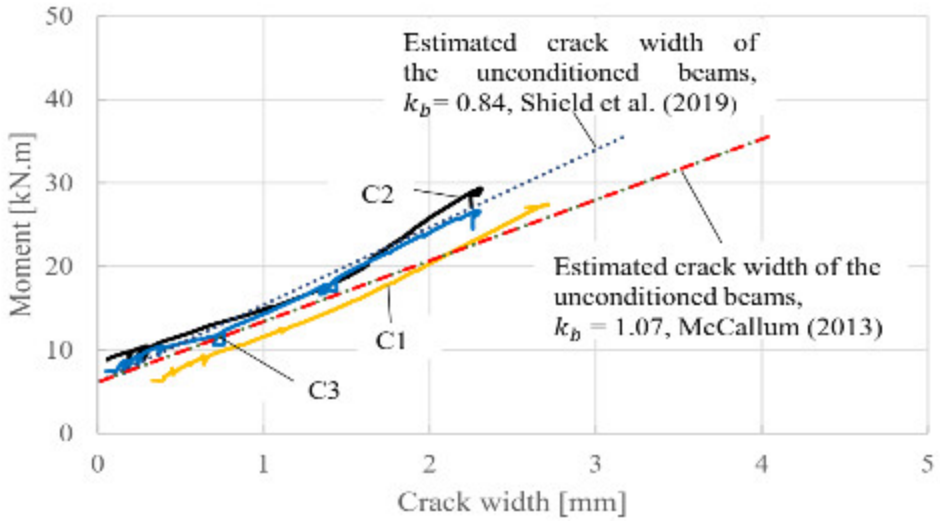

Fig. 4-19. Comparison of the crack widths of the unconditioned beams (calculated values) and the conditioned beams (experimental values)

4.5. Conclusions

A total of eight RC beams (four unconditioned and four conditioned beams) were constructed using early generation of sand coated GFRP bars. The conditioned beams were exposed to the combined effect of natural environmental conditioning and high sustained bending stress (40% of the ultimate tensile strength of the GFRP bars) for 10 years in a field site in Halifax (Nova Scotia, Canada). During the exposure, the conditioned beams sustained temperature fluctuations ranging from -25°C to 35°C with numerous freeze–thaw and wet–dry cycles. In order to achieve the objectives of this study, two sets of tests were carried out: (1) destructive testing in which the structural flexural behavior of the beams up to the failure was evaluated using a four point bending setup and (2) non-destructive testing in which physiochemical changes in the GFRP bar properties due to the likelihood of degradation were examined on the microstructural scale. Based on the obtained results, the following conclusions can be drawn:

1- The outcomes indicate a strength reduction of only 16% in the tested beams despite the high level of sustained load applied to the GFRP RC beams. Since the maximum stress at serviceability limit states specified in CSA S806 (CSA 2012) is based on the guaranteed tensile strength, the amplitude of the applied stress to the GFRP bars considered in our study was even higher than 40% of the characteristic value. This value is almost double the allowable maximum stress specified in CSA S806 (CSA 2012).
2- The analytical model proposed in ACI440.1R (ACI 2015) could predict the short term deflection of the conditioned beams with a reliable accuracy.

3- The similar number and spacing of the cracks, as well as the slight change in stiffness of the conditioned and the unconditioned beams, can relate to the negligible effect of conditioning on the bond strength. The results of the optical microscopy and SEM analysis on the conditioned beams also reconfirmed this conclusion at all targeted stress levels.

4- The T_g, infrared spectra of the FTIR, and interlaminar shear strength values for the GFRP bars from the beams under natural conditioning for 10 years remained almost unchanged for the cores extracted from the GFRP bars at all targeted stress levels (0% to 40%).

5- This study involved an early generation of GFRP bars. Since the quality, physical properties, mechanical properties, and durability performance of more recent generations have improved, it can be supposed that the thresholds specified for GFRP stress limits in design codes are conservative. It should be noted, however, that the experimental results were based on the limited number of tested beams. Additional tests need to be conducted with the new generation of GFRP bars to assess and support these findings.

NOTATION

d_c = distance from the centroid of the tension reinforcement to the extreme tension surface of concrete, mm

E_c = elastic modulus of concrete

E_f = elastic modulus of FRP bar

E_s = elastic modulus of steel

f_f = stress in the tension FRP reinforcement

f_{fu}^* = guaranteed ultimate tensile strength of the FRP product

h_1 = distance from the centroid of tension reinforcement to the neutral axis

h_2 = distance from the extreme flexural tension surface to the neutral axis

I_{cr} = moment of inertia of cracked section transformed to concrete

I_e = effective moment of inertia

I_g = moment of inertia of the gross section

k_b = coefficient depending on bond between the FRP and concrete

L = span of the beam

L_a = distance from the support

M_c = moment corresponding to a maximum concrete compressive strain of 0.001 in the section

M_{cr} = cracking moment

M_{ult} = ultimate moment capacity of the section

P = total concentrated load

s = spacing of tensile reinforcement

S_u= interlaminar shear strength

$\varepsilon_{fu}{}^{*}$= guaranteed rupture strain of the FRP product

CHAPTER 5 GENERAL CONCLUSIONS AND RECOMMENDATIONS

5.1. Summary

This thesis presents the results of two sets of experimental investigation including a) 150 GFRP bar specimens tested for creep rupture strength assessment; and b) eight GFRP-RC beams tested for evaluation of retained flexural strength after 10 years natural weathering. The former experiment was performed on the new generation of GFRP bars in laboratory setting and the latter experimental program was a field study and carried out on an earlier generation of GFRP bars. The main objective of this study was to assess the long-term performance of GFRP bars subjected to various environmental conditions under high sustained loads.

The first phase (Phase I) evaluated a design creep strength and environmental coefficient factor of GFRP bars through performing creep test on 150 bar specimens made of ECR fibers and vinyl ester resin. The bars were exposed to three different environmental conditions, and concurrently applied sustained load ranging from 40% to 90% UTS. The conditioned bars were exposed to a) normal laboratory conditions, b) immersed in alkaline solution with normal laboratory conditions at 23˚C, and c) immersed in alkaline solution with elevated temperature of 60˚C.

In the second phase (Phase II), a total of eight RC beams (four unconditioned and four conditioned beams) were constructed using early generation of sand-coated GFRP bars. The conditioned beams were exposed to the combined effect of natural environmental conditioning and high sustained bending stress (40% of the ultimate tensile strength of the GFRP bars) for 10 years in a field site in Halifax (Nova Scotia, Canada). During the exposure, the conditioned beams sustained temperature fluctuations ranging from -25°C to 35°C with numerous freeze–thaw and wet–dry cycles. In order to achieve the objectives of this study, two methods of performing test were considered: (1) destructive testing in which the structural flexural behavior of the beams up to the failure was evaluated using a four point bending setup and (2) non-destructive testing in which physiochemical changes in the GFRP bar properties due to the likelihood of degradation were examined on the microstructural scale.

5.2. Conclusions

Based on the experimental testing and the analysis conducted in this research program, the following conclusions are drawn:

5.2.1. Assessment of Creep Rupture Strength of GFRP Bars Subjected to Different Environmental Exposures under Sustained Loads

1- The consistency of Weibull distribution in accounting for variabilities of creep test of GFRP composite materials was verified by a correlation of coefficient of more than 95% for the predicted and experimental data points.

2- The extrapolation of the creep-rupture results of GFRP bars from Group A with sizes #3, #4, #5A and #5B at 10^6 h endurance time resulted in mean creep-rupture strengths equal to 47%, 48%, 50%, 51% UTS, respectively. These values were decreased due to additional exposure to alkaline solution at 23°C by 3%, 8%, 13%, and 11% UTS for GFRP bars #3, #4, #5A and #5B, respectively (i.e. the extrapolated creep-rupture strengths were 44%, 40%, 37% and 40%, respectively). Moreover, when increasing the conditioning temperature to 60°C, the extrapolated mean creep strengths of bars #4 and #5A were 32% and 29% UTS, showing a reduction of 16% and 21%, respectively, in respect to the sole creep-rupture test results of the same bars.

3- It was evident that larger bar size exhibited higher degradation rate than smaller bar in all conditioning groups. Therefore, it can be concluded that the correlation between the bar diameter and creep strength reduction is reverse.

4- A guaranteed creep-rupture threshold associated with the 99.9th strength percentile at an endurance time of 106 h equal to 0.41 can be used for the tested bars (#3, #4, #5A, and #5B). This value is approximately 37% and 105% higher than the 0.30 and

0.2 coefficients currently recommended by AASHTO LRFD (2018) and the ACI 440.1R (2015), respectively

5- The guaranteed creep-rupture strengths at 106 h endurance time obtained for the bars exposed to conditioning Group B and C showed that the product of the environmental factors (*CE* = 0.8 for members not exposed to earth or weather) multiplied by creep rupture strength limits (*Cc* = 0.2-0.3) were conservatively above the creep strength limits by the codes. The resulted $C_c \times C_E$ at an endurance time of 10^6 h of the tested GFRP bar in Group B was at least 0.3, which is 25% and 87% higher than the limits required by the AASHTO LRFD (2018) and ACI 440.1R (2015). Furthermore, the obtained design creep-rupture limit (0.30) at 23°C is 20% higher than that required by Canadian Standards [CSA S806 (2012), CSA S6 (2019)] of 25% GTS.

6- The results showed that a *CE* factor of 1 can be used with the creep rupture limits specified by the codes for GFRP bars not exposed to earth or weathering. A lower *CE* factor was obtained for GFRP bars conditioned at 60°C temperature that have been used in the current study as accelerated again, however, such a high service temperature is rarely existing.

7- The microstructural observations on functioning GFRP bars under sustained loads of 50% UTS did not show a significant difference between the bars of conditioning Group B and their associated control specimens (intact bars). This confirms that the degradation process becomes slower at lower sustained loads.

5.2.2. Performance of GFRP-RC Beams Subjected to High Sustained Load and Natural Aging for 10 Years

8- The outcomes indicate a strength reduction of only 16% in the tested beams despite the high level of sustained load applied to the GFRP RC beams. Since the maximum stress at serviceability limit states specified in CSA S806 (2012) is based on the guaranteed tensile strength, the amplitude of the applied stress to the GFRP bars considered in our study was even higher than 40% of the characteristic value. This value is almost double the allowable maximum stress specified in CSA S806 (2012).

9- The analytical model proposed in ACI 440. 1R (2015) could predict the short-term deflection of the conditioned beams with a reliable accuracy.

10- The similar number and spacing of the cracks, as well as the slight change in stiffness of the conditioned and the unconditioned beams, can relate to the negligible effect of conditioning on the bond strength. The results of the optical microscopy and SEM analysis on the conditioned beams also reconfirmed this conclusion at all targeted stress levels.

11- The T_g, infrared spectra of the FTIR, and interlaminar shear strength values for the GFRP bars from the beams under natural conditioning for 10 years remained almost unchanged for the cores extracted from the GFRP bars at all targeted stress levels (0% to 40%).

12- This study involved an early generation of GFRP bars. Since the quality, physical properties, mechanical properties, and durability performance of more recent generations have improved, it can be supposed that the thresholds specified for GFRP

stress limits in design codes are conservative. It should be noted, however, that the experimental results were based on the limited number of tested beams. Additional tests need to be conducted with the new generation of GFRP bars to assess and support these findings.

5.3. Recommendations for Future Work

The current research demonstrated the acceptable durability performance of the tested GFRP bars. It, also, provided an understanding of the durability behavior of GFRP bars and the variables that affect their performance. The scope of this investigation was limited to the test conditions and parameters studied herein. Consequently, further research investigations should be conducted in this field, some suggested recommendations for future work are as follows:

- A similar experiment as the phase I can be performed to investigate the combined effect of environmental conditioning and sustained load using retained strength method. It can be postulated that the effect of conditioning in strength reduction is more pronounced when the sustained load level is low.
- New microstructural testing techniques should be developed to examine the in-service structures with more precession.
- The same experiment as the phase II of the study can be performed in 20-30 years-time to estimate the actual life span of the GFRP bars embedded in concrete exposed to natural harsh weathering.

- More experimental field studies are needed to investigate the durability performance of GFRP-RC structures.

5.4. Résumé

Cette thèse présente les résultats de deux séries de recherches expérimentales comprenant : a) 170 échantillons de barres de PRFV testés pour l'évaluation de la résistance à la rupture par fluage, et b) huit poutres en béton armé de PRFV testées pour l'évaluation de la résistance retenue à la flexion après 10 ans d'exposition aux intempéries naturelles. La première série d'essais a été réalisée sur la nouvelle génération de barres de PRFV en laboratoire et le second programme expérimental était une étude de terrain et a été réalisé sur une génération antérieure de barres de PRFV. L'objectif principal de cette étude était d'évaluer la performance à long terme des barres de PRFV soumises à diverses conditions environnementales et charges soutenues élevées.

La première phase (phase I) a évalué la résistance au fluage et le coefficient environnemental des barres de PRFV en effectuant un essai de fluage sur 170 barres fabriquées à l'aide de fibres de type ECR et de résine vinylester. Les barres ont été exposées à trois conditions environnementales différentes et ont été soumises simultanément à une charge soutenue allant de 40 à 90 % de la résistance ultime à la traction des barres. Les barres conditionnées ont été exposées à : a) des conditions normales de laboratoire, b) immersion dans une solution alcaline dans des conditions normales de laboratoire à 23°C, et c) immersion dans une solution alcaline à une température élevée de 60°C.

Dans la deuxième phase (Phase II), huit poutres en béton armé (quatre poutres non conditionnées et quatre poutres conditionnées) ont été fabriquées en utilisant la première génération de barres de PRFV revêtues de sable. Les poutres conditionnées ont été exposées à l'effet combiné d'un conditionnement environnemental naturel et d'une contrainte de flexion soutenue élevée (40 % de la résistance ultime à la traction des barres de PRFV) pendant 10 ans sur un site à Halifax (Nouvelle-Écosse, Canada). Pendant l'exposition, les poutres conditionnées ont subi des fluctuations de température allant de -25°C à 35°C avec de nombreux cycles de gel-dégel et de séchage par voie humide. Afin d'atteindre les objectifs de cette étude, deux méthodes d'essais ont été envisagées : (1) un essai destructif dans lequel le comportement structural en flexion des poutres jusqu'à la rupture a été évalué en utilisant un essai de flexion quatre points et (2) un essai non destructif dans lequel les changements physicochimiques des propriétés des barres de PRFV dus à la probabilité de dégradation ont été examinés à l'échelle microstructurale.

5.5. Conclusions

Sur la base des essais expérimentaux et de l'analyse menée dans le cadre de ce programme de recherche, les conclusions suivantes sont tirées :

5.5.1. Évaluation de la résistance à la rupture par fluage des barres de PRFV soumises à différentes expositions environnementales et charges soutenues

1- La cohérence de la distribution de Weibull dans la prise en compte des variabilités de l'essai de fluage des matériaux composites de PRFV a été vérifiée à l'aide d'un coefficient de corrélation de plus de 95 % pour les données prédites et expérimentales.

2- L'extrapolation des résultats des essais de rupture par fluage des barres No 3, No 4, No 5A et No 5B en PRFV du groupe A, pour un temps d'endurance de 10^6 h a donné des résistances moyennes de rupture par fluage égales à 47 %, 48 %, 50 %, et 51 % de la résistance ultime en traction des barres, respectivement. Ces valeurs ont diminué de 3 %, 8 %, 13 % et 11 % de la résistance ultime en traction des barres en raison d'une exposition supplémentaire à une solution alcaline à 23 °C pour les barres de PRFV No 3, 4, 5A et 5B, respectivement (c'est-à-dire que les résistances de rupture par fluage extrapolées étaient de 44 %, 40 %, 37 % et 40 %, respectivement). De plus, en augmentant la température de conditionnement à 60°C, les résistances moyennes de rupture par fluage extrapolées des barres No 4 et No 5A étaient de 32 % et 29 % de la résistance ultime en traction, montrant ainsi une réduction de 16 % et 21 %, respectivement, par rapport aux résultats uniques des essais de rupture par fluage des mêmes barres.

3- Il était évident que les barres de grand diamètre présentaient un taux de dégradation plus élevé que les barres plus petites dans tous les groupes de conditionnement. Par conséquent, on peut conclure que la corrélation entre le diamètre de la barre et la réduction de la résistance au fluage est inverse.

4- Un seuil de rupture par fluage garanti associé au 99,9e percentile de la résistance à un temps d'endurance de million d'heures égal à 0,41 peut être utilisé pour les barres testées (No 3, No 4, No 5A et No 5B). Cette valeur est supérieure d'environ 37 % et 105 % aux coefficients de 0,30 et 0,2 actuellement recommandés par l'AASHTO LRFD (2018) et l'ACI 440.1R (2015), respectivement.

5- Les résistances à la rupture par fluage garanties à million d'heures d'endurance obtenues pour les barres exposées du groupe de conditionnement B et C ont montré que le produit des facteurs environnementaux (CE = 0,8 pour les éléments non exposés au sol ou aux intempéries) multiplié par les limites de résistance au fluage (Cc = 0,2-0,3) était conservateur et supérieur aux limites de résistance au fluage fixées par les codes. Le résultat $C_c \times C_E$ pour un temps d'endurance de million d'heures de la barre de PRFV testée dans le groupe B était d'au moins 0,3, ce qui est supérieur de 25 % et 87 % aux limites requises par l'AASHTO LRFD (2018) et l'ACI 440.1R (2015). De plus, la limite de rupture par fluage (0,30) à 23°C obtenue est supérieure de 20 % à celle exigée par les normes canadiennes [CSA S806 (2012), CSA S6 (2019)] de 25% de la résistance à la traction garantie (RTG).

6- Les résultats ont montré qu'un facteur CE de 1 peut être utilisé avec les limites de rupture par fluage spécifiées par les codes pour les barres de PRFV non

exposées au sol ou aux intempéries. Un facteur *CE* plus faible a été obtenu pour les barres de PRFV conditionnées à une température de 60°C qui ont été utilisées dans la présente étude comme spécimens pour un essai accéléré, cependant, une température de service aussi élevée existe rarement.

7- Les observations microstructurales sur les barres de PRFV sous charges soutenues de 50 % de la résistance ultime en traction des barres n'ont pas montré de différence significative entre les barres du groupe de conditionnement B et leurs échantillons de référence associés (barres intactes). Cela confirme que le processus de dégradation devient plus lent à des charges soutenues plus faibles.

5.5.2. Performance des poutres en béton armé de PRFV soumises à une charge élevée et à un vieillissement naturel pendant 10 ans

8- Les résultats indiquent une réduction de la résistance de seulement 16 % dans les poutres testées malgré le niveau élevé de charge soutenue appliquée aux poutres en béton armé de PRFV. Étant donné que la contrainte maximale aux états limites de service spécifiée dans la norme CSA S806 (2012) est basée sur la résistance à la traction garantie, la contrainte appliquée aux barres de PRFV considérées dans notre étude était encore supérieure à 40 % de la valeur caractéristique. Cette valeur est presque le double de la contrainte maximale admissible spécifiée dans la norme CSA S806 (2012).

9- Le modèle analytique proposé dans l'ACI 440. 1R (2015) pourrait prédire la flèche à court terme des poutres conditionnées avec une précision fiable.

10- La similarité du nombre et de l'espacement des fissures, ainsi que le léger changement de la rigidité observés dans les poutres conditionnées et non conditionnées peuvent être liés à l'effet négligeable du conditionnement sur la résistance d'adhérence. Les résultats de la microscopie optique et de l'analyse

MEB sur les poutres conditionnées ont également confirmé cette conclusion à tous les niveaux de contrainte ciblés.

11- Les valeurs de *Tg*, de la spectroscopie IRTF (infrarouge à transformée de Fourier) et de la résistance au cisaillement interlaminaire des barres de PRFV des poutres sous conditionnement naturel pendant 10 ans sont restées pratiquement inchangées pour les carottes des barres de PRFV extraites, à tous les niveaux de contrainte ciblés (0 à 40 %).

12- Cette étude a porté sur une première génération de barres de PRFV. Comme la qualité, les propriétés physiques, les propriétés mécaniques et la durabilité des générations de barres plus récentes se sont améliorées, on peut supposer que les seuils spécifiés pour les limites de contrainte des barres de PRFV dans les codes de conception sont conservateurs. Il convient toutefois de noter que les résultats expérimentaux étaient basés sur un nombre limité de poutres testées. Des essais supplémentaires doivent être effectués avec la nouvelle génération de barres de PRFV pour évaluer et appuyer ces résultats.

5.6. Recommandations pour les travaux futurs

La recherche actuelle a démontré une durabilité acceptable des barres de PRFV testées. Elle a également permis de comprendre la durabilité des barres de PRFV et les variables qui affectent leur performance. La portée de cette recherche a été limitée aux conditions d'essai et aux paramètres étudiés ici. En conséquence, des recherches supplémentaires devraient être menées dans ce domaine. Voici quelques recommandations pour les travaux futurs :

- Une expérience similaire à la phase I peut être réalisée pour étudier l'effet combiné du conditionnement environnemental et de la charge soutenue en

utilisant la méthode de la résistance retenue. On peut supposer que l'effet du conditionnement sur la réduction de la résistance est plus prononcé lorsque le niveau de charge soutenue est faible.

- De nouvelles techniques d'essais microstructuraux devraient être développées pour examiner les structures en service avec davantage de précession.
- Le même essai que dans la phase II peut être réalisé dans 20 à 30 ans pour estimer la durée de vie réelle des barres de PRFV noyées dans le béton exposé aux intempéries naturelles.
- Des études expérimentales sur le terrain sont nécessaires pour étudier les performances de durabilité des structures en béton armé de PRFV.

REFERENCES

AASHTO. (2018). “LRFD Bridge Design Guide Specifications for GFRP-Reinforced Concrete, second ed.” *American Association of State Highway and Transportation Officials*, American Association of State Highway and Transportation Officials, Washington, DC.

ACI (American Concrete Institute). (2015). “Guide for the Design and Construction of Structural Concrete Reinforced with FRP Bars.” *ACI440.1R*, ACI, Farmington Hills, MI:, 88.

ACI 440.1R-15. (2015). “Guide for the Design and Construction of structural concrete reinforced with Fiber Reinforced Polymer (FRP) bars.” ACI Committee 440, American Concrete Institute Farmington Hills, MI.

Ali, A. H., Benmokrane, B., Mohamed, H. M., Manalo, A., and El-Safty, A. (2018). “Statistical analysis and theoretical predictions of the tensile-strength retention of glass fiber-reinforced polymer bars based on resin type.” *Journal of Composite Materials*, SAGE Publications Sage UK: London, England, 52(21), 2929–2948.

Arczewska, P. 2018. “Deterioration of glass fiber-reinforced polymer (GFRP) bars in concrete environment.” In Proc., 10th Int. Conf. on Short and Medium Span Bridges (SMSB 2018), edited by K. Sennah, 157-1:11. Quebec, Canada: CSCE.

ASTM D4475. (2016). “Standard Test Method for Apparent Horizontal Shear Strength of Pultruded Reinforced Plastic Rods By the Short-Beam Method 1.” ASTM International, 3–5.

ASTM D570. (2018). “Standard Test Method for Water Absorption of Plastics.” ASTM Standards, West Conshohocken, PA, 1–4.

ASTM D578. (2018). “Standard specification for glass fiber strands.” ASTM International, West Conshohocken, PA.

ASTM D7205 / D7205M-06. (2016). “Standard test method for tensile properties of fiber reinforced polymer matrix composite bars.” ASTM International, West Conshohocken, PA.

ASTM D7337 / D7337M-12. (2019). “Standard test method for tensile creep rupture of Fiber Reinforced Polymer matrix.” ASTM International, West Conshohocken, PA, 1–6.

ASTM D7705 / D7705M - 12. (2019). “Standard test method for alkali resistance of fiber reinforced polymer (FRP) matrix composite bars used in concrete construction.” ASTM International, West Conshohocken, PA.

ASTM D7957 / D7957M-17. (2017). “Standard specification for solid round glass fiber reinforced polymer bars for concrete reinforcement.” ASTM International, West Conshohocken, PA.

ASTM E1356. (2014). “Standard Test Method for Assignment of the Glass Transition Temperatures by Differential Scanning Calorimetry.” ASTM International, West

Conshohocken, PA, 1–4.

Bakis, C. E., Schaut, R. A., Pantano, C. G., and Boothby, T. E. (2005). "Tensile Strength of GFRP Bars Under Sustained Loading in Concrete Beams." *ACI Symposium Publication*, 230, 1429–1446.

Benmokrane, B., Brown, V. L., Ali, A. H., Mohamed, K., and Shield, C. (2020). "Reconsideration of the Environmental Reduction Factor C E for GFRP Reinforcing Bars in Concrete Structures." *Journal of Composites for Construction*, 24(4), 06020001.

Benmokrane, B., Brown, V. L., Mohamed, K., Nanni, A., Rossini, M., and Shield, C. (2019). "Creep-Rupture Limit for GFRP Bars Subjected to Sustained Loads." *Journal of Composites for Construction*, 23(6), 1–7.

Benmokrane, B., Manalo, A., Bouhet, J. C., Mohamed, K., and Robert, M. (2017). "Effects of Diameter on the Durability of Glass Fiber-Reinforced Polymer Bars Conditioned in Alkaline Solution." *Journal of Composites for Construction*, 21(5), 1–12.

Benmokrane, B., Nazair, C., Loranger, M.-A., and Manalo, A. (2018). "Field Durability Study of Vinyl-Ester–Based GFRP Rebars in Concrete Bridge Barriers." *Journal of Bridge Engineering*, 23(12), 04018094.

Benmokrane, B., Wang, P., Ton-That, T. M., Rahman, H., and Robert, J.-F. (2002a). "Durability of Glass Fiber-Reinforced Polymer Reinforcing Bars in Concrete Environment." *Journal of Composites for Construction*, 6(3), 143–153.

Benmokrane, B., Wang, P., Ton-That, T. M., Rahman, H., and Robert, J.-F. (2002b). "Durability of Glass Fiber-Reinforced Polymer Reinforcing Bars in Concrete Environment." *Journal of Composites for Construction*, 6(3), 143–153.

Bischoff, P. H., and Gross, S. P. (2011). "Equivalent moment of inertia based on integration of curvature." *Journal of Composites for Construction*, 15(June), 263–273.

Can, S., Yu, Z., Jianbin, Y., and Dongguan, S. L. (2017). "Long-term creep behavior experiment of gfrp bars under different service loads and environmental." 19–21.

Chen, Y., Davalos, J. F., and Ray, I. (2006). "Durability Prediction for GFRP Reinforcing Bars Using Short-Term Data of Accelerated Aging Tests." *Journal of Composites for Construction*, 10(4), 279–286.

CSA (Canadian Standards Association). (2012). "Design and construction of building structures with fiber reinforced polymers." *CSA-S806*, CSA, Rexdale, ON, Canada.

CSA (Canadian Standards Association). (2019a). "Canadian Highway Bridge Design code." *CSA-S6*, CSA, Mississauga, ON, 1185.

CSA (Canadian Standards Association). (2019b). "Specification for fibre-reinforced polymers." *CSA-S807*, CSA, Rexdale, ON, Canada:

Davalos, J. F., Chen, Y., and Ray, I. (2012). "Long-term durability prediction models for GFRP bars in concrete environment." *Journal of Composite Materials*, 46(16), 1899–1914.

Dejke, V., and Tepfers, R. (2001). “Durability and service life prediction of GFRP for concrete reinforcement.” *Proceedings of the 5th International Symposium on Fiber Reinforced Polymer Reinforcement for Concrete Structures - FRPRCS-5*, 515–520.

Devalapura, R. ., Greenwood, M. E., Gauchel, J. V., and Humphrey. (1998). “Evaluation of GFRP performance using accelerated test methods.” *1st Int. Conf. on Durability of Fiber Reinforced Polymer (FRP) Composites for Construction and Rehabilitation of Structures*, B. Benmokrane and H. Rahman, ed., Quebec: University of Sherbrooke., 107–116.

Dong, Z., Wu, G., Zhao, X. L., and Wang, Z. K. (2017). “A refined prediction method for the long-term performance of BFRP bars serviced in field environments.” *Construction and Building Materials*, 155, 1072–1080.

D'Antino, T., Pisani, M.A., and Poggi, C. (2018). " Effect of the environment on the performance of GFRP reinforcing bars." Composites Part B 141 (2018) 123–136.

El-Hassan, H., El Maaddawy, T., Alsallamin, A., and Al-Saidy, A. (2017). “Performance evaluation and microstructural characterization of GFRP bars in seawater-contaminated concrete.” *Construction and Building Materials*, 147, 66–78.

El-Hassan, H., and El Maaddawy, T. (2019). " Review Article Microstructure Characteristics of GFRP Reinforcing Bars in Harsh Environment." Advances in Materials Science and Engineering, 2019(8053843), 19 pp., https://doi.org/10.1155/2019/8053843

European Standard EN 1992. (2014). *Eurocode - Basis of structural design*. *Dictionary*

Geotechnical Engineering/Wörterbuch GeoTechnik.

Franke, L., and Meyer, H. J. (1992). "Predicting the tensile strength and creep-rupture behaviour of pultruded glass-reinforced polymer rods." *Journal of Materials Science*, 27(18), 4899–4908.

Gooranorimi, O., and Nanni, A. (2017). "GFRP Reinforcement in Concrete after 15 Years of Service." 21(5), 1–9.

Greenwood, M. E. (2002). "Creep-rupture testing to predict long-term performance." *2nd Int. Conf. on Durability of Fiber Reinforced Polymer (FRP) Composites for Construction*, ISIS, Canada, Montréal.

He, X. J., Dai, L., and Yang, W. R. (2017). "Durability and degradation mechanism of GFRP bars embedded in concrete beams with cracks." *Plastics, Rubber and Composites*, 46(1), 17–24.

He, X., Jingnan, Y., and Bakis, C. E. (2013). "Tensile Strength Characteristics of GFRP Bars in Concrete Beams with Work Cracks under Sustained Loading and Severe Environments." *Wuhan University of Technology and SpringerVerlag Berlin Heidelberg*, 28(5), 934–937.

Helbling, C., Abanilla, M., Lee, L., and Karbhari, V. M. (2006). "Issues of variability and durability under synergistic exposure conditions related to advanced polymer composites in the civil infrastructure." *Composites Part A: Applied Science and Manufacturing*, 37(8), 1102–1110.

ISIS Canada. (2007). *Reinforcing Concrete Structures with Fibre Reinforced Polymers*. *Winnipeg, Manitoba*.

Kumar, D. S., Shukla, M. J., Mahato, K. K., Rathore, D. K., Prusty, R. K., and Ray, B. C. (2015). "Effect of post-curing on thermal and mechanical behavior of GFRP composites." *IOP Conference Series: Materials Science and Engineering*, 75(1).

Manalo, A., Maranan, G., Benmokrane, B., Cousin, P., Ferdous, W., Liang, R., and Hota, G. (2020). " Comparative durability of GFRP composite reinforcing bars in concrete and in simulated concrete environments." Cement and Concrete Composites, 109(2020), 103564. https://doi.org/10.1016/j.cemconcomp.2020.103564.

Mccallum, B. (2013). "Experimental Evaluation of the Bond Dependent Coefficient." Dalhousie University, Halifax, Nova Scotia.

Micelli, F., and Nanni, A. (2004). "Durability of FRP rods for concrete structures." *Construction and Building Materials*, 18, 491–503.

Mota, C., Alminar, S., and Svecova, D. (2006). "Critical Review of Deflection Formulas for FRP-RC Members." *Journal of Composites for Construction*, 10(June), 183–194.

Mufti, A. A., Onofrei, M., Benmokrane, B., Banthia, N., Boulfiza, M., Newhook, J. P., Bakht, B., Tadros, G. S., and Brett, P. (2007). "Field study of glass-fibre-reinforced polymer durability in concrete." *Canadian Journal of Civil Engineering*, 34(3), 355–366.

Mukherjee, A., and Arwikar, S. J. (2005). "Performance of Glass Fiber-Reinforced Polymer

Reinforcing Bars in Tropical Environments— Part II: Microstructural Tests." *ACI Structural Journal*, 102(6), 632.

Mukherjee, A., and Arwikar, S. J. (2006). "Performance of glass fiber-reinforced polymer reinforcing bars in tropical environments - Part 1: Structural scale tests." *ACI Structural Journal*, 103(4), 632.

Nanni, A. (1993). "Flexural Behavior and Design of RC Members Using FRP Reinforcement. Journal of Structural Engineering." *ASCE, Structural Engineering*, 119(11), 3344–3359.

Nkurunziza, G., Debaiky, A., Cousin, P., and Benmokrane, B. (2005). "Durability of GFRP bars: A critical review of the literature." *Progress in Structural Engineering and Materials*, 7(4), 194–209.

Noël, M. (2019). "Probabilistic fatigue life modelling of FRP composites for construction." *Construction and Building Materials*, 206, 279–286.

Park, Y., Kim, Y. H., and Lee, S. H. (2014). "Long-term flexural behaviors of GFRP reinforced concrete beams exposed to accelerated aging exposure conditions." *Polymers*, 6(6), 1773–1793.

Renaud, C. M., and Greenwood, M. E. (2000). "Effect of Glass Fibres and Environments on Long-Term Durability of GFRP Composites." *Presentation*.

Robert, M., Wang, P., Cousin, P., and Benmokrane, B. (2010). "Temperature as an Accelerating Factor for Long-Term Durability Testing of FRPs: Should There Be Any

Limitations?" *Journal of Composites for Construction*, 14(4), 361–367.

Rossini, M., Saqan, E., and Nanni, A. (2019). "Prediction of the creep rupture strength of GFRP bars." *Construction and Building Materials*, 227.

Seki, H., Sekijima, K., and Konno, T. (1997). "Test Method on Creep of Continuous Fiber Reinforcing Materials." *International symposium; 3rd, Non-metallic (FRP) reinforcement for concrete structures*, Japan Concrete Institute, Sapporo; Japan, 195–202.

Shi, J., Wang, X., Wu, Z., and Zhu, Z. (2017). "Fatigue behavior of basalt fiber-reinforced polymer tendons under a marine environment." *Construction and Building Materials*, 137, 46–54.

Shield, C., Brown, V., Bakis, C. E., and Gross, S. (2019). "A Recalibration of the Crack Width Bond-Dependent Coefficient for GFRP-Reinforced Concrete." *Journal of Composites for Construction*, 23(4), 1–8.

The official website of the Government of Canada. (2019). "Historical Climate Data."

Thériault, M., and Benmokrane, B. (1998). "Effects of FRP Reinforcement Ratio and Concrete Strength on Flexural Behavior of Concrete Beams." *Journal of Composites for Construction*, American Society of Civil Engineers, 2(1), 7–16.

Tobbi, H., Farghaly, A., and Benmokrane, B. (2012). "Concrete Columns Reinforced Longitudinally and Transversally with Glass Fiber-Reinforced Polymer Bars." *Aci Structural Journal*, 109.

Trejo, D., Kim, J. J., and Gardoni, P. (2011). "Long-Term Performance of Glass Fiber-Reinforced Polymer Reinforcement Embedded in Concrete." *Materials Journal*, 108(6).

Wang, L., Ma, Y., Ding, W., Zhang, J., and Liu, Y. (2012). "Comparative Study of Flexural Behavior of Corroded Beams with Different Types of Steel Bars." *Journal of Performance of Constructed Facilities*, 1–9.

Weber, A. (2005). *Durability tests performed on straight ComBAR GFRP bars with standard coating d=16mm.* G. Baden - Baden, Germany:

Wu, G., Dong, Z., Wang, X., Zhu, Y., and Wu, Z. (2014). "Prediction of Long-Term Performance and Durability of BFRP Bars under the Combined Effect of Sustained Load and Corrosive Solutions." *Journal of Composites for Construction*, 19(3), 4014058.

Yamaguchi, T., Kato, Y., Nishimura, T., and Uomoto, T. (1997). "Creep Rupture of FRP Rods Made of Aramid, Carbon and Glass Fibers." *International symposium; 3rd, Non-metallic (FRP) reinforcement for concrete structures*, Japan Concrete Institute;, 179–186.

Yilmaz, V. T. (1992). "Chemical attack on alkali-resistant glass fibres in a hydrating cement matrix: characterization of corrosion products." *Journal of Non-Crystalline Solids*, 151(3), 236–244.

Yilmaz, V. T., Lachowski, E. E., and Glasser, F. P. (1991). "Chemical and Microstructural

Changes at Alkali-Resistant Glass Fiber–Cement Interfaces." *Journal of the American Ceramic Society*, 74(12), 3054–3060.